Low Air Pressure Partial Discharge Recognition Using Statistical Analysis of Time-Domain Pulse Features

by

Saeed Shahabi

A Thesis submitted to the Faculty of Graduate Studies of
The University of Manitoba
in partial fulfilment of the requirements of the degree of

Doctor of Philosophy

Department of Electrical and Computer Engineering
University of Manitoba
Winnipeg, Canada

Examining Committee

This thesis was examined and approved by the following examining committee on March 20, 2019. The oral examination was chaired by **Dr. Ehab El-Salakawy** from Department of Civil Engineering.

- **Dr. Behzad Kordi** (advisor)
  Department of Electrical and Computer Engineering
  University of Manitoba
- **Dr. Namal Fernando**
  Department of Electrical and Computer Engineering
  University of Manitoba
- **Dr. Madjid Birouk**
  Department of Mechanical Engineering
  University of Manitoba
- **Dr. Kaveh Niayesh**
  Department of Electric Power Engineering
  Norwegian University of Science and Technology (NTNU)

Abstract

The heavy mechanical, hydraulic and pneumatic based systems in modern aircraft are going to be replaced by electrical systems to make them more compact and light. The growth of electrical equipment in modern aircraft is achieved by increasing the voltage of electrical power supplies that may cause partial discharges (PD). At higher voltages, the partial discharges can be disruptive and causes insulation failure. Furthermore, an aircraft experiences a wide range of operating pressures during ascending and descending. The air pressure at high altitudes drops as low as 30%. It is widely known from Paschen's law that the dielectric strength of air decreases with altitude and hence increases the risk of partial discharges (PD). The performance of electric power system components of an aircraft must be reliable at high altitude under sub-atmospheric pressures. Electric actuators used in more-electric aircraft are fed by inverter drives that generate pulse width modulated (PWM) voltages. Under sub-atmospheric pressures, these PD signals are covered by the interfering signals from inverter that makes them difficult to be detected. Because of this, PD activity measurement under sub-atmospheric pressures has been a topic of interest for the evaluation of aircraft insulation system.

The ultimate goal of this dissertation is to show a powerful diagnostic method for the evaluation of insulation condition and PD source recognition under sub-atmospheric pressures. A method based on the combination of wavelet and energy techniques is proposed to detect PD pulses in an extremely polluted noisy environment under typical aircraft's operating air pressure. For separation of PD sources, the time-domain features are calculated from PD pulse signal. Three of the features are selected to make a three dimensional (3D) space and the calculated features of all PD signals are mapped in the 3D space for separation of superimposed PD sources. The statistical moments of feature distributions are used for classification of PD sources. In order to have a good combination of available statistical moments and high speed of classification, kernel support vector machine (KSVM) algorithm is employed as a classifier for PD recognition under sub-atmospheric pressures.

Acknowledgements

This dissertation would not have been possible without the guidance, support, and cooperation of several individuals whom in different ways contributed and extended their valuable assistance in the preparation and completion of this work.

First and foremost my utter gratitude to my adviser, Prof. Behzad Kordi, whose inspirational guidance, great patience, and cheerful encouragements, supported me through this process and propelled me to finish this study.

I would like to express my appreciation to my committee members, Dr. Namal Fernando, Dr. Kaveh Niayesh and Dr. Madjid Birouk for their efforts put into reviewing the thesis, and their invaluable comments and suggestions.

I would also like to extend my thanks to our High Voltage (HV) lab technologist, Mr. Daryl Hamelin for his invaluable support in experimental setup.

A lot of gratitude goes to the University of Manitoba, and its high voltage lab facilities, and the National Science and Engineering Research Council of Canada (NSERC), for providing financial support on this work.

I also am deeply in debt to my parents, whose unconditional love and support give me the possibility of pursuing my dreams and education.

Finally, I indeed am grateful for having my lovely wife, Zahra Taban whose endless love and support made this path more comfortable for me; I would like to sincerely thank her for sharing these moments of studying life with me.

Table of Contents

List of Figures

List of Tables

Chapter 1

Introduction

1.1 Motivation

Aircraft manufacturers are replacing heavy, mechanical, hydraulic, and pneumatic based systems with electrical systems to make them more compact and light. More-electric system architecture is going to be used in modern aircraft which is called More-Electric Aircraft (MEA). Boeing quotes that the benefits of MEA are more efficient power generation and distribution, better fuel efficiency, lower maintenance costs, and less drag and noise [1]. The growth of electrical equipment in modern aircraft can be achieved by increasing either the current or the voltage of the electrical power supplies. Increasing the electric current of power supply increases the cable carrying current capacity. A cable with greater size is required for higher level of current carrying capacity. Increasing the size of cables leads to heavier conductors which is unfavorable. Therefore, the manufacturers' focus is on increasing the voltage to increase the power supply [2, 3]. On the other hand, the increase of source voltage (235 VAC and 540 VDC) leads to higher levels of partial discharges. partial discharge (PD) is a localized dielectric breakdown of a small portion of an electrical insulation system under high voltage stress, which partially bridge the space between two conductors. Partial discharges (PD) will be disruptive that leads to insulation failure [1, 4].

Aircraft experiences a wide range of operating pressures during ascending and descending. Compared to the sea level atmospheric pressure (101 kPa), the pressure at high altitudes of 33,000 to 46,000 feet (10 to 14 km) drops to less than 30% of the pressure at sea level [2, 5]. The standard atmosphere pressure above sea level versus altitude is shown in Figure 1.1 [5]. As shown in Figure 1.1, the atmosphere pressure decreases with altitude. It is widely known from Paschen's law that the dielectric strength of air as a gas insulation is pressure dependent [6]. Paschen's law states that as the pressure is reduced, the dielectric strength of air reaches a minimum value and then, as the pressure is further reduced, the dielectric strength rises sharply as shown in Figure 1.2 [6]. Typical cruise altitude of commercial aircraft is somewhere between 12 and 15 km above sea level [4, 7]. As such, the performance of the electric power system components of the aircraft must be reliable at high altitude under sub-atmospheric pressures.

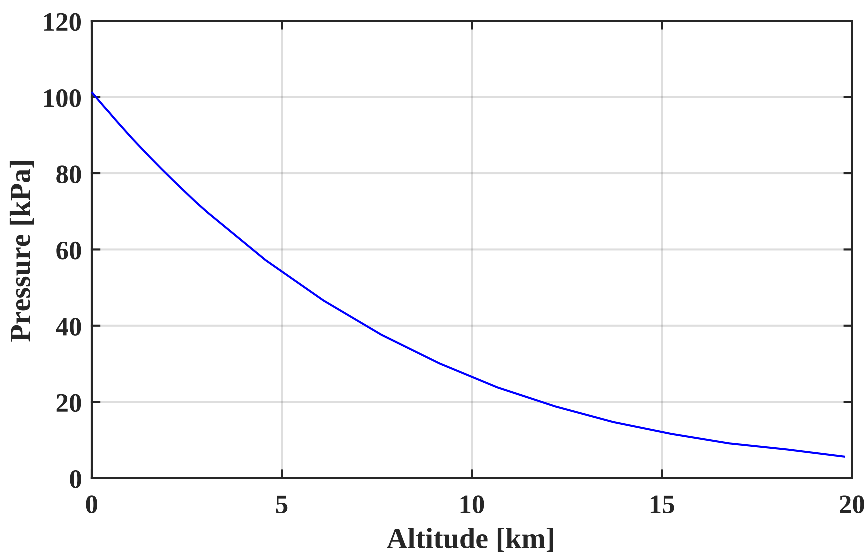

Fig. 1.1: Standard atmosphere pressure vs. altitude above sea level.

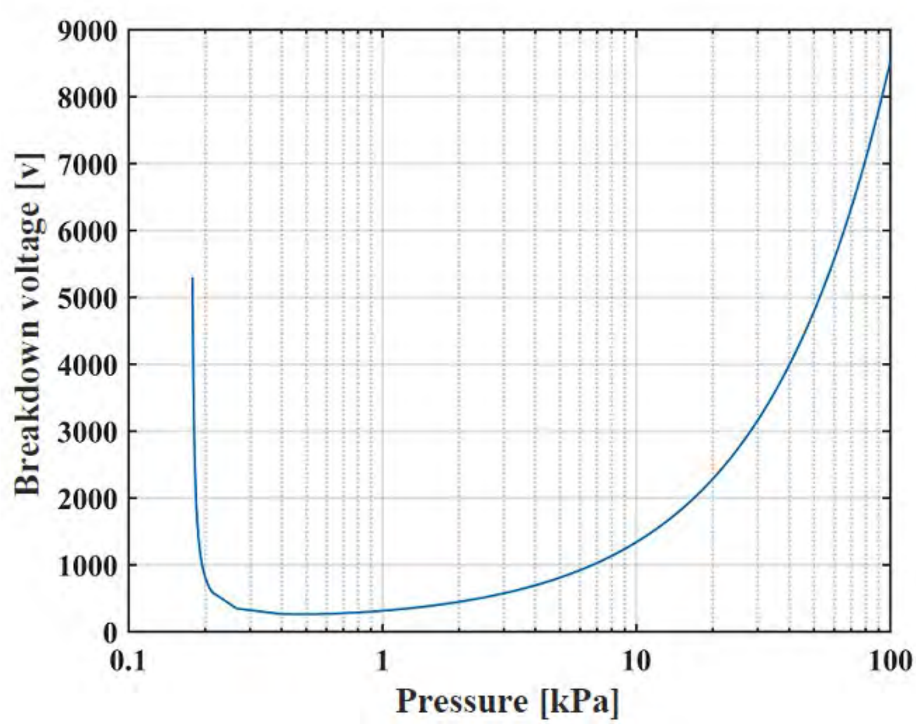

Fig. 1.2: Experimental results for breakdown voltage of air at different pressure (gap distance=2.5 mm) [6].

As shown in Figures 1.1 and 1.2, at an altitude of 12 km the atmospheric pressure is less than 20 kPa and the risk of partial discharges will increase according to Paschen's law. The health and performance of the insulation system of generators and electric actuators in MEA is a serious concern under operating conditions [8]. Partial discharges can erode the insulation system of MEA and eventually lead to its breakdown [9]. In recent years, due to the availability of high-speed data processors and well-developed statistical techniques in machine learning, automated detection and classification of PD pulses seems to be more reliable [10]. Using an automated method based on machine learning technique for classification of PD sources are more accurate and efficient. In this way, the ability to detect insulation defects in early stages can lead to an increase in safe operation of electrical devices [11]. Therefore, the partial discharge (PD) identification and classification under sub-atmospheric pressures has been a topic of interest for evaluation of the insulation system.

1.2 Objectives

The main objective of this PhD thesis is the identification of simultaneous PD sources under sub-atmospheric pressure condition and square wave voltage. In order to identify PD sources that are activated simultaneously, partial discharge detection and classification are required. Multiple PD sources sometimes occur in insulation system of aircraft and their identification is very serious for aircraft industry. Despite the PD detection techniques used by many manufacturers, they are not beneficial under sub-atmospheric pressure condition. In this thesis, a new PD detection technique is developed that can be used for PD measurement in low air pressure area. This detection technique can be used for identifying concurrent PD sources, as well as a single PD source. The new technique can detect small-amplitude PD pulses in excessive noisy environment very well. A high performance algorithm based on machine learning technique is developed for the separation and classification of simultaneous multiple PD sources. This algorithm is powerful in the separation and classification of multiple PD sources in excessive noisy environment under sub-atmospheric pressure.

In order to test the performance of the proposed detection and classification technique, measurements are conducted on different artificial defects that are implemented in small laboratory test cells. A needle-plane electrode arrangement and a twisted pair of insulated conductors are the main electrode arrangements used for the experiments. The discharge current created by insulation defects of test samples are recorded for further analysis. To generate a dataset as an input of the classification algorithm, a comprehensive investigation and analysis is performed on PD pulse waveforms captured under square wave applied voltage. The automated identification of insulation condition is carried out on the generated dataset. In general, the purpose of this thesis is to show a powerful diagnostic method for evaluation of insulation condition and PD source recognition.

1.3 Methodology and Contributions

This thesis introduces an efficient method for monitoring of insulation operations under sub-atmospheric condition as well as separation and classification of PD pulses based on effective statistical features. The applied voltage waveform used for measurement is either a square or sinusoidal. The artificial defects that are simulated in low pressure test cells are connected in parallel. The air pressure inside the test cells is reduced to as low as 30 kPa which is equal to air pressure level at an altitude of 10 km. The current going through the ground connection is measured and recorded for analysis. The current signal contains both PD and noise pulses. The PD pulses are detected based on the combination of wavelet and differential energy techniques. The differential energy pattern of PD signals, which shows the occurrence of PD activities in reference to the phase angle of the applied voltage, is a valuable PD identification tool in a noisy environment.

In order to classify PD sources, a data acquisition system with a high time resolution is managed to record pulses for feature generation. Parameters of pulses are calculated to generate time-domain features. The pulse parameters that represent the significant fingerprints of the PD sources are rise time, fall time, and pulse width. The statistical-based features of pulse parameters are used for the separation of pulse sources. The PD pulses are identified and seperated from noise pulses based on pulse signal parameters. The statistical moments of feature distributions are computed. Subsequently, a classifier algorithm based on support vector machine (SVM) is implemented for the classification of PD sources.

The contributions of this PhD thesis are:

- Partial discharges were detected in excessive noisy environment using wavelet and differential energy technique at three level of air pressure. The air pressure levels used for experiments were 33, 67, and 101 kPa.

- The waveform of applied voltage used for PD measurements was either a square or sinusoidal. The applied voltage frequency used for the measurements was between 10 Hz and 5 kHz. The square wave applied voltage was symmetrical in shape with 50% duty cycle and the minimum rise time of 10 μS.

- The effects of air pressure and applied voltage frequency on Partial Discharge Inception Voltage (PDIV) and PD pulse parameters such as rise time, fall time, slew rate, and pulse width have been investigated. Also, the effects of pressure and frequency on differential energy pattern of PD signals have been explored.

- A clustering technique based on pulse parameters was used for separation of simultaneously active PD sources.

- Identification of partial discharge sources under sub-atmospheric pressures and then classification of new unknown data that is a mixture of PD pulses and noise signals based on machine learning technique.

1.4 Publications

The outcomes of this research have been published in one conference paper and two journal papers on have been submitted.

Journal papers:

1. S. Shahabi, A. N. Esfahani, G. C. Stone, and B. Kordi, "Corona Discharge Detection in Noisy Environment and Low Air Pressure", *IEEE Transactions on Aerospace and Electronic Systems*, Submitted.

2. S. Shahabi, H. Janani, and B. Kordi, "Separation and Classification of Concurrent Partial Discharge Sources Using Statistical-Based Feature Analysis for Gas Insulated Substation", *IEEE Transactions on Dielectric and Electrical Insulation*, Submitted.

Conference paper:

1. A. N. Esfahani, S. Shahabi, G. Stone and B. Kordi, "Investigation of Corona Partial Discharge Characteristics Under Variable Frequency and Air Pressure," *2018 IEEE Electrical Insulation Conference (EIC)*, San Antonio, TX, 2018, pp. 31-34.

Chapter 2

Background and Literature Review

In this chapter, the definition of partial discharge in gaseous dielectrics and its mechanism are presented. Then, a review of existing investigation on partial discharge activity under sub-atmospheric pressure and detection methods is reported.

2.1 Partial Discharge

One of the major problems for electrical systems is insulation failure. The factors that contribute to insulation failure are cracking of insulation, defective insulation material, porosity in the insulation material, and contamination. These risk factors are required for initiation of partial discharges (PD) inside the insulation or on the surface of insulation. When the electric field strength between two conductors exceeds the dielectric strength of the insulation between the conductors, partial discharge can occur. In electrical engineering, partial discharge (PD) is the most common type of electrical discharge or spark that bridges a small portion of a solid or fluid electrical insulation (gaseous void in solid dielectric and gas bubble in liquid dielectric) between two conductors while the remaining parts of insulation are healthy [12]. The remaining healthy part of the insulation is affected by partial discharge and the dielectric breakdown may happen. When the dielectric breakdown occurs, the discharge fully bridges the conductors and then the insulation failure happens. In general, partial discharges appear as pulses having a duration of much less than 1 μs. More continuous forms can, however, occur that are the so-called pulse discharges in gaseous dielectrics [13].

2.2 Partial Discharge in Gaseous Insulating Media

Gas discharge refers to an electric current that flows through an ionized gas. When there is no external ionization source (normal condition), the electrical conduction of the gaseous medium is very low. In reality, there is a small amount of charged particles in the air due to cosmic rays and radiation that exists on the earth [12, 14]. At normal condition, the charged particles move erratically that makes the average current approximately equals to zero. When a weak electric field is applied to the gas, the movements of charged particles will be in the direction of electric field. These movements leads to a small electric current. When the electric field in the gaseous medium becomes strong enough, the electrical conduction of the gaseous medium suddenly increases which leads to a high electric current. At this condition, the gas will not function as insulation anymore. The transition from the state of insulating to conductive condition is called breakdown. The minimum voltage in the gas that causes to have breakdown, is called "breakdown voltage (Ub)"[14].

In the study of gas discharge, six particles are considered: electron, photon, ground-state atoms or molecules, excited atoms or molecules, cation and anion [15]. The collision of charged particles leads to a change in their state. When an electron becomes attached to a neutral atom, a negative ion is generated. However, a positive ion is generated through ejection of an electron from a neutral atom. The mass of an atom in comparison to that of an electron is much higher so that the mass of an atom is assumed approximately equal to the corresponding ion. The drift velocity of an electron is significantly higher than an ion because the mass of an electron is lower than the mas of an ion. Due to the low drift velocity of ions, they can be considered stationary from the place at which they are generated. Therefor, the discharge process is mostly precipitated by generated free electrons [14, 15, 16].

Two types of mechanisms are used to describe gas discharge phenomena which are non-self sustaining discharge and self-sustaining discharge. In non-self sustaining gas discharges, an external ionization source is required to generate electrons for maintaining discharge phenomenon. When the applied voltage between conductors exceeds a critical value, the formation of discharge becomes independent of the external ionization source, which is called self-sustaining discharge [14, 15].

According to Townsend discharge theory, a rapid increase in the number of space charges in the gas discharge is resulted by three ionization processes as following [14]:

- The initial free electrons move toward the energized conductor at positive polarity and collide with other particles. A huge number of positive ions and electrons are generated which is known as the α process.

- Positive ions move toward the electrode at negative polarity and collide with gas particles. The number of electrons and positive ions which are produced as a result of this process are small in comparison to the α process. This ionization process is known as the β process and is not considered in the study of gas discharge under normal conditions. The reason is that the positive ions cannot obtain the required kinetic energy to ionize gas particles.

- When the positive ions strike the cathode, an average number of secondary electrons are emitted (secondary electron emission). This process is known as the γ ionization process.

2.3 PD Activity under Sub-atmospheric Pressure Conditions

The partial discharges (PD) occurring in different types of insulation (oil, air, paper, ...) at ground level atmospheric pressure has been studied by many researchers. The purpose of most investigations on partial discharges was to detect, localize, analyze, and classify the PDs. The experiments were carried out on different electrode configurations and gases under standard atmospheric pressure condition (i.e. 101.3 kPa). However, few investigations are available for monitoring and measuring PDs under sub-atmospheric pressure conditions. This section reviews literature covering partial discharge activity under sub-atmospheric pressure conditions.

Husain and Nema [17] investigated surface partial discharge in dry air at different pressure levels. The range of air pressure was from 91.333 down to 0.067 kPa. PD tests were performed on Rogowski profile electrodes, which create a uniform electric field in the space between electrodes, with various thickness of solid insulation. They reported that the PD inception voltage (PDIV) changes with air pressure and also the thickness of dielectric has no significant impact on PDIV at low pressures. PDIV is the lowest voltage at which partial discharges occur when the test voltage is gradually increased from a lower value [12]. However, samples with higher insulation thickness show higher PD inception voltage near atmospheric pressures. The main observation of this study is that the breakdown voltage of solid-gas insulation system is 20% to 30% lower than that predicted by Paschen curve.

PD tests at various pressure values (from a vacuum pressure of 100 mPa to an atmospheric pressure of 101 kPa) under non-uniform electric field were performed by Okubo *et al.* [18, 19]. The applied voltage was a DC positive voltage and various electrode configurations were used in the vacuum chamber. At high-altitude space where satellites and space shuttles fly, helium and argon are significant components of residual gas. Because of this reason, the gases used for PD tests were helium, argon and air. The electric field (E) distributions in the gap distance of two electrodes under various gas pressure (P) were studied. In [18], it was shown that the electric field strength increases with pressure. They used spatial distribution of E/P for the investigation of PD where E and P are electric field and gas pressure, respectively. The spatial distribution is obtained by dividing E by the corresponding pressure. It was concluded that there is a critical value for spatial distribution of E/P (kV/mm/Pa) for which PD was dependent on the gas medium but independent from the non-uniformity of the electric field. It was suggested that partial discharge occurs in the gap distance where the value of E/P exceeds the critical value.

Li *et al.* [20, 21] studied positive and negative corona discharge in air under pressures from 20 kPa to 100 kPa. The electrodes were hemispherically-tipped pointed electrode and concave hemispherical electrode. Positive/negative DC voltage was applied to hemispherically-tipped pointed electrode, whereas the concave hemispherical electrode was grounded. It was reported that the onset voltages for both positive and negative corona increase with air pressure.

The PD pulse characteristics in air and argon at different pressures (13.3 Pa to 101.3 kPa) were investigated by Kasten *et al.* [5, 22]. The point-plane electrode configuration in a vacuum chamber was used. A 60-Hz AC voltage was applied to the point electrode with the plane electrode grounded. The typical waveforms of discharge current pulses at different pressures were measured. The rise time of discharge current pulses were obtained and the corresponding frequency contents were estimated. Based on the experimental results, the negative discharge current pulses have a lower frequency content than the positive ones under the same pressure for both air and argon. The frequency contents of positive and negative discharge pulses for argon compared to air under the same pressure are lower. It was concluded that the pressure has a significant influence on the frequency content of discharge current pulses. At low pressures the frequency content of discharge pulses was lower than the frequency content at atmospheric pressure.

Tabrizchi *et al.* [23, 24] investigated the effects of pressure and temperature on ion mobility of corona discharges. The ion mobility is defined as the ratio of drift velocity of ions to applied electric field. Dry nitrogen was used as testing media at different pressure levels (from 2 kPa to 101 kPa). The moisture level of nitrogen gas was less than 20 ppm (parts per million). It was reported that the ion mobility of corona discharge increases with reducing pressure while the ignition potential decreased. The ignition potential is the threshold voltage necessary for ignition which is often referred as breakdown voltage.

PD tests in argon, helium, and air under pressures from 101.3 kPa down to 0.27 kPa for both AC and DC applied voltages were carried out by Liu *et al.* [25, 26]. A twisted pair of insulated conductors mounted in the experimental chamber was used for the investigations. For AC tests, the PD inception voltage was determined for each gas. Then, the PD current pulses were recorded for an applied voltage of 5% and 20% above the inception voltage. For DC tests, a bipolar voltage source with an amplitude of 50 kV was used. Authors concluded that the PD current pulse waveform characteristics (rise time, fall time, amplitude, and width) are pressure dependent for argon, helium, and air. They reported that the average amplitude of the PD pulses increases with increasing pressure for argon and helium and for air as well. The rise time of the PD current pulses decreases with decreasing pressure for argon. On the other hand, the rise time of PD waveforms increases with decreasing pressure for helium and air. The characteristics of PD current pulse waveforms at the applied voltage of 5% and 20% above inception voltage (PDIV) were studied. The maximum amplitude at 20% above inception voltage is larger than that measured at 5% over the inception voltage.

PD measurement in the disc-shaped cavities in polycarbonate material was investigated by Forssen and Edin [27, 28]. The frequency range of the applied voltage was 100 Hz down to 0.01 Hz. It was shown that PD activity depends on the applied voltage frequency and the rate of this dependency changes with the applied voltage magnitude. PD measurements showed that PD magnitude increases with increasing the frequency when the magnitude of applied voltage is less than 10 kV. On the other hand, PD number increases with increasing the frequency when the magnitude of applied voltage is more than 10 kV. Also, the size and location of the cavity affect PD frequency dependence. It was indicated that PD activity in the small cavities is independent of frequency while the number of PDs increases with increasing the frequency for larger cavities.

PD pulse characteristics of two electrode arrangements, a point-plane electrode and a twisted-pair of insulated conductors were studied by Grosjean *et al.* [7, 29]. PD measurements were carried out under pressures from 101.3 kPa down to 0.27 kPa for 60-Hz AC energization in air, argon, and helium. The incompatibility of standard methods for PD measurement and calibration for low pressure were described. The incompatibility is that the PD pulse rise time estimated at low pressures in air is much longer than the one measured at ground level air pressure. Because of this reason, PD frequency content may be below the low cutoff frequency of measuring devices. The modification of the standard procedures is necessary to measure PD under sub-atmospheric pressure. It was concluded that a very long rise time and pulse width of PD current waveforms can be detected at low pressures by using a suitable filter. Using a bandpass filter with a low cutoff frequency of 30 kHz and a high cutoff frequency of 50 kHz, one can measure PD with long pulse width at low pressures.

The positive and negative corona discharges at various pressure and humidity level were investigated by Bian *et al.* [30, 31]. A needle-plane electrode arrangement in a pressure chamber was used for the investigation. For a constant applied voltage, it was observed that the corona discharge current decreases when the air pressure or humidity increases. It was concluded that the PD inception voltage for both of the negative and positive corona discharge decreases with increasing the humidity and decreasing the air pressure.

Rui and Cotton [2] reported the effect of pressure on partial discharge characteristics. PD tests were carried out on different samples in a pressure range of 10 kPa to 100 kPa. One pair of twisted insulated wires and a piece of insulated wire wound with a metallic conductor were used as PD test samples. It was shown that the inception voltage increases while the pressure rises from a low pressure (10 kPa) to atmospheric pressure. On the other hand, it was shown that the magnitude and number of partial discharge pulses increase as the air pressure decreases. The most significant finding in this paper is that the partial discharge magnitude significantly increases when pressure decreases.

Sattari *et al.* [32, 33] studied the effect of air pressure on Trichel pulse characteristics under DC applied voltage. Trichel pulse is a typical kind of negative corona discharge current. This type of corona discharge current consists of the repetitive pulses that regularly occur with short rise time and durations, and long intervals. It was first observed by Trichel in 1934 and named after him [34]. The numerical model of corona discharge pulses was introduced in [32, 33]. Negative and positive oxygen ions, and electrons were considered for simulating Trichel pulses in air. Then the authors compared the numerical results with experimental data. It was shown that the numerical results were in good agreement with experimental results. It was reported that the duration of Trichel pulses and the occurrence frequency of pulses are affected by air pressure level. The duration of Trichel pulses as well as the occurrence frequency of pulses increase with decreasing the air pressure.

The Trichel pulses generated by the needle-plane electrode arrangement in the low air pressure area (0.134 kPa to 6.67 kPa) under a negative DC voltage were investigated by Shou *et al.* [35]. Current-voltage characteristics of negative corona discharge were obtained for different stages of discharge phenomena. It was shown that the voltage across the test cell increasing with current for the pre-discharge stage. Then, the average current increases abruptly while the voltage drops and the Trichel pulses are initiated (corona discharge stage). Further increasing the current leads to transition from corona discharge to glow discharge. Within this stage, the voltage is almost unaltered during current raising and pulses disappear suddenly. It was reported that the peak current of PD is greater at higher pressure since the more electron avalanches can be produced due to the higher air density.

Cavallini *et al.* [36] performed partial discharge measurements on varnished coils at sub-atmospheric pressures. The waveforms of applied voltage used in this study were repetitive square and sinusoidal. A high frequency current transformer (HFCT) placed around the ground connection was used for PD monitoring and the applied voltage was sinusoidal. When a square voltage generator was used to supply a system, the disturbance from the voltage supply interfered with PD signals. The patterns of PDs were not distinct from voltage supply noise in the data collected using the HFCT sensor. Because of this reason, authors introduced a second sensor which works in ultra-high frequency (UHF) range to suppress the inverter interference. It was reported that the partial discharge inception voltage (PDIV) decreases with pressure under sinusoidal and repetitive square voltage waveforms. PDIV obtained from sinusoidal voltage waveforms were higher than that obtained from repetitive square voltage waveforms. It was shown that PD monitoring is feasible using UHF techniques for aircraft under operating conditions. However, the UHF technique loses sensitivity with increasing altitude. At high altitude, PD pulses lose high frequency content.

Abadie *et al.* [37] studied the influence of pressure on frequency spectra of partial discharges under pulse width modulated (PWM) and AC power supply. The influence of the cut-off frequency of high-pass filter on PD signals at pressure less than 10 kPa was studied. Partial discharge measurements were performed on twisted pairs of enamel wires subjected to both repetitive square and sinusoidal voltage waveforms at various pressures. At low pressure (10 kPa), the PD inception voltage (PDIV) for different cut-off frequencies (50, 90, and 200 MHz) was measured. In the case of 200 MHz, the PDIV was three times greater than the one with cut-off frequency of 50 MHz. On the other hand, the cut-off frequency of the high-pass filter has no effect on the PDIV at atmospheric pressure. It was concluded that when the pressure decreases, the amplitudes of the low frequency components increase, but the high frequency ones decrease. In conclusion, for partial discharge detection at low pressures, the bandwidth of sensors and filters must be optimized.

The impact of air pressure on the positive corona current pulses was studied by Li *et al.* [38]. PD experiments were performed on a coaxial conductor-cylinder electrode structure with a corona point on the conductor. The electrode was mounted in a pressure chamber. The air pressure in the chamber was varied from 60 kPa up to 100 kPa. It was shown that the air pressure affects PD pulse characteristics under the same ratio of the applied voltage to the PD inception voltage. The pulse amplitude decreases with decreasing the air pressure. However, rise time, pulse width, pulse duration, and pulse repetition frequency increases with decreasing the air pressure.

Partial discharge measurements on magnet wires used in electric actuator and feeder cables were carried out by Billard *et al.* [4]. The results obtained from different PD tests showed that the PD inception voltage (PDIV) of typical magnet wire decreases with pressure. On the other hand, PD amplitude at low pressure is several times higher than the amplitude at atmospheric pressure. Under DC voltages, the frequency spectra of PD current waveform is not affected by pressure.

Liu *et al.* [39, 40] conducted a research on the effects of applied voltage waveform on PD occurrence. The authors performed PD experiments on polyimide films under AC sinusoidal voltage waveform at a frequency range of 5 kHz to 30 kHz. Further experiments were conducted under triangle and bipolar square waves repeating at a rate of 1 kHz at atmospheric pressure. A sphere-to-plane electrode configuration was mounted in the chamber with polyimide films as the dielectric barrier. An electric current transducer with a wide bandwidth (0.5 to 120 MHz) was employed to detect PD pulses. The minimum sensitivity of current transducer to measure PD pulse current is 1 mA. It was reported that partial discharges mostly occur during the falling and rising edges of the applied voltage. It was shown that the total number of PDs increases with frequency. On the other hand, the maximum of PD pulse magnitude decreases when the frequency increases. These two obtained parameters indicated that the lifetime of insulation system decreases as the voltage power supply with higher frequencies are used. The main factor that affects the insulation lifetime is the peak-to-peak value and frequency, however the influence of rise time can be ignored. It was concluded that the sinusoidal and square voltage waveforms with equal applied frequencies and peak-to-peak voltages, affect the lifetime of insulation system approximately identical.

PD measurements on a point-plane electrode at different frequencies of applied voltage (from 0.1 Hz to 50 Hz) were conducted by Zhou *et al* [41]. It was reported that the PD inception voltage decreases by increasing the applied voltage frequency. It was shown that the magnitude of corona discharges in the negative half cycle is significantly smaller than that in the positive half cycle. By increasing the applied voltage, the magnitude of discharge pulses in the positive half cycle increases while the discharge magnitude decreases in the negative half cycle. Analysis of phase resolved PD (PRPD) pattern indicated that the discharge patterns are frequency dependent. It was observed that the inception phase of PD shifts to the right side of the obtained pattern and discharge phase range decreases with increasing the applied frequency. Under Trichel pulse mode, increasing the magnitude of applied voltage leads to an elevation in the pulse repetition and reduction in the time interval of pulses because of the strong electric field around the needle tip.

Xing *et al.* [42] carried out a study on the effect of air pressure on negative corona-generated space charge via computational approaches. A rod-plane electrode was used to model corona discharge under different air pressure (50 kPa to 100 kPa). It was observed that when the air pressure is low, the drift velocities of gas particles such as electrons or ions significantly increase which leads to higher kinetic energy when subjected to an external electric field. In addition, the number of electrons and ions produced during corona discharge are much higher at low air pressure since the kinetic energy of gas particles is much less dissipated as a consequence of less collisions. It was concluded that PD inception voltage is lower at sub-atmospheric pressures and the number of charged particles increases with raising the applied voltage.

The effect of temperature and pressure on partial discharge degradation of silicone-coated printed circuit boards (PCB) using a 50 Hz sinusoidal AC voltage signal was studied by Emersic *et al.* [43, 44]. Two mirror-curved tracks on printed circuit board coated with different thicknesses of silicone layer were used as test samples. The experiments were conducted under air pressure levels of 11.6 and 50 kPa at room temperature. Then, two experiments were carried out at temperatures of -55°C and +70°C under atmospheric pressure. It was observed that the surface of test samples were subjected to partial discharges despite the good quality of coating. The partial discharges created cracks on the surface of silicon layer. At low air pressure, the number of cracks on the surface of silicon coating increased significantly, specially for the coating thicknesses less than 100 μm. Also, it was shown that the temperature has an impact on the growth of surface cracks and damage rate. The authors concluded that the silicone coating thicknesses greater than 250 μm prevents partial discharge occurrence on the surface of silicon-coated PCB during operating condition.

2.4 Partial Discharge Detection Techniques

Partial discharges are detected through the detection of their electrical pulses, electromagnetic emission, acoustic emission, chemical reaction, light emission. Based on these physical manifestations, several detection methods have been developed to measure partial discharges. Many of these methods use commercial PD detectors to monitor PD. There are some standard methods used by many manufacturers for off-line or on-line PD testing [45]. Each method has advantages and disadvantages. In off-line PD testing, the measurement devices work in low frequency domain and have low rate of error due to low noise. On the other hand, for off-line PD test, an external power supply is required. For on-line PD test, an external power supply is not required, so it is less expensive and PD behavior can be observed during operation conditions. Because of high rate of noise, the measurement devices should work in high frequency domain to minimize the risk of errors. Most of the detection methods are being focused on wide-band acquisitions through applying distinct methods and sensors under atmospheric pressure (101 kPa). However, these techniques are not beneficial under sub-atmospheric pressure. The following subsections are a review of the detection techniques mostly used in industry.

2.4.1 Electrical Technique

The most straightforward method for PD detection is the electrical method. This method has been widely used by researchers because it is easy to use in various insulation systems and system noises can be better suppressed compared to other detection methods [46]. The IEC standard 60270 provides the conventional PD detection method for wide-band PD instruments with lower and upper frequencies of 30 and 500 kHz [13]. The electrical detection method described by IEC standards is based on the discharge current.

A standard partial discharge measurement system consists of a coupling device, a transmission system, and a measurement system. The coupling device converts the input current to a voltage signal. The voltage signal is transmitted to a measurement system by the transmission system. The two fundamental test circuits mostly used for PD measurement are shown in Figure 2.1 [13].

In Figure 2.1, the test object is shown as a capacitor C_a and the coupling capacitor is specified as C_k. CC and MI are the connecting cable and the measuring instrument, respectively. The coupling capacitor has low level of partial discharges (less than 2 pC at 26.7 kV) in order to measure the specified partial discharges of the test object. An impedance Z is used as a filter to reduce the background noise from the power supply voltage. As recommended by the IEC standard 60270 [13], the apparent charge of partial

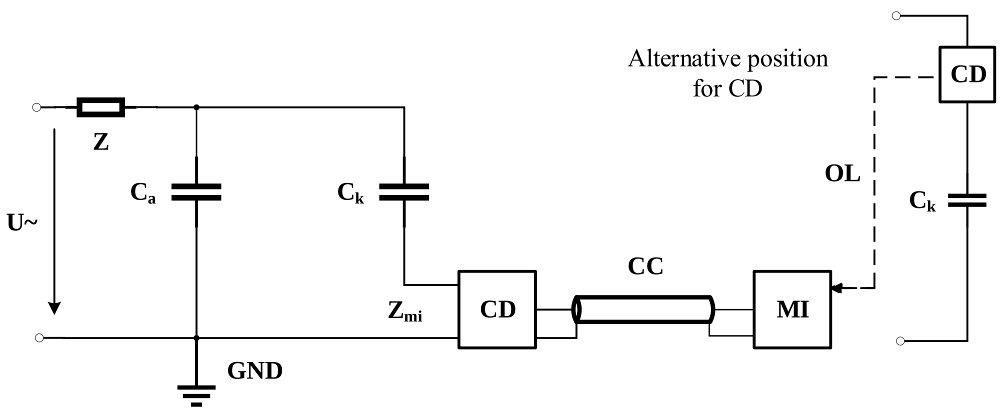

(a) Coupling device (CD) in series with coupling capacitor (C_k)

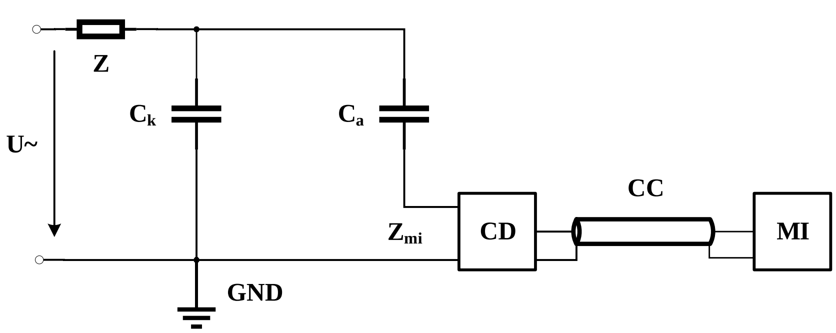

(b) Coupling device (CD) on the ground side of the test object (C_a)

Fig. 2.1: General test circuits for PD measurement [13].

discharge injected from the test object is measured. The PD current pulse generated by the same amount of injected apparent charge can be read by PD measuring device, instantly. The apparent charge is usually expressed in picocoulombs (pC).

Over the years, many digital PD detectors have been developed to analyze partial discharges. For the evaluation and analysis of partial discharge data, two different types of data patterns have been used, phase-resolved data and time-resolved data [47]. Phase-resolved partial discharge (PRPD) pattern is obtained with respect to the phase angle of the AC test voltage and the fast rise-time voltage pulses. Time-resolved partial discharge (TRPD) pattern is used to observe the PD current pulse waveforms and identify the origin of the pulses based on their shape and other characteristics. The advantage of TRPD is that the the physical characteristics of PD pulse waveforms can be better realized.

The electrical method is useful for PD detection in laboratory conditions, however it is difficult to have precise recordings of PDs for on-site conditions because the electromagnetic interference level is high and it is difficult to have an accurate calibration [45, 48].

2.4.2 Electromagnetic Interference Technique

Electromagnetic interference (EMI) measuring devices working in the very high frequency (VHF) range have been used to evaluate the condition of the insulation. Electric utility companies usually use the EMI method because of both on-line and off-line detection capabilities. This method is based on electrical coupling which includes coupling capacitors, coaxial cable sensors, and high frequency current transformers (HFCT) [25]. Since PD pulses have a very fast rise time (in the nanosecond range), corresponding to high frequency components, HFCTs and coupling capacitors are used to transfer high frequencies to the measuring system. Note that the capacitors used as coupling devices need to be PD free at operating condition for on-line monitoring [49]. The injected charges caused by PD occurrence change the voltage of discharge site, immediately. PD pulses propagate in both directions from the location of injected charges towards the coupling capacitor or the HFCT.

PD signals are attenuated during propagation because of the impedance along the path that the PD signal have to travel. The attenuation of PD signals during propagation reduces the signal to noise ratio at the detection site. De-noising methods are needed to process PD signals where the detection sensitivity is low. The output signals of the capacitors or HFCT are voltage or current pulses, respectively, which can be measured with an oscilloscope. The measured results are analyzed to assess the insulation condition [50].

2.4.3 Radio Frequency Technique

Partial discharge pulses generate electromagnetic waves. These electromagnetic waves propagate away from the discharge sites and contain radio frequencies (RF) from 100 kHz to GHz range. An RF sensor with a suitable antenna can be used to detect the RF electromagnetic waves radiated from PD sites. RF method is used to find the locations of PD in high-voltage winding of electric machinery [50]. This sensor can be used for both off-line and on-line PD tests. For off-line test, the machine winding is energized at nominal voltages and the antenna should be moved along the stator to detect PD pulses [51]. As an example of UHF antennas used for on-line PD testing, one can name the stator slot coupler (SSC) that is installed in the stator slots. Note that this type of UHF sensor is more sensitive than the VHF sensors used in the EMI method [49].

2.5 PD Source Identification and Classification

In practice, there are multiple, simultaneously-activated PD sources that affect the insulation reliability. These multi-source PDs are often partially overlapped during PD measurement. This overlapping has influence on PD classification that leads to unfavorable evaluation of the insulation quality [11]. During the past few years, discrimination of PD sources has been progressively studied in order to have proper evaluation of insulation condition and PD classification. Different techniques have been developed for the separation of PD pulses. Each type of PD source has its own discharge mechanism and features that results in a unique discharge pattern. Various methods based on PD pulse waveform analysis have been reported by many researchers. In the most proposed methods, the PD sources were classified based on phase-resolved PD (PRPD) patterns. However, these methods are barely robust in real situations because of overlapping. In practical situations, where multiple PD sources are activated simultaneously, PRPD patterns are often overlapped that results in misclassification of PD sources[52, 53].

For the separation of PD pulses, various methods and algorithms have developed and proposed based on PD pulse waveform analysis. The recognition of two simultaneous activated PD sources using a five-parameter additive Weibull distribution was presented in [54]. It was reported that this function fits well on the partial discharge height distributions in order to analyze the probability distribution associated with each of the PD defects.

In order to discriminate the collected pulses into homogeneous clusters and considering noise disturbance, time-frequency analysis method has been proposed using a fuzzy classifier (FC) in [55, 56]. It has been reported that the PD pulses created from a PD source have the same characteristic which can be useful in the separation of overlapped PD pulses. The equivalent time-frequency analysis method has been used for separation of PD pulses from noises. In this method, separations were performed through mapping the pulse waveforms in a two-dimensional (time-frequency) space. The features considered for mapping the pulse waveforms were the average time and dominant frequency of PD signal that contains the total energy of the signal [56].

The auto-correlation technique has been proposed for automatic PD source classification [57, 58]. The proposed technique is based on the comparison of the auto-correlation function (ACF) of the PD shape signals. The assumption was that there is a similarity between ACF of the recorded PD signal shapes generated from the same PD source.

The use of envelope comparison of ultra-high-frequency (UHF) signals to separate PD pulses coming from multiple sources has been proposed in [59]. The comparison of ultra-high-frequency (UHF) envelopes were performed through applying a Gaussian kernel smoothing to the data set.

A new method based on the comparison of signal energies was introduced for the identification of PD pulse signals in [60]. In this method, wavelet decomposition combined with principle component analysis (PCA) was used for the estimation of signal energies and dimensionality reduction of the data.

Feature extraction technique using S Transform (ST) based on time-frequency representation has been proposed in [52, 61] to separate PD pulses. In this procedure, features extracted from PD signals were performed using non-negative matrix factorization (NMF). Then, the classification of PD sources was achieved by a fuzzy C-means clustering algorithm.

Partial discharge recognition of insulation defects in GIS has been studied in [62, 63]. A UHF signal feature extraction algorithm based on cumulative energy technique has been presented in [63] for the classification and separation of mixed PD pulses. Blind source separation theory, combined with complex wavelet transform, has been used for the separation of concurrent pulse sources in [62].

In [64, 65, 66], the spectral power ratios analysis technique has been proposed for the classification of PD sources and noise. The ratios of spectral power in the selected frequency bands and total spectral power for each detected PD pulse signal were calculated and mapped in a two-dimensional space for PD identification.

Time-frequency sparsity map based on decomposition methods has been presented in [67] for the separation of different PD sources. The decomposition methods used for detected PD signals in this method were wavelet transform and mathematical morphology decompositions.

The use of mathematical morphology for feature extraction from optical PD data and sparse representation classification has been presented in [68]. This classification technique discriminates the PD sources on the principle of using least amount of resources which is used for the imperfect and noisy PD signal.

A new method based on two-step logistic regression (LR) model for the probabilistic identification of multi-source PDs has been introduced in [11]. In this method, principal component analysis (PCA) technique was implemented on a database to create a low dimensional space associated with single-source PDs. The dataset of multiple PD sources were mapped into this space and one-class kernel support vector machine (SVM) was employed to discriminate the multiple PD sources. Then, the classification was performed by the probability estimation of each PRPD pattern created by different multi-source PDs based on LR model.

The PD pulse separation and classification methods mentioned above are effective if managed by a skilled operator because of the complexity of algorithms [10, 69]. In real electrical apparatus, the separation of simultaneously activated PD sources without any human intervention is still a significant problem and needs more investigation. Because of this reason, there is a great interest for utilities to have an automated system for separation and classification of multi-source PD pulses.

In the last decade, many studies have been reported on PD activities at low air pressure. In these studies, the PD measurements were carried out in an environment with low level of noises and the external interferences have not been considered by the researchers. In real situations, the external interference and noises may affect the measurements. Because of these shortcommings, two developed methods are introduced in this thesis for PD source recognition under sub-atmospheric pressure and excessively noise environment.

2.6 Summary

In this chapter, a brief review of partial discharge definition and gas discharge mechanism, and PD identification history in low pressure area in More-Electric Aircraft (MEA) insulation systems was presented. Also, different partial discharge detection techniques as the standard methods for off-line PD detection were explained. Finally, PD source classification methods presented by researchers were briefly discussed. In the next chapter, partial discharge detection in low air pressure area with the implementation details of its different steps for identification of PD sources in MEA insulation system based on using differential energy patterns of PD pulses is presented.

Chapter 3

Partial Discharge Detection in Noisy Low Air Pressure Environment

3.1 Noise Interferences in PD Measurement

Partial Discharge (PD) measurement is a non-destructive method for assessment of insulation condition [13]. Noise interference from external sources affects the measurement of PD signals and reduces the accuracy of the measurements. Repetitive switching noise that comes from a switching-type power source and PD occurring in neighboring apparatus are the main external sources of interference. A variable frequency AC system is used in MEA power distribution system. The frequency of the system can vary from 360 Hz to 900 Hz. The power electronic converters that are used in electrical AC power system of MEA are the sources of switching noises. The high frequency switching signals can penetrate to the AC power system and combine with PD signals [70].

The other sources of switching noise in MEA are inverter drives that generate Pulse

Width Modulation (PWM) voltages. PWM inverters are used to feed high power and low voltage electric motors [4, 71]. Electrical rotating machines such as generators and motors are receiving more attention in MEA. In such aircraft, generators are required to supply extra power for electric actuators, wing ice protection, braking, and engine start [1]. An electric actuator is an induction motor that converts electrical energy into torque which then moves a mechanism. Electric actuators are fed by Pulse Width Modulation (PWM) inverters which is a multi-level voltage source inverter. The use of multi-level voltage source inverters allows improvement in speed control of induction motors and voltage level control of PWM [4, 71, 72]. In an electric PWM fed actuator, overvoltage is created during polarity inversion of voltage because of impedance mismatch between the power supply and the terminals of the electric actuator. In the worst case, the overvoltage can reach two times of the rated voltage. The overvoltage will be created during switching operation of inverter. The measuring system display this transient overvoltage as a pulse signal, which is an interfering signal. The insulation system is affected by electrical stresses caused by the transient overvoltages. Although, the insulation system is prefectly designed to withstand the full phase-to-phase and phase-to-ground voltages, transient overvoltages can affect the insulation systems. Partial discharges may occur during such overvoltage whose detection can be helpful for the evaluation of the health of insulation system [71].

The type of stator winding structure used in PWM fed actuator is random-wound stator. Random-wound stators are used for machines that operate at voltages less than 1000 V and a power rating of less than a few hundreds of kW. The insulated copper conductors used for random-wound stators are magnet wires. The magnet wire insulation can be affected by partial discharges, because the insulation is organic and not resistant to PDs. The PD breaks the chemical bindings of dielectric insulation that causes erosion of the insulation material. Because of this reason, the PD increases the dielectric losses and contribute to insulation failure [48].

At ground-level atmospheric pressure, a typical PD pulse has a rise time of a few nanoseconds (2 to 5 ns) [25, 49]. Under sub-atmospheric pressures, the rise time of the PD pulse is much longer, up to hundreds of microseconds. Because of this reason, PD pulses at low pressures have lower frequency contents [37]. These PD pulses can be covered by the interfering signals from inverter that make them difficult to be detected [26, 36]. Also, traditional PD measurement is carried out at a single frequency of 50/60 Hz in atmospheric pressure which cannot give information about PD characteristics at a higher frequency in low air pressure [27, 28]. When the waveform of suppy voltage is sinusoidal, the supply voltage frequency has effects on the insulation system. So, the PD characteristics caused by insulation defects can be affected by the frequency of the supply voltage as well as the air pressure [39, 73].

Background noise is a form of external interference. The background noise with a high level of intensity can affect the measurements at a low level of air pressure. Corona signal amplitude in low air pressure is significantly lower than the one at ground-level atmospheric pressure due to the reduction in particle density and production of free electrons. The magnitude of corona pulses may decrease to a value close to the magnitude of background noise which ultimately results in overlapping of the background noise and corona discharge signals. Because of this reason, the combination of noise and corona signals forms a resultant signal with the same amplitude of corona signal that makes the detection of corona discharge difficult. In the on-line measurement, switching and background noises are the most challenging noises to tackle. Using wavelet transform techniques and digital filtering to remove noises are not sufficient because these techniques attenuate the corona signals, significantly [35]. Partial discharge (PD) detection techniques are very important for evaluation of insulation systems and materials in excessive noisy environment [45].

Figure 3.1 shows a measured noisy signal for one cycle of applied voltage. A sine wave voltage with a frequency of 1 kHz was applied to the needle-plane electrode. The measurement was carried out at a pressure of 67 kPa.

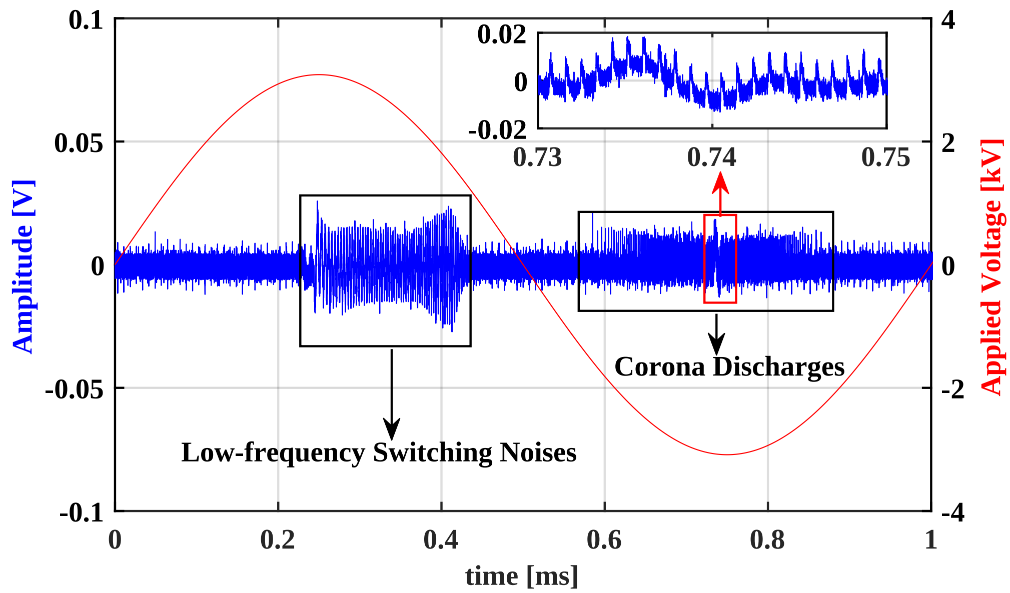

Fig. 3.1: Noisy measured PD signals under sine wave applied voltage.

As shown in Fig. 3.1, the measured signal consists of low-frequency switching noise, background noise and corona discharges. Corona discharges happen when the polarity of the sine wave voltage is negative. According to Fig. 3.1, the voltage magnitude of corona discharges is too small that makes corona detection difficult.

A wavelet-based technique is used to attenuate the continuous background noises and low-frequency voltage ripple of the measured signals. Selecting wavelet mother is a key task in the de-noising of the PD signal. It is shown that high orders of Symlet family provide good results in removing the background noises from PD signals [74, 75]. As shown in Fig. 3.2, PD signals with high-frequency switching interferences are obtained after using the wavelet technique. The voltage magnitude of corona discharge pulses as well as the frequency content is close to those of the switching pulses. Using filtering or wavelet technique to remove switching pulses will attenuate corona discharges as well. Therefore, in order to remove the effect of switching pulses and obtain PD pulses, more data analysis is required.

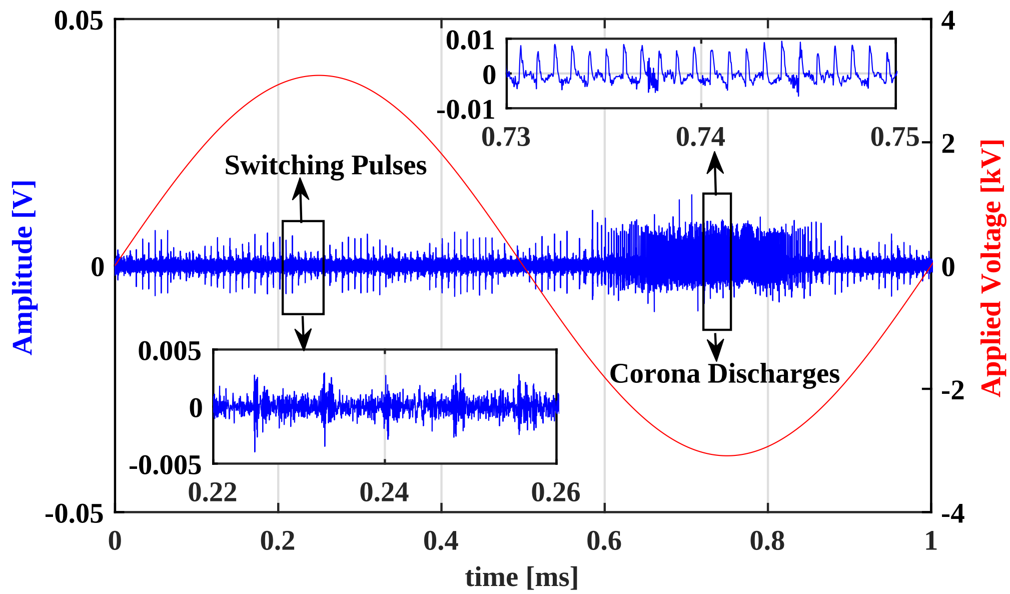

Fig. 3.2: Measured PD signals under sine wave applied voltage after using wavelet technique.

In this chapter, a new technique for on-line monitoring of PD under the low air pressure area and excessive noisy environment is presented. To evaluate the new technique, PD tests are performed on two test cells under different levels of air pressure and frequency.

3.2 Experimental Setup

The experimental setup shown in Fig. 3.3 was utilized to detect the PD pulses at different range of air pressure. The experiments were conducted on artificial defects in a high voltage laboratory. Two different artificial defects were developed to generate PD pulse signals. Each defect was simulated in a controllable pressure test cell.

As shown in Fig. 3.3, the experimental setup consists of a power source for energizing the test cells, a coupling capacitor ($C_k = 1nF$) for sensing partial discharges, a measuring

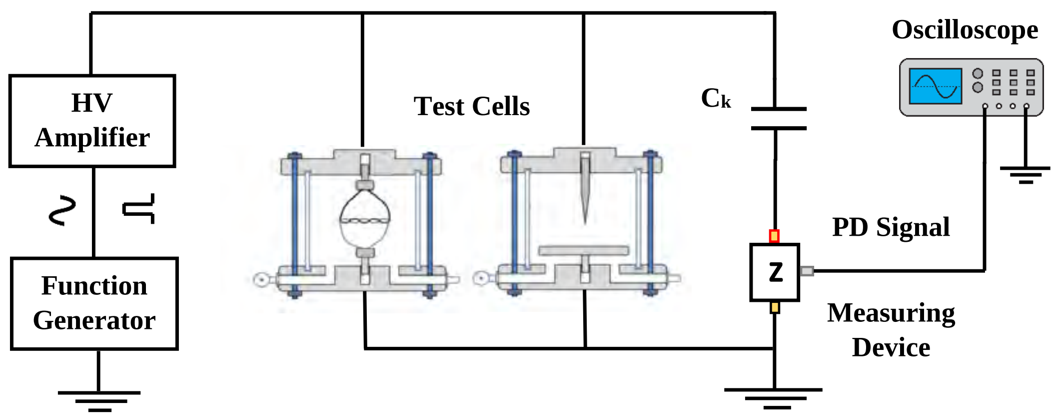

(a) Test circuit for partial discharge measurement

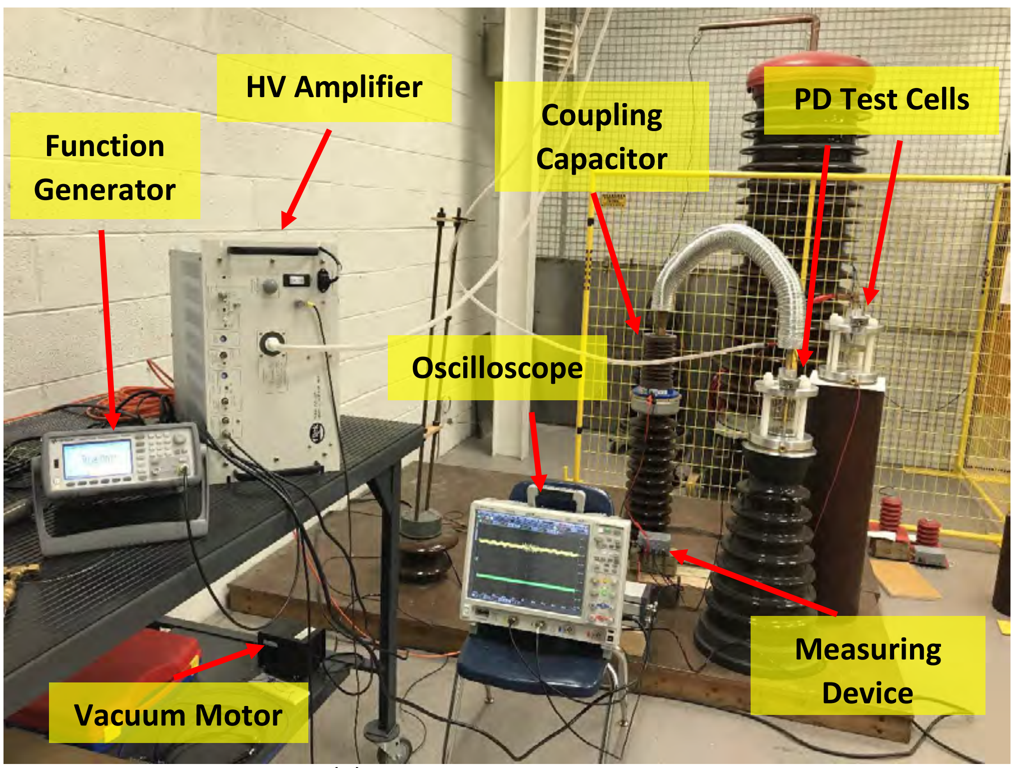

(b) Photo of the experimental setup.

Fig. 3.3: Experimental setup of two-source PDs consists of an HV source, a coupling capacitor, two PD source cells, a measuring device, and a oscilloscope.

impedance (Omicron CPL 542) for sending PDs as voltage signals to an oscilloscope for signal processing. The power source consists of a linear high-voltage power amplifier and a signal generator. The main role of the signal generator is to provide a signal at the desired frequency and voltage. The high-voltage power amplifier (TREK Model PD05034) was connected in series with the output channel of the signal generator to step up the voltage magnitude. The high voltage amplifier used in experimental setup can generate square waveform voltages with rise time or fall time of longer than 5 μs.

3.2.1 PD Test Cell Models

In this dissertation, we simulate two common insulation defects of the aircraft power system and model their corresponding PD source types in the small-scale laboratory test cells. One type of discharge is the corona discharge that occurs in the non-uniform high electric field around a sharp edge, loose wire strand, or transmission conductor in aircraft power system [76]. Another type of discharge is the partial discharge that occurs in an air gap between motor winding turns. The type of stator winding structure used in low voltage electric machines is random-wound stator. The insulated copper conductors used for random-wound stators are magnet wires. The magnet wire insulation can be affected by partial discharges because the insulation is organic and not resistant to PDs. Partial discharge may occur in the air gap between winding turns. The presence of air gap between winding turns as well as the difference in the permittivity of the air and insulation material of the wires can lead to partial discharges in the air pockets [48].

To model corona discharge and the air gap between winding turns, a needle-plane electrode and a twisted pair of magnet wires were built in the small-scale test cells as shown in Fig. 3.4.

The test cells can tolerate vacuum pressure condition. Each test cell is a round perspex glass chamber with aluminum top and base plates. We used a pressure gauge and a vacuum

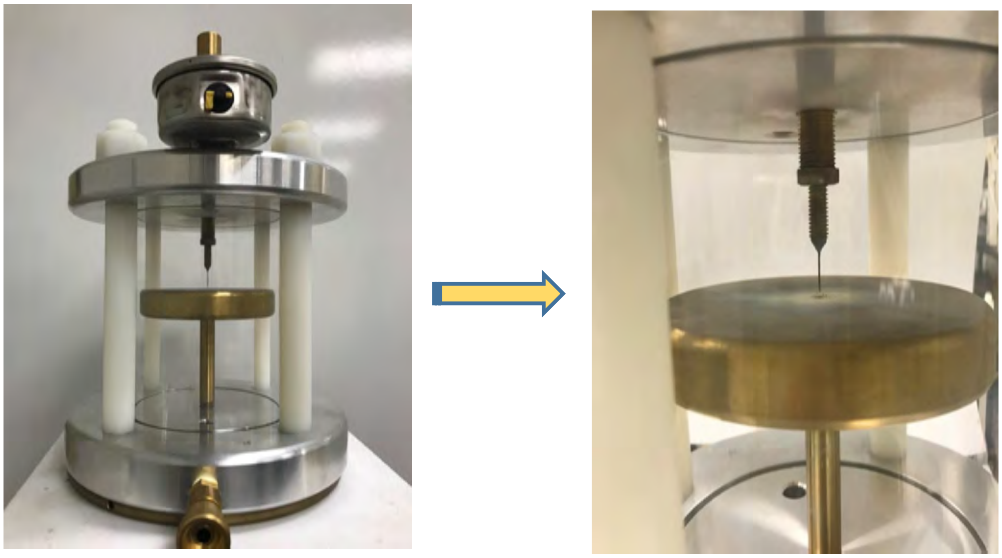

(a) Needle-plane electrode configuration

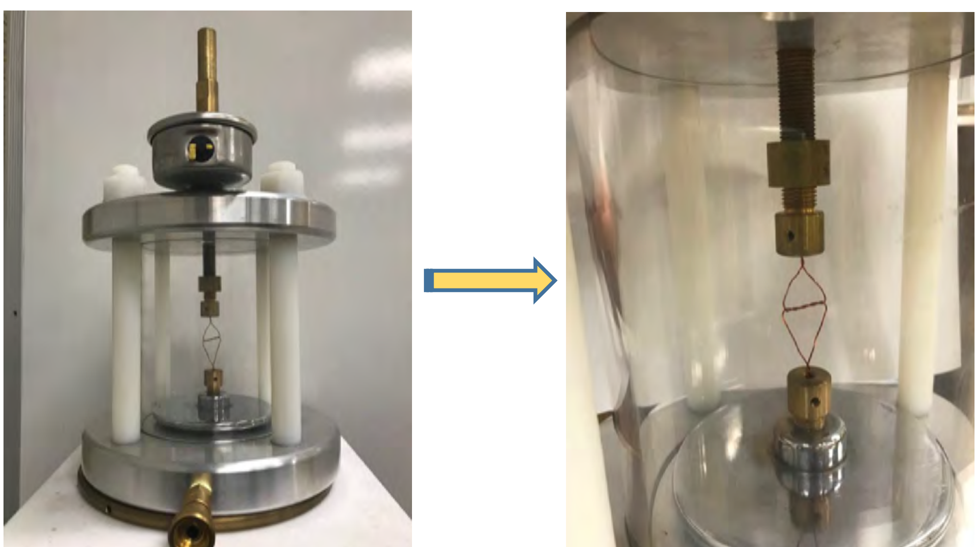

(b) Twisted-pair of magnet wires

Fig. 3.4: PD source test cell models, needle-plane electrode and twisted-pair magnet wires.

pump to adjust the air pressure in the test cells. The needle used for needle-plane electrode is made of tungsten with a tip diameter of 20 μm. The insulation type of magnet wires (NEMA MW 35-C) is made of a heavy polyester layer coated with a layer of polyamide to remove the problem of PD occurrence on the insulation surface. The magnet wires are having a wire gauge of 24 AWG and jacket diameter of 0.58 mm with a temperature rating of 200 °C. The procedure for the preparation of twisted pair sample was performed according to IEC 60851-5 standard [77]. The magnet wires were twisted three times on each other over a distance of 3 cm.

3.2.2 PD Measurement Setup

The measurement procedure and system calibration were carried out according to IEC 60270 standard [13]. The wide band detection technique in the 50 kHz to 600 kHz range as described in IEC standard was used for PD measurements. IEC standard assumes that the test objects are capacitive and the coupling capacitor detects PDs. The measuring impedance was connected between the coupling capacitor and the ground. The applied voltage and the PD signal are separated to V and PD outputs by the frequency diplexers embedded in measuring impedance device. The PD and V outputs of the measuring device were sent to the oscilloscope as voltage signals for further processing. A data acquisition system with long time duration of PD measurements and high time resolution is required for signal analyzing. Because of this, a high-speed digital oscilloscope (Agilent DSO9254A) with a bandwidth of 2.5 GHz and a sampling rate of 20 GSa/s was employed.

3.2.3 PD Test Procedure

PD measurements were carried out on each of test cells to determine their partial discharge inception voltage (PDIV). Sine and square wave voltages at different frequencies were applied to the test cells. The rise time of applied square wave voltage with a duty cycle of

50% was set to 10 μs. The air pressure inside the test cells can be decreased from 101 kPa down to 33 kPa which is approximately 30% of the sea-level pressure. The amplitude of the applied voltage was increased to 70% of the expected PDIV value and then slowly raised in step of 100 volts. Each voltage step were maintained for 30s. The reason for this long time is that the number of gas molecules and photons reduces with decreasing air pressure and thus the air needs more time to initiate photo-ionization [78]. Because of stochastic nature of PD measurments, PDIV values from repeated tests are different. To overcome the variability in the measurements, 10 PDIV tests were carried out on each of the test samples to determine the PDIV value for each test condition. Mean of the measured values is determined as a PDIV value.

After determining the PDIV of each test cell at different frequencies, the experiments were carried out on the parallel test cells. Test cells were connected in parallel to have two PD sources that can be activated, simultaneously. The sine and square wave voltages at different frequencies were applied to the parallel test cells. The applied voltage was increased to 80% of PDIV related to twisted-pair wires and PD measurement was carried out. PD measurement shows only interference noises. Then, the applied voltage was increased from 80% to 120% of PDIV related to twisted-pair wires. The applied voltage magnitude was maintained at 120% of PDIV and PD measurement was carried out. The measurement shows noises and partial discharges generated by twisted-pair wires. Then again, the applied voltage was increased to 20% higher than PDIV related to needle-plane electrode and maintained to have PD measurement. It is certain that both defects were involved in PD activity simultaneously. The measurements were recorded and transmitted to a personal computer for further analysis.

3.3 PD Detection Method

In the on-line PD measurement, the captured PD signal is weak due to the environmental noises and parasitic impedances. In addition, the amplitude of PD discharge decreases at low air pressures and PD pulses can be masked by the noise. Therefore, a technique is needed to identify the PD pulses in the measured noisy environment for further investigation.

In the PD measurement setup as shown in Fig. 3.3, the high voltage amplifier is the main source of switching noises. It operates based on high frequency switching of electronic devices. The switching frequency results in output ripple voltage and switching noises. Furthermore, the background noise level of the high voltage lab is less than 5 pC. The background noise level of HV lab was measured with a commercial device (Omicron MPD 600) used for PD measurement. The system calibration was carried out according to IEC 60270 standard [13].

Fig. 3.5 shows the measured noisy signal for one cycle of applied voltage. The bipolar square wave and sine wave voltages with a frequency of 2 kHz was applied to the test cells. The measurement was carried out under a pressure of 33 kPa. As shown in Fig. 3.5, the measured signal consists of switching noise, background noise, voltage ripple, PD pulse, and corona discharge. The switching noise is generated by polarity inversion of square waveform voltage. The PD pulses come from twisted-pair insulated conductor occur during voltage falling and rising flanks. Corona discharges happen when the polarity of the square wave voltage is negative. According to Fig. 3.5, the voltage magnitude of corona discharges is too small that makes corona detection difficult. Because of this, a new method is presented for corona discharge detection in an excessive noisy environment.

In this new detection method, a series of signal processing techniques are executed on the measured noisy signals to attenuate noise signals. A MATLAB code was developed for signal processing in terms of phase and differential energy magnitude of PD pulses with respect to the applied voltage waveform. The processing technique involves:

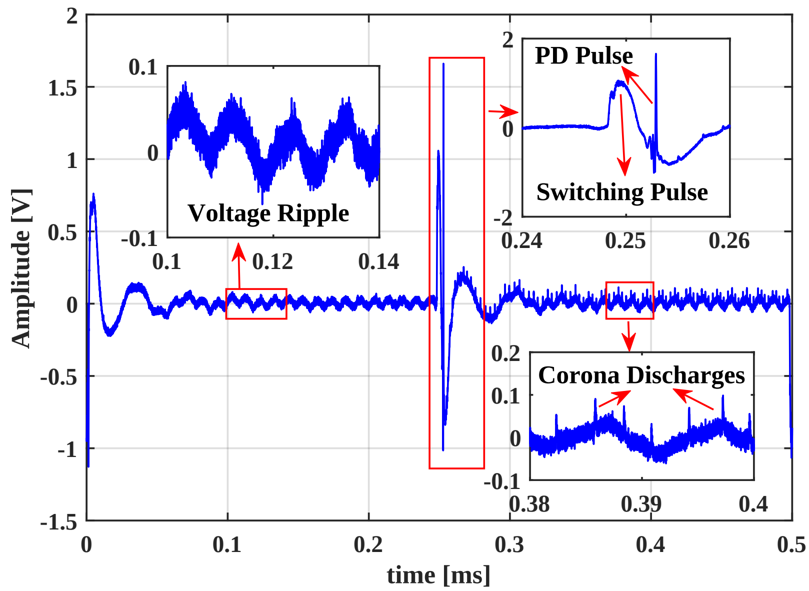

(a)

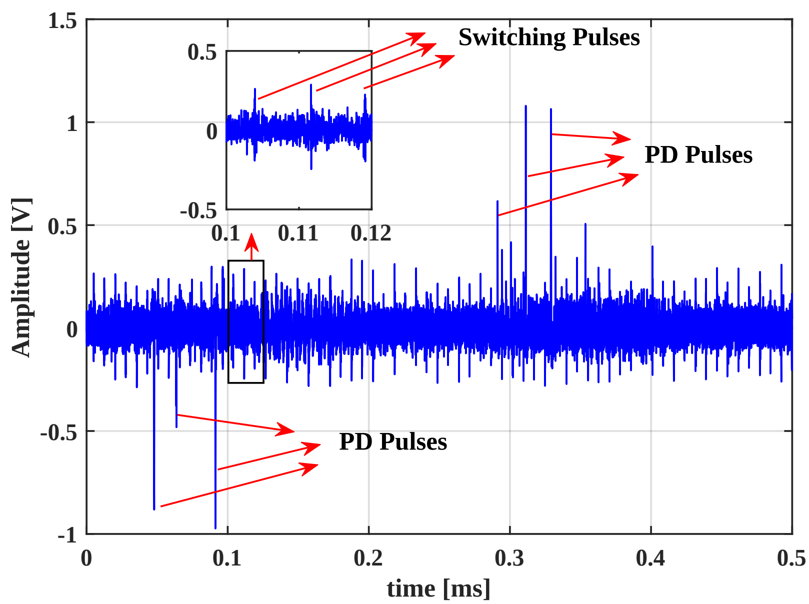

(b)

Fig. 3.5: Measured noisy signal under an applied voltage frequency of 2 kHz and air pressure level of 33 kPa, (a) bipolar square wave voltage source, (b) sine wave voltage source.

- Attenuation of the continuous background noise of measured signals

- Detection of PD pulses

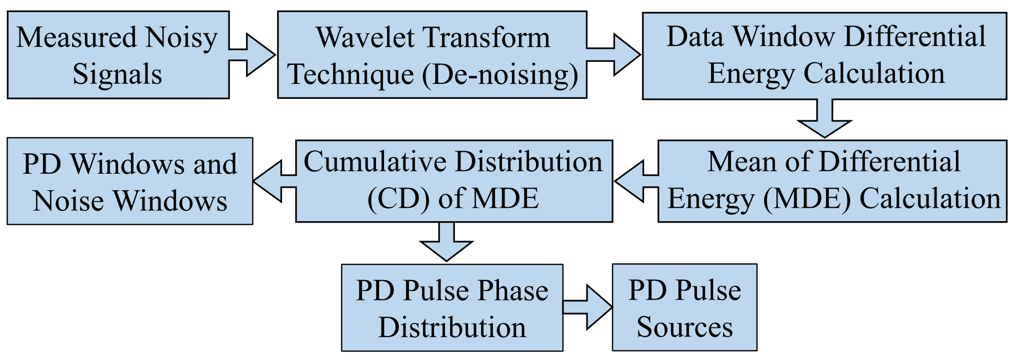

Fig. 3.6: Proposed algorithm for PD detection.

The duration of measurement recorded by oscilloscope is equal to 20 cycles of the voltage waveform. So, the total number of data windows (M) is equivalent to 20 ($M = 20$). A wavelet-based technique is used to attenuate the continuous background noises and low-frequency voltage ripple of the measured voltage signals. Wavelet transform (WT) is a powerful method for signal analyzing which has been widely used in PD pulse extraction [79, 80, 81]. Discrete wavelet transform (DWT) has been found as an efficient algorithm for pattern recognition and signal filtering. The output of this algorithm is wavelet coefficients which are derived by splitting the signal spectrum in two equal parts, a low-pass and a high-pass part. The low-pass part of the signal spectrum contains much more data compare to the high-pass part. Therefore, we split the low-pass part of the signal spectrum for constructing the next level. The number of levels is defined by user. These levels are called decomposition levels and represent a signal at various frequency ranges. In this way, we have created iterated two-band filter bank. The output of low-pass and high-pass filters at each level creates approximation coefficients and detail coefficients, respectively. These coefficients contain the signal's characteristics which can be utilized to rebuild the signal in the reconstruction process [60, 82]. The background noises contain high frequency spectrum. In order to attenuate background noises, the Symlet filter of order 9 was used in DWT algorithm and the signal was decomposed into 9 levels. On the other hand, the low-frequency voltage ripple can be obtained using Symlet filter of order 3. In order to get rid of both background noises and voltage ripple, the output signal of DWT used Symlet filter of order 9 was subtracted from the output of DWT used Symlet filter of order 3. The result of subtraction represents the PD signals polluted with switching noises. The output of this step gives PD pulses generated by twisted-pair of magnet wires, corona discharge pulses, and switching interferences. Fig. 3.7 shows the results of this step for the applied voltage of sine and square wave voltages.

As shown in Fig. 3.7, the magnitude of corona discharge pulses is still less than the switching pulses. In order to remove the effect of switching pulses, more data analysis is required. Therefore, the obtained single-cycle data windows is divided into multiple equal sub-windows. The time length of each sub-window is 2 μs which is much more than the time duration of PD pulses. Therefore, the total number of sub-windows (N) in a single-cycle data window depends on the applied voltage frequency. For example, when the applied voltage frequency is 2 kHz, the total number of sub-windows (N) in a single-cycle data window will be equivalent to 250 ($N = 250$). The energy-based technique, which is called the differential energy (DE), is used to detect sub-windows with PD pulses and then separate them from the noisy sub-windows [72]. The energy sum in the j^{th} sub-window, E_j, is calculated using

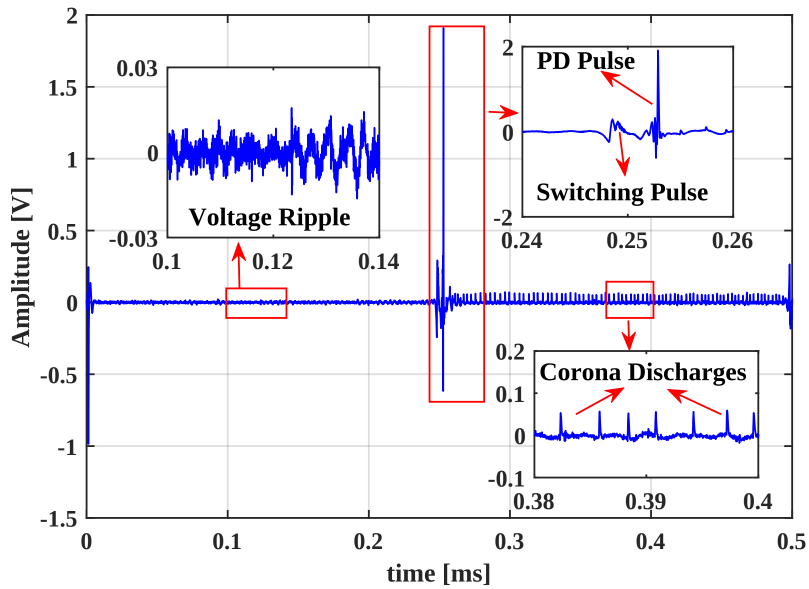

(a)

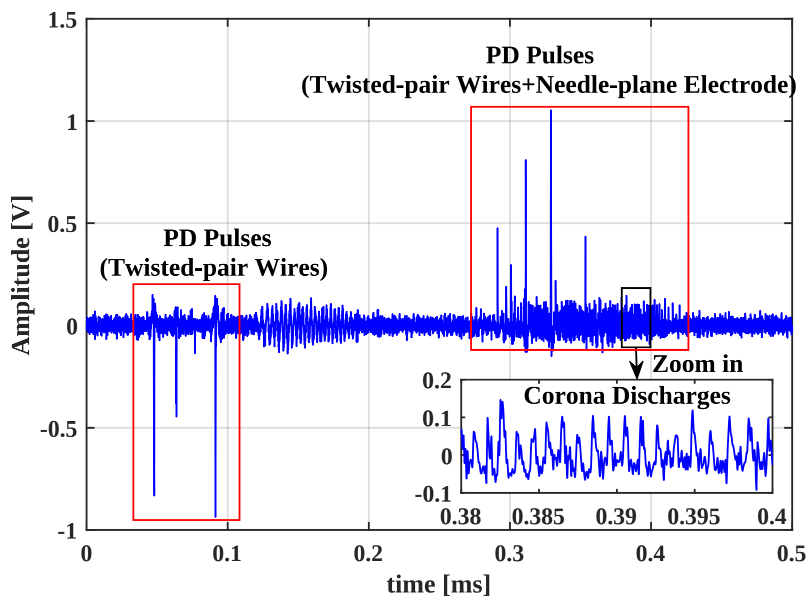

(b)

Fig. 3.7: PD signals after using wavelet transform technique, (a) bipolar square wave voltage source, (b) sine wave voltage source.

$$E_j = \sum_i k_i.(x_i)^2 \tag{3.1}$$

where x_i represents the recorded signal that are located in the j^{th} sub-window and

$$k_i = \begin{cases} +1, & \text{if } x_i \geq 0 \\ -1, & \text{if } x_i < 0 \end{cases}$$

Because of the symmetrical characteristics of low-frequency switching signals, the differential energy (E_j) of signal in a sub-window with switching signal will be very small in magnitude ($E_j \cong 0$). On the other hand, the magnitude of the differential energy (E_j) of signal in a sub-window with PD signal will be high enough to reveal PD signal phase location. Fig. 3.8 shows the phase-resolved pattern of partial discharge differential energy caused by two simultaneously activated sources (twisted-pair of magnet wires and needle-plane electrode) for the applied voltage of sine and square wave voltages.

Within each $2\pi/N$-wide phase window, there are M different values corresponding to E_j . The mean of M values is calculated for each of the $2\pi/N$-wide phase windows that creates a distribution of N values in 2π phase angle window as given by

$$E_w = \frac{\sum_{j=1}^{M} E_{j,w}}{M} \tag{3.2}$$

where

$$w = 1, ..., N$$

E_w is the mean of differential energy (MDE) values in the corresponding phase window (w), and $E_{j,w}$ is the differential energy of a signal (E_j) in the corresponding phase window (w). These N values are assigned as MDE in reference to phase angle. The phase-resolved pattern of MDE values caused by two simultaneously activated sources (twisted-pair of

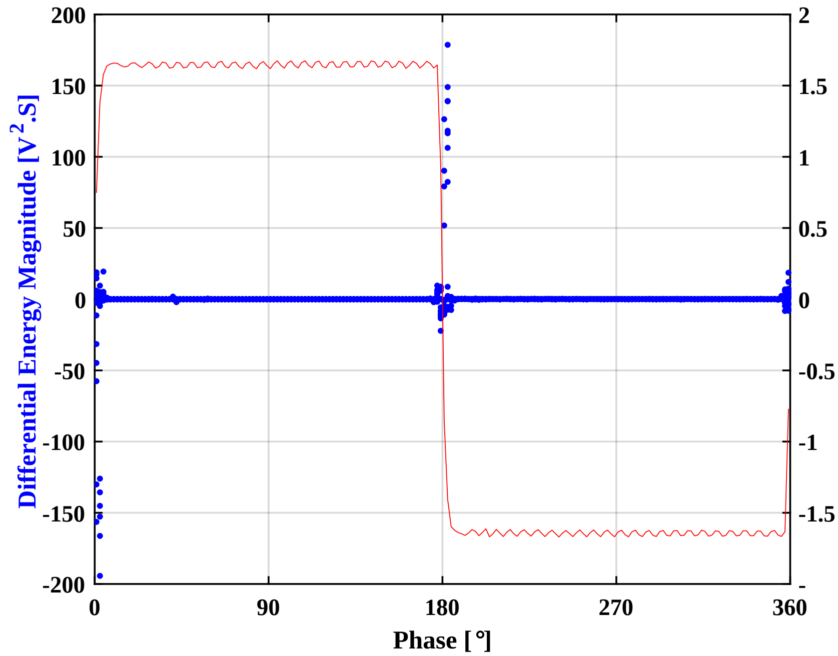

(a)

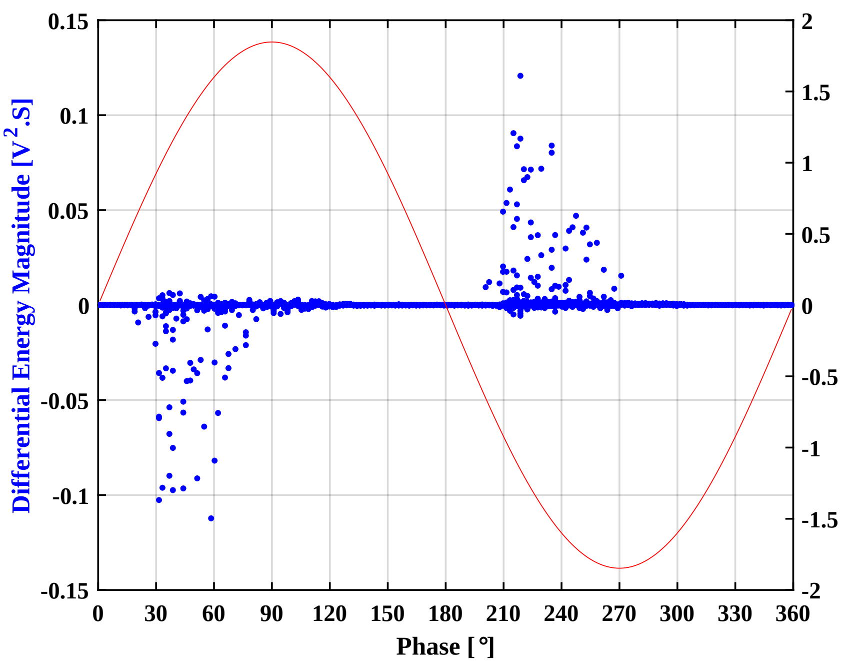

(b)

Fig. 3.8: Differential energy (DE) pattern of PD signal in reference to the phase angle, (a) bipolar square wave voltage source, (b) sine wave voltage source.

magnet wires and needle-plane electrode) for both applied voltage of sine and square wave voltages are shown in Fig. 3.9.

The expanding phase window calculates the sum of all data values as phase windows progresses according to 3.3. For example, within phase window 1, within phase window 1 and 2 together, within phase window 1, 2, and 3 together, and so on. Therefore, the expanding phase window calculation gives the cumulative distribution (CD) of MDE values over a 2π phase angle window.

$$CD_n = \sum_{w=1}^{n} E_w \text{ ; } n \leq N \tag{3.3}$$

where n is the phase window number.

Figure 3.10 shows the cumulative distribution (CD) of MDE values ($CDMDE$) caused by two simultaneously activated sources (twisted-pair of magnet wires and needle-plane electrode) in reference to the phase angle which is called the phase-resolved cumulative distribution (PRCD) pattern. The PRCD pattern is an automatic approach for PD detection under low air pressure. It can be seen that PRCD starts to rise/fall where PD pulses occur. On the other hand, the value of PRCD is constant where there is no PD pulse. In other words, the gradient of the PRCD shows the occurrence phase angle of PDs. According to Fig. 3.10a, the gradient of $CDMDE$ with respect to the phase angle at negative half cycle of the square wave voltage is $10/\pi$ $[V^2.s/rad]$ that confirms the occurrence of corona discharges. Figure 3.10b shows that PDs occur in both positive and negative half cycles because the $CDMDE$ drops to -0.022 $[V^2.s]$ and then rises up to 0.01 $[V^2.s]$ in negative and positive half cycles, respectively.

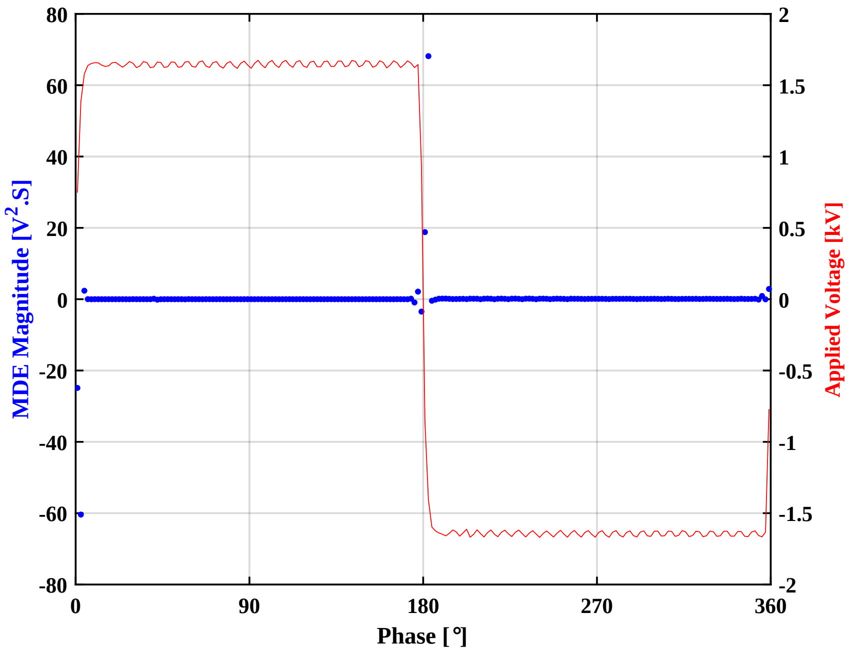

(a)

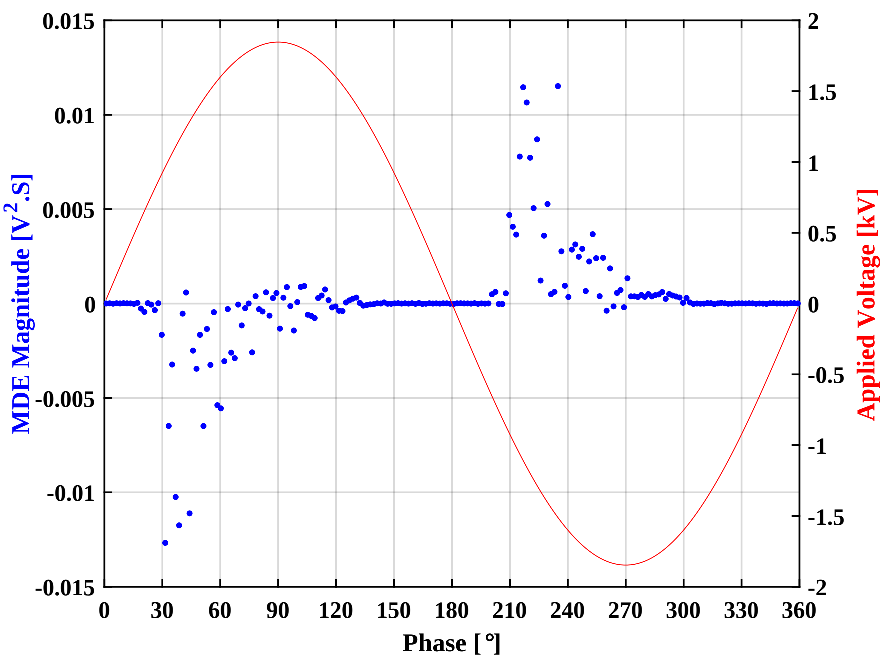

(b)

Fig. 3.9: Mean of differential energy (MDE) values in reference to the phase angle, (a) bipolar square wave voltage source, (b) sine wave voltage source.

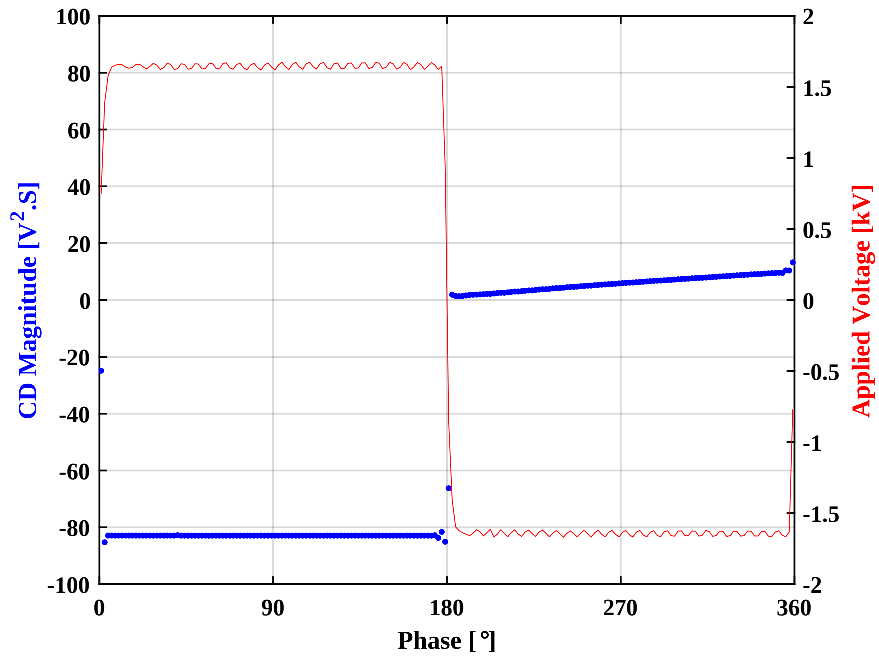

(a) Bipolar Square Wave Voltage Source.

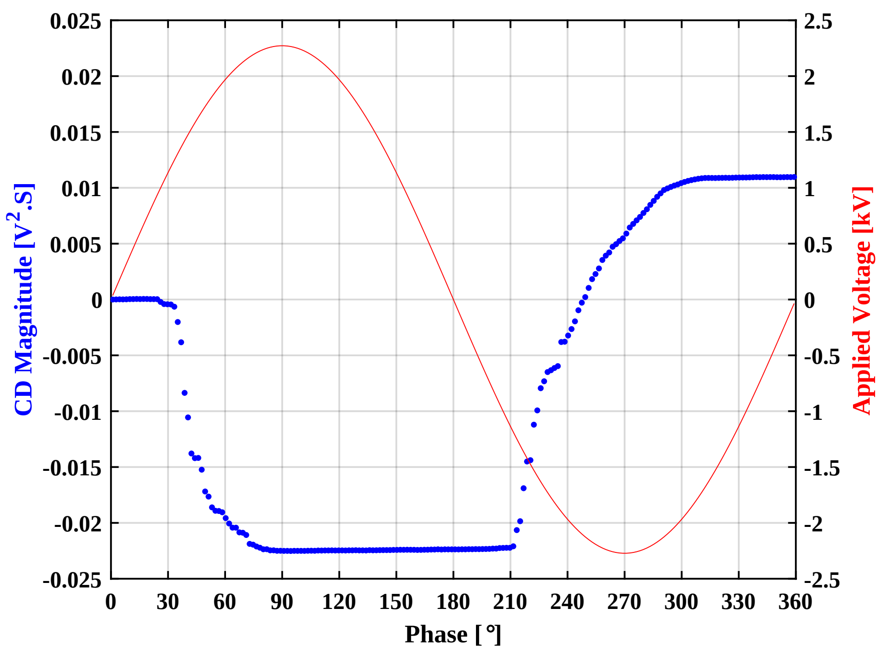

(b) Sine Wave Voltage Source.

Fig. 3.10: Cumulative distribution pattern of MDE values ($CDMDE$) in reference to the phase angle, (a) bipolar square wave voltage source, (b) sine wave voltage source.

3.4 Influence of Pressure and Frequency on PDIV

In this section, the PD experiments on each of the test cells at different air pressure levels and frequencies were performed in the HV laboratory, individually. To determine the partial discharge inception voltage (PDIV), the detection method explained in the previous section was used. The amplitude of the applied voltage was increased to 70% of the expected PDIV value and then the voltage amplitude was raised in steps of 100 volts (V). When the phase-resolved cumulative distribution pattern start to show changes, the related applied voltage was considered as the PDIV. The rate of rise of applied voltage amplitude should decrease with reducing the air pressure because the number of gas molecules and photons are reduced. Therefore, gas needs much more time to initiate ionization at lower air pressure [78]. Because of this reason, under 101, 67, and 33 (kPa), each voltage step is maintained for 3, 10 and 30 (s), respectively.

As mentioned earlier, 10 measurement tests were carried out on each test sample to determine the PDIV value. It is worth mentioning that the first obtained PDIV was larger for each measurement. The reason for this observation is that the first discharge generate more free electrons in the air gap. Therefore, electron avalanches occur easily and the PDIV decreases for the next PDIV measurement. To avoid this, the entire air in the test cell was changed before each measurement. The mean of the measured values is determined as the PDIV.

The PDIV as a function of frequency under the three different air pressure levels for needle-plane electrode and twisted-pair of insulated magnet wires were shown in Fig. 3.11. The applied voltage was an AC excitation voltage with a variable frequency. The air gap length for the needle-plane electrode was 3 mm. The reason for the PDIV measurement of needle-plane electrode up to 2 kHz is due to the maximum current limitation of HV amplifier. It can be seen that both the frequency and the air pressure have a significant effect on the PDIV values.

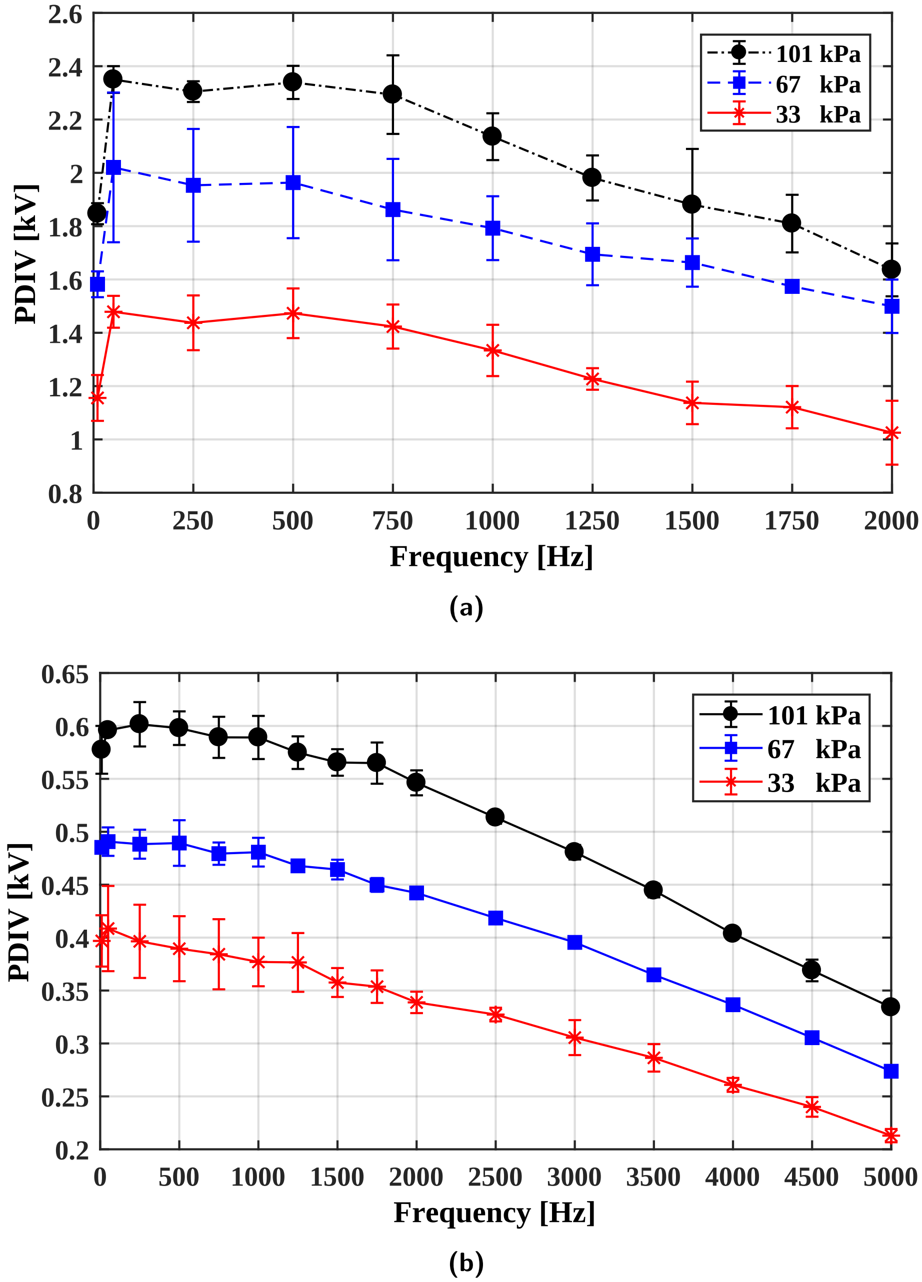

Fig. 3.11: PDIV as a function of frequency and pressure under applied sine wave voltage for (a) needle-plane electrode, and (b) twisted-pair magnet wires.

As shown in Fig. 3.11, the PDIV for sine wave voltage decreases with increasing frequency and increases with air pressure. The rationale for this trend is that the density of air molecules increases as the air pressure is raised. As a result, the probability of an electron collision with other gas particles increases as it travels in the direction of the anode. Because of dissipation of energy at each collision, a higher applied electric field intensity or a higher applied voltage is needed to supply electrons with kinetic energy necessary for ionization via collision to initiate electron avalanches [12, 14, 16].

It can be seen that the PDIV for a twisted pair of insulated wires is much lower than the needle-plane electrode. Under an applied frequency of 500 Hz, when the air pressure drops from 101 to 33 kPa, the PDIV for the needle-plane electrode and twisted-pair of magnet wires configuration decreases from 2.3 and 0.6 kV to 1.5 and 0.39 kV, respectively. This reduction in PDIV indicates that the gap distance of energized conductors and the insulation type of conductors used in the electric machines must be considered in the design of MEA equipment under operating conditions.

There are two factors that affect the discharge mechanism and its dependence on the frequency. The first factor is the effective discharge time which is the time that PDs are active during one cycle of the applied voltage. When the needle has a negative polarity and the applied voltage is still lower than the inception voltage, the positive ions are accumulated around the tip of the electrode. Increasing the applied voltage frequency causes the positive ions to have less time to dissipate due to lower drift velocity compared to electrons. This accumulation of positive ions around the needle tip enhances the external applied voltage in the ionization region. The second factor is the number of positive ions accumulated in the vicinity of the tip of the electrode during the negative half cycle, which increases with an increase of the frequency. With increasing the frequency, the contribution of these two factors to the external electric field leads to a lower applied voltage or a lower electric field intensity sufficient to initiate electron avalanches. This explanation can be used for the reduction in PDIV of twisted-pair of magnet wires with an increase of the frequency because of the non-uniform electric field in the air gap between turns [41].

Figure 3.12 shows the PDIV measurements for twisted pair of insulated wires under an applied voltage of bipolar square waveform. It can be observed that the PDIV decreases when the air pressure increases. However, the frequency does not have any significant influence on the PDIV when the applied voltage is a square waveform.

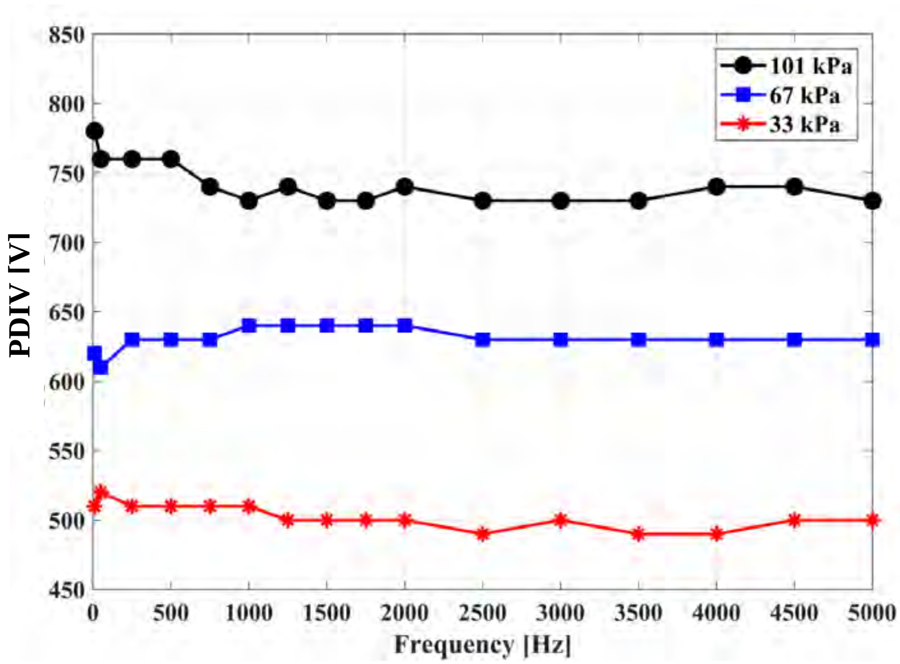

Fig. 3.12: PDIV for the twisted-pair magnet wires under square waveform voltage.

3.5 Accuracy of Estimation

In previous sections, the reported PDIV was calculated as the average of 10 measurements. In order to evaluate the accuracy of the estimated PDIV, the bootstrap method is used.

Bootstrapping is a resampling technique used to derive estimates of confidence intervals around the measured PDIV values [83, 84]. This technique allows the estimation of the sampling distribution using a random sampling method. The simplest implementation of the bootstrap method involves taking the original data set of PDIV values (10 measured values in our research) and take random samples to create a new data set which is called the bootstrap sample. The size of the bootstrap sample is the same as the original data set. This process is repeated many times (1000 times in this research). For each of these bootstrap samples we compute its mean which is called the bootstrap estimates. We now can create a histogram of bootstrap means. This histogram provides an estimate of the shape of the distribution of the sample mean that shows how the mean varies across the samples.

Tables 3.1 and 3.2 show the 90% confidence interval around the PDIV measured values under an AC applied voltage for the needle-plane electrode and the twisted-pair of magnet wires, respectively. As shown in these tables, the mean of PDIV values for all conditions are in the confidence intervals obtained from bootstrapping method. Thus, the calculated PDIV shown in Figures 3.11a and 3.11b are within the 90% confidence interval.

Table 3.1: Confidence intervals of the measured PDIV values in kilovolts (kV) under an AC applied voltage for the needle-plane electrode using bootstrap method.

Frequency [Hz]	90% Confidence Interval [kV]		
	101 kPa	67 kPa	33 kPa
10	1.81 - 1.87	1.55 - 1.61	1.11 - 1.23
50	2.30 - 2.37	1.84 - 2.22	1.45 - 1.54
250	2.27 - 2.33	1.81 - 2.09	1.40 - 1.52
500	2.28 - 2.36	1.81 - 2.08	1.39 - 1.50
750	2.15 - 2.36	1.75 - 2.03	1.36 - 1.46
1000	2.08 - 2.19	1.69 - 1.85	1.27 - 1.38
1250	1.94 - 2.05	1.60 - 1.76	1.22 - 1.27
1500	1.78 - 2.07	1.59 - 1.72	1.11 - 1.21
1750	1.74 - 1.88	1.56 - 1.57	1.10 - 1.19
2000	1.57 - 1.71	1.40 - 1.54	0.97 - 1.09

Table 3.2: Confidence intervals of the measured PDIV values in kilovolts (kV) under AC applied voltage for the twisted-pair of magnet wires using bootstrap method.

Frequency [Hz]	90% Confidence Interval [kV]		
	101 kPa	67 kPa	33 kPa
10	0.56 - 0.59	0.48 - 0.49	0.38 - 0.41
500	0.58 - 0.60	0.48 - 0.51	0.37 - 0.46
1000	0.57 - 0.60	0.47 - 0.48	0.36 - 0.39
1500	0.55 - 0.57	0.45 - 0.47	0.35 - 0.37
2000	0.53 - 0.55	0.439 - 0.444	0.33 - 0.34
2500	0.50 - 0.52	0.41 - 0.42	0.32 - 0.33
3000	0.47 - 0.48	0.392 - 0.398	0.30 - 0.32
3500	0.44 - 0.45	0.361 - 0.366	0.28 - 0.30
4000	0.40 - 0.41	0.33 - 0.34	0.257 - 0.266
4500	0.36 - 0.37	0.304 - 0.306	0.235 - 0.247
5000	0.331 - 0.336	0.272 - 0.274	0.209 - 0.217

Figure 3.13, for example, shows the probability density estimate of bootstrap distribution of the sample means for the needle-plane electrode under the air pressure of 33 kPa and frequency of 1 kHz. It can be seen that the 90% probability of PDIV is between applied voltage of 1.27 and 1.38 kV. A similar plot for the twisted pair of magnet wires is shown in Fig. 3.14 where the 90% probability falls between 0.36 and 0.39 kV.

3.6 Summary

The PD detection procedure was described in this chapter. A technique was proposed to detect discharge pulses under low air pressure and excessive noisy environment that can be implemented for on-line condition monitoring of the insulation system in the aircraft electrical system. This method is based on the combination of the wavelet and differential energy techniques. The phased-resolved cumulative distribution pattern of PD pulses can give the inception voltage and also the phase location of PD occurrence. The absolute value of the gradient of CD magnitude revealed the phase duration that PDs were activated in one cycle of the applied voltage. The non-zero value of gradient shows PD phase occurrence.

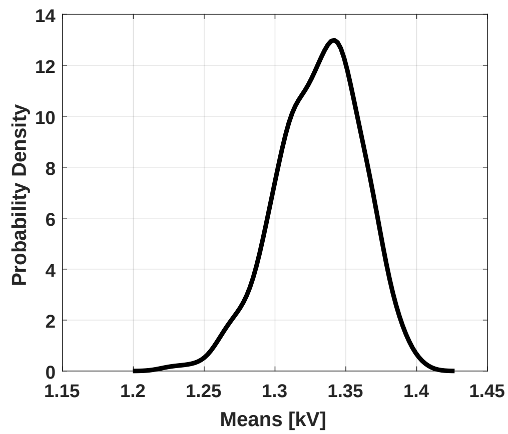

Fig. 3.13: The probability density of the sample means for the needle-plane electrode under air pressure of 33 kPa and applied voltage frequency of 1 kHz.

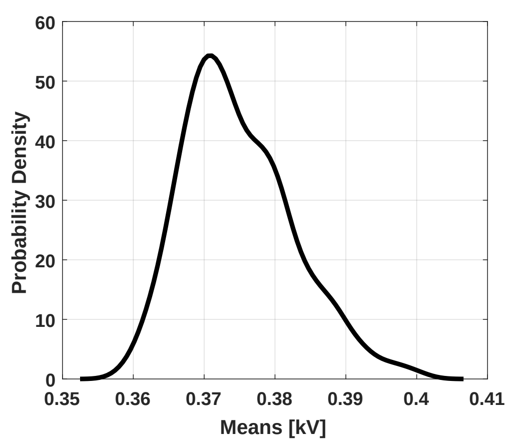

Fig. 3.14: The probability density of the sample means for the twisted-pair of magnet wires under air pressure of 33 kPa and applied voltage frequency of 1 kHz.

The influence of air pressure and applied voltage frequency on PDIV was investigated in this chapter. The results show that the air pressure and frequency have significant effects on the PDIV when the applied voltage is sinusoidal. The PDIV increases with air pressure but decreases with frequency. When the applied voltage is a square waveform, the air pressure has significant effect on PDIV, however the frequency of applied voltage has no influence. In order to evaluate the accuracy of PDIV estimation, the bootstrapping method was used. The bootstrapping technique was shown that the reported PDIV are within the 90% confidence interval.

Chapter 4

Phased-Resolved Cumulative Distribution Pattern of PD Signals

In this chapter, the performance of proposed PD detection method is examined upon different measured noisy signals. The phase-resolved patterns of cumulative distribution of measured PD signal differential energy are studied to identify the extent of PD occurrence. The PD measurements are carried out at different air pressure levels and frequencies. The air pressure levels are 33, 67, and 101 kPa. Sine and bipolar square waveforms are used as the applied voltage to experimental test cells. The sinusoidal applied voltage frequencies used for experiments are 500 Hz and 1 kHz. The reason for choosing these frequencies is that the output frequency of an aircraft generator varies from 360 to 900 Hz [70]. The square wave applied voltage used for experiments are 2 and 5 kHz. The multi-level voltage source inverters are used to feed the electric actuators. The frequency of output voltage of inverters has to be high enough to have a constant speed for electric actuators. Because of the maximum current limitation of high voltage (HV) amplifier, the maximum frequency used for experiments was 5 kHz. When the power supply frequency increases to more than 5 kHz, the current that must be supplied by the HV amplifier exceeds the limit value that results in operation of protection devices and then tripping of the system.

The experiment procedure and system calibration are carried out according to IEC 60270 standard [13]. In all experiments, the applied voltage for the PD measurement was set to 20% higher than PDIV value under a predetermined frequency and air pressure. The PD signals are recorded with an oscilloscope for further processing. The PD measurement and signal processing were carried out based on the detection method explained in Section 3.3.

4.1 Single Source PD Pattern

In this section, the Phased-Resolved Cumulative Distribution (PRCD) pattern of each electrode configuration as a single PD source is investigated. The configurations used for experiments are a needle-plane electrode and a twisted-pair of insulated wires.

4.1.1 Needle-to-Plane Electrode

A needle-plane electrode is mounted in a chamber with a gap length of 3 mm to investigate corona discharges. The test circuit components are the same as those shown in Fig. 3.4 while the test cell of twisted-pair of magnet wires is disconnected from the measurement setup and the needle-plane electrode was the only PD source for generating PD pulses.

The experimental results for the needle-plane electrode configuration under both AC and square-wave voltages are shown in Fig. 4.1 to Fig. 4.4. The relevant DE patterns have been shown in Appendix A. Figure 4.1 shows the results of corona discharge pulses acquisition in Mean of Differential Energy (MDE) pattern in reference to the phase angle at three levels of air pressure when the frequency of applied voltage is 1 kHz. The sinusoidal waveform voltage was used as the applied voltage. It can be seen that the shapes of the phased-resolved MDE pattern changes with air pressure. At pressure levels of 101 and 67 kPa, the MDE patterns are similar to wave-like and triangle patterns, respectively. At a low air pressure level of 33 kPa, MDE pattern is similar to the so-called rabbit-ear pattern [85].

PRCD pattern of corona discharge signals caused by needle-plane electrode is shown in Fig. 4.2. The PRCD gives the occurrence phase angle of partial discharges under AC applied voltage when the voltage frequency is 1 kHz. It can be observed that PDs occur at negative half cycle of the applied voltage and the negative corona discharges start at a phase of 210°. The reason is that the positive ions accumulated in the vicinity of needle tip curvature create an internal electric field which enhances the external electric field. This results in higher electric field intensity that is sufficiently strong for electron avalanches to be initiated. It can be seen that the CD magnitude increases by reducing air pressure level that demonstrates an increase in PD activities at high altitude.

Fig. 4.3 shows the Mean of Differential Energy (MDE) pattern of corona discharge signals in reference to the phase angle at three levels of air pressure when the frequency of applied voltage is 2 kHz. A bipolar square wave voltage was used as an applied voltage. It can be observed that the phased-resolved MDE pattern changes with air pressure. The PD activity in the negative half cycle increases when the air pressure is reduced. However, the magnitude of discharge voltage decreases because of particle density. Lower pressure leads to lower particle density and less electrons can be produced. Because of this, lower discharge current will be produced that causes to have lower voltages.

As shown in Fig. 4.3, the dispersion of MDE values related to corona discharges under an air pressure level of 33 kPa is low in comparison with others. At lower air pressure, the number of oxygen molecules is low that causes ions to have less frequent collisions with neutral molecules and move faster. Therefor, the discharge pulse period decreases while the number of discharge pulses and pulse duration increase [32].

The PRCD pattern of corona discharge signals is shown in Fig. 4.4 under three levels of air pressure. It can be observed that the CD magnitude starts to rise where PD pulses

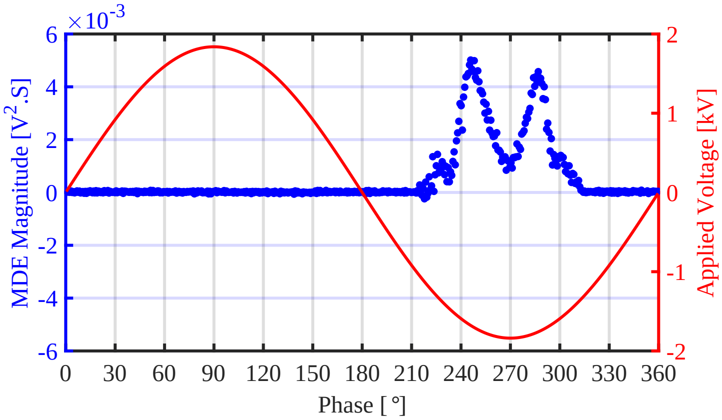

(a)

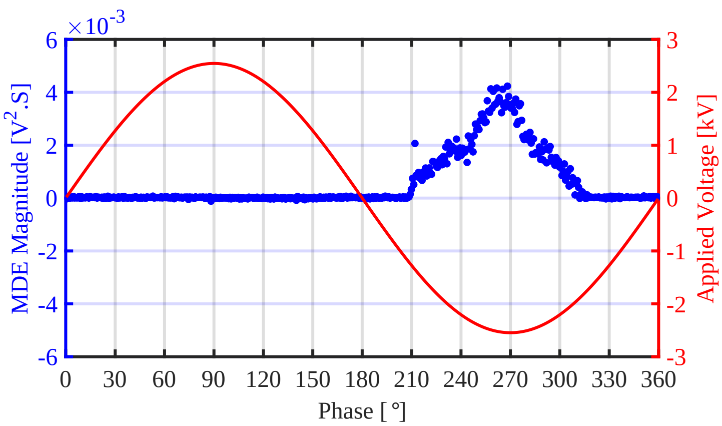

(b)

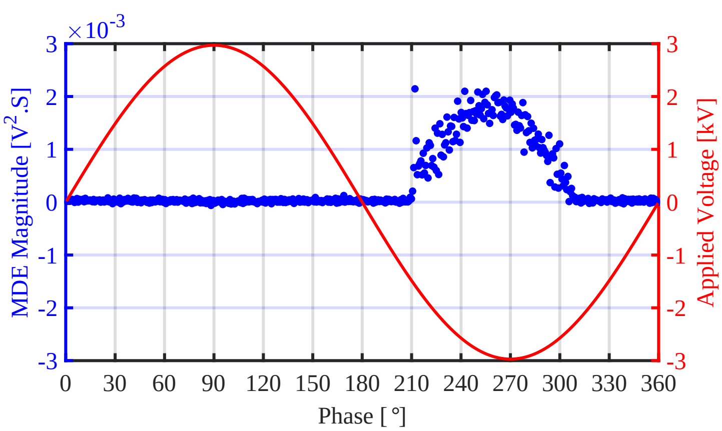

(c)

Fig. 4.1: MDE patterns for needle-to-plane corona discharges under AC voltage frequency of 1 kHz and air pressure level of (a) 33 kPa, (b) 67 kPa, and (c) 101 kPa.

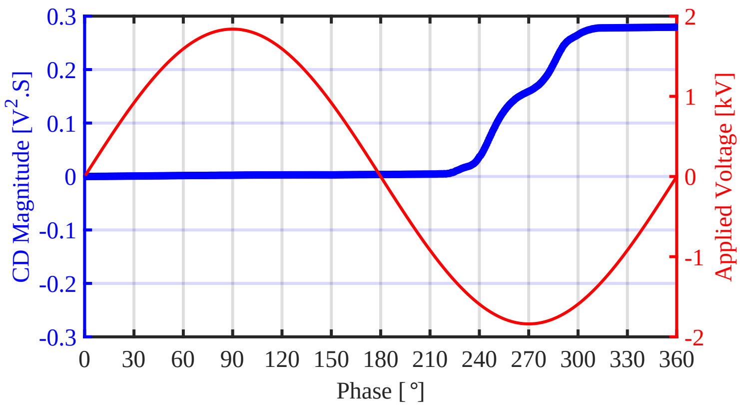

(a)

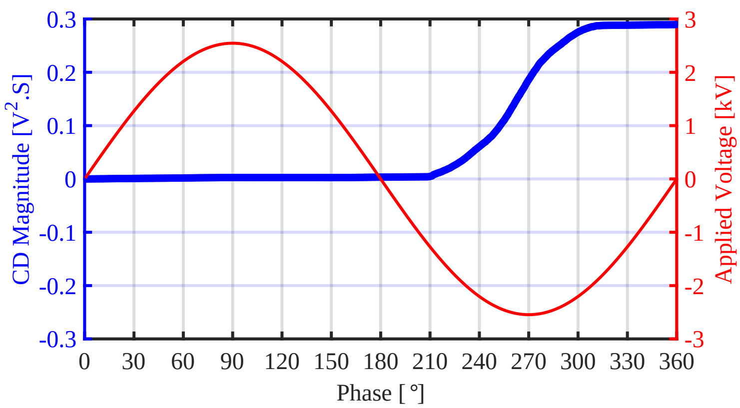

(b)

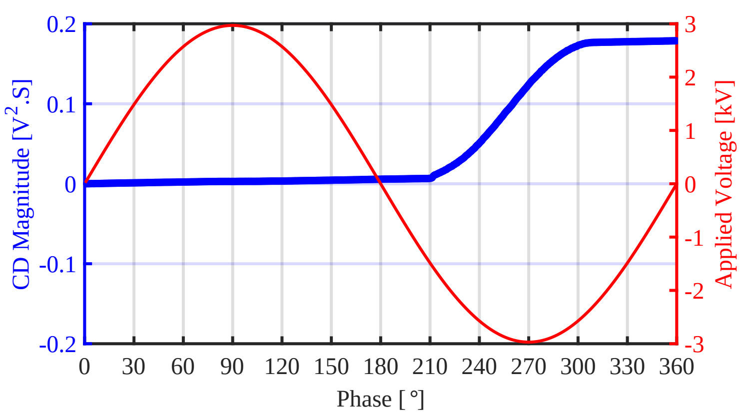

(c)

Fig. 4.2: PRCD patterns for needle-to-plane corona discharges under AC voltage frequency of 1 kHz and air pressure level of (a) 33 kPa, (b) 67 kPa, and (c) 101 kPa.

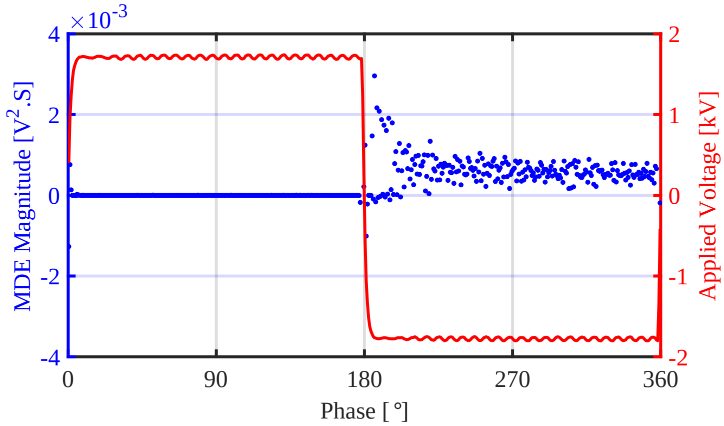

(a)

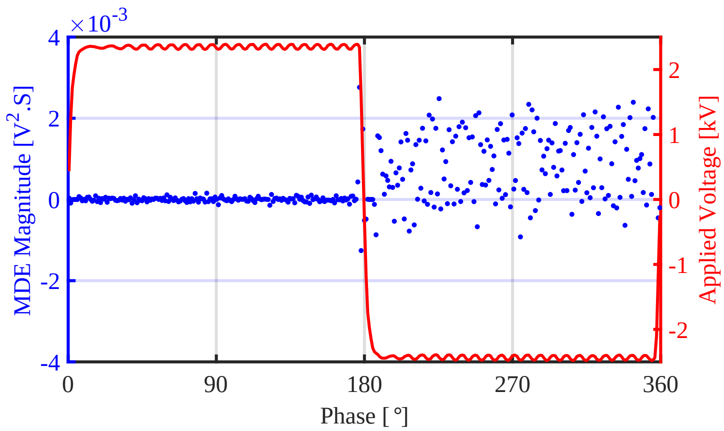

(b)

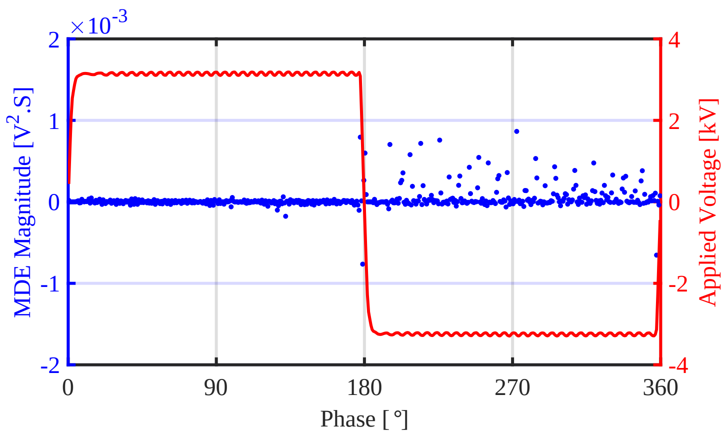

(c)

Fig. 4.3: MDE patterns for needle-to-plane corona discharges under square wave voltage frequency of 2 kHz and air pressure level of (a) 33 kPa, (b) 67 kPa, and (c) 101 kPa.

occur. On the other hand, the value of CD magnitude is constant where there is no PD pulse. According to Fig. 4.4, the PD activity increases when the air pressure is reduced. The reason is that the gradient of CD magnitude under 33 and 67 kPa air pressures are higher than that under 101 kPa air pressure. The results of the PRCD pattern indicate that the needle-to-plane corona discharges have an asymmetrical pattern with an increase only on one half side of the applied voltage.

According to Fig. 4.3, Fig. 4.4, and the related DE patterns shown in Fig. A.2, Trichel pulses caused by corona were observed in the negative half cycle of the applied voltage [33, 86]. However, under an air pressure level of 33 kPa, the amplitude of the first PD pulse after polarity reversal is much higher than the rest of pulses. This is due to the stronger avalanche ionization at lower air pressure. According to Boltzmann equation, the ionization coefficient depend on the electric field (E), and the air pressure (P). This coefficient can be measured as a function of E/P [87]. The electric field is a function of applied voltage. In our study, the amplitude of applied voltage for the experiment under an air pressure level of 33 kPa was 60% of that under the atmospheric pressure. Therefore, the ionization coefficient increases by reducing the air pressure that results in stronger avalanche ionization. Due to this, the total charge of electrons and positive ions is larger which results in a much higher amplitude.

Therefore, at high altitude, the occurrence rate of negative PDs is high enough to be considered in MEA under both AC and square-wave voltages. Also, the CD magnitude increases by reducing air pressure which demonstrates an increase in PD activities at high altitude.

4.1.2 Twisted-Pair of Insulated Wires

A twisted-pair of magnet wires is mounted in a chamber to investigate partial discharges occur between winding turns of electric motors. The test circuit components are the same as

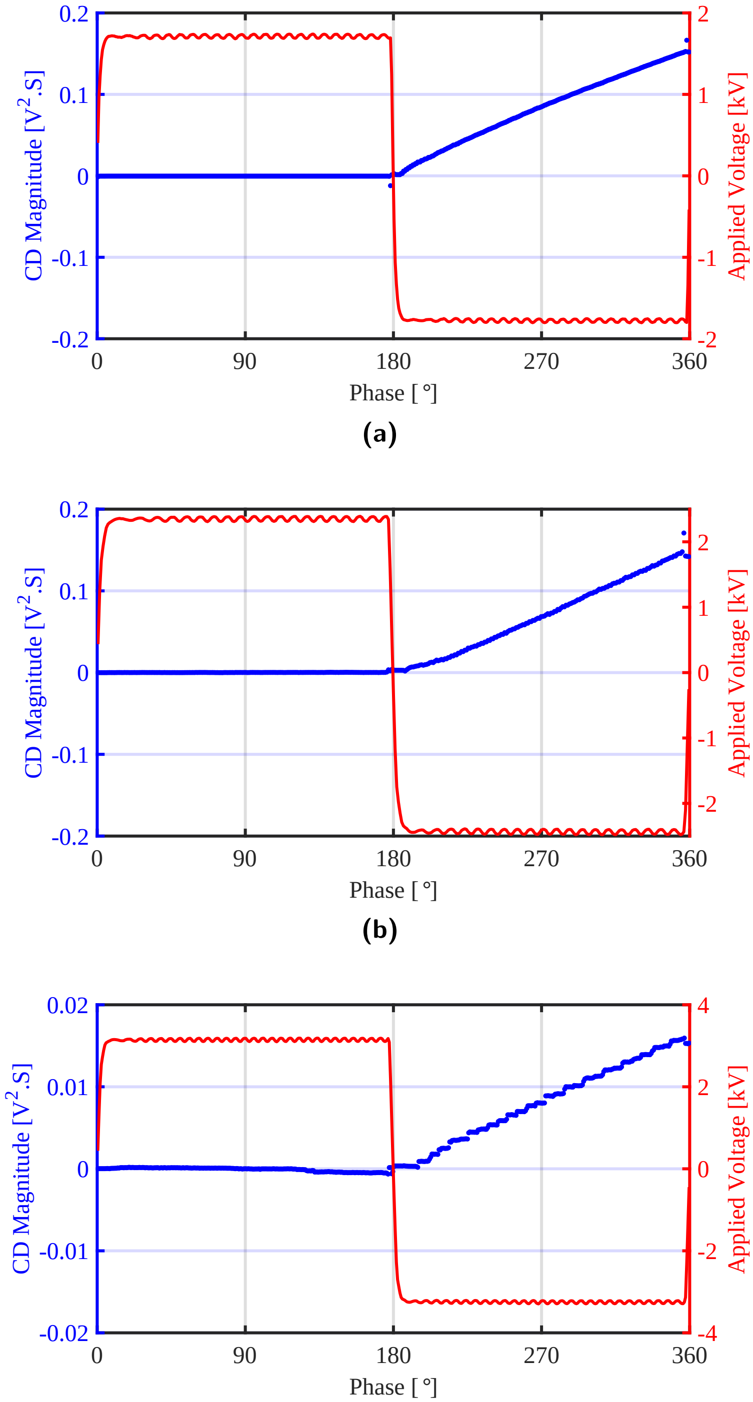

(a)

(b)

(c)

Fig. 4.4: PRCD patterns for needle-to-plane corona discharges under square wave voltage frequency of 2 kHz and air pressure level of (a) 33 kPa, (b) 67 kPa, and (c) 101 kPa.

those shown in Fig. 3.4 while the chamber containing needle-plane electrode is disconnected from the measurement setup. The twisted-pair of magnet wires is the only PD source for generating PD pulses.

The experimental results for the configuration of twisted-pair of magnet wires under both AC and square-wave voltages are shown in Fig. 4.5 to Fig. 4.8. The relevant DE patterns are shown in Appendix A. As shown in Fig. 4.5, and Fig. 4.6, the partial discharges occur on both negative and positive half cycles of the applied voltage. It can be seen that the shapes of the MDE pattern in both half cycles of the applied voltage are the same. The CD magnitude falls abruptly in the positive half cycle when the PDs start ignition and then rises to a value close to zero in the negative half cycle. The results show that the cumulative distribution of the MDE values in both positive and negative half cycles are almost the same. Therefore, the PRCD pattern of a twisted-pair of insulated wire is symmetric.

The results shown in Fig. 4.7 and Fig. 4.8 indicate that the PRCD pattern of PDs generated by the twisted-pair of magnet wires under square wave applied voltage is symmetrical as well. The PD pulses occur during the polarity inverse of the applied voltage at all pressure levels. However, under air pressure level of 33 kPa, the first PD pulse is much higher than the rest of the pulses.

4.2 Multi-source PD Pattern

Detection and identification of multiple simultaneously activated partial discharges occur in the power system of an aircraft is a challenge at high altitude and in a noisy environment. In order to activate the PD sources simultaneously, the twisted pair of magnet wires is connected in parallel with the needle-plane electrode as shown in Fig. 3.3. The measurements are carried out at different air pressure levels. Sinusoidal and square waveform voltages are applied. The frequency of sine and square wave applied voltages are 500 Hz and 5 kHz,

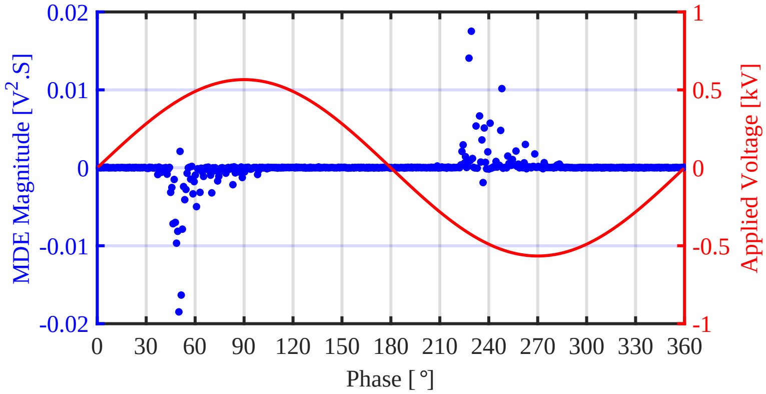

(a)

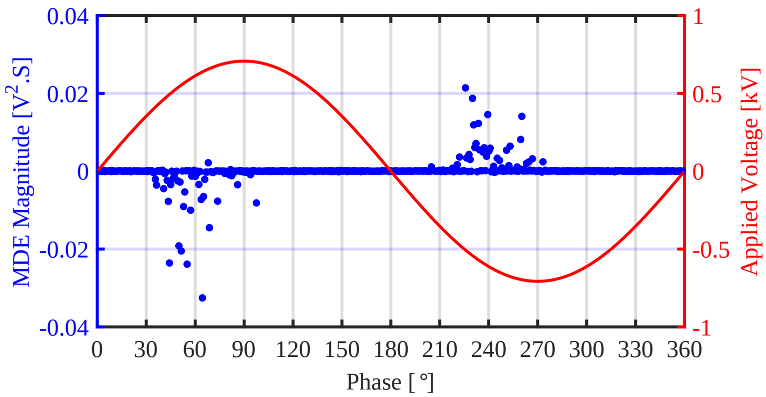

(b)

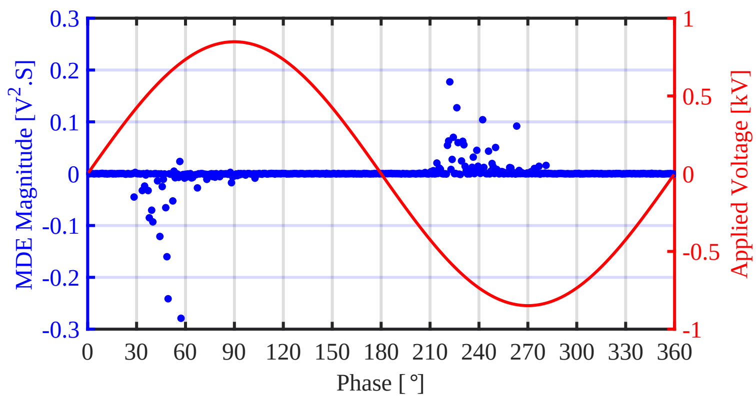

(c)

Fig. 4.5: MDE patterns caused by twisted-pair of magnet wires under AC voltage frequency of 1 kHz and air pressure level of (a) 33 kPa, (b) 67 kPa, and (c) 101 kPa.

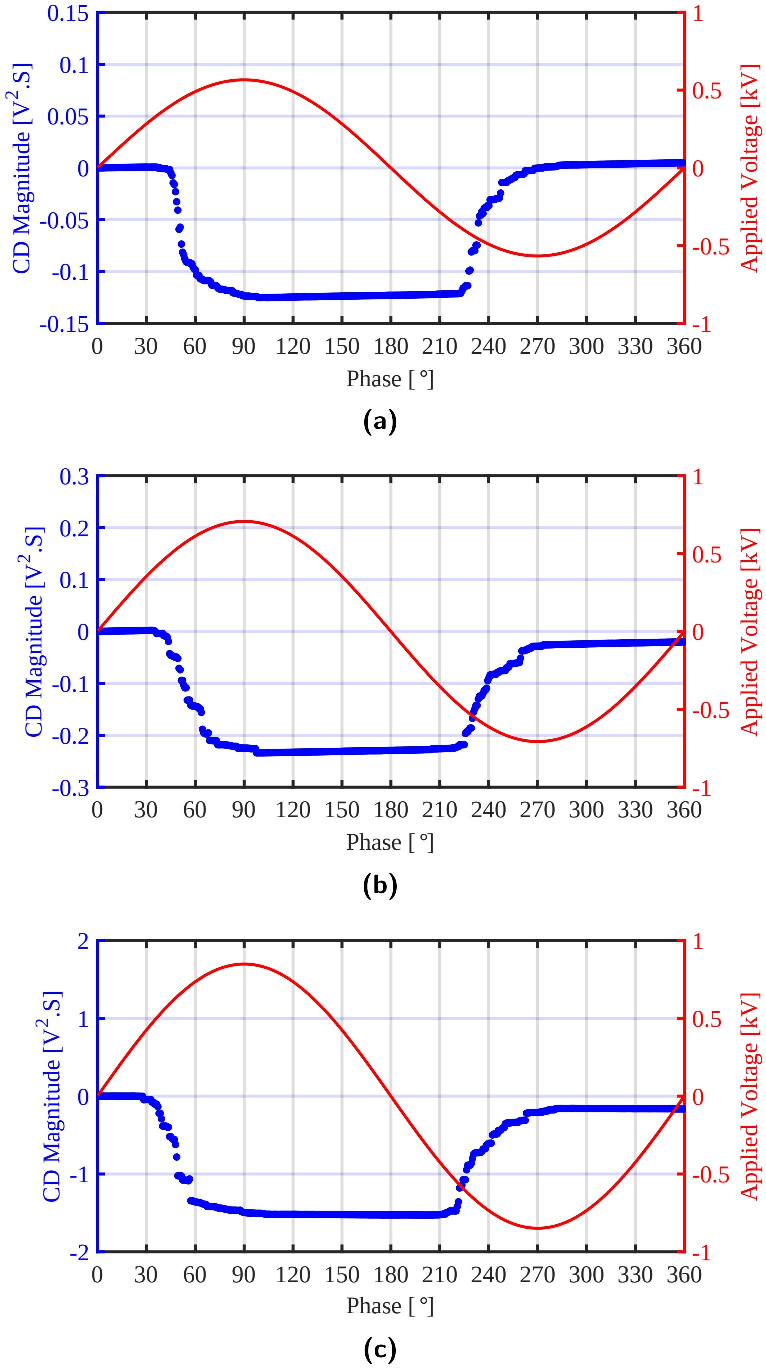

Fig. 4.6: PRCD patterns caused by twisted-pair of insulated wires under AC voltage frequency of 1 kHz and air pressure level of (a) 33 kPa, (b) 67 kPa, and (c) 101 kPa.

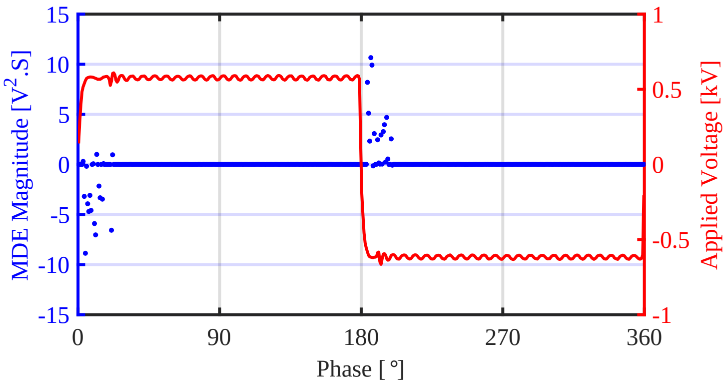

(a)

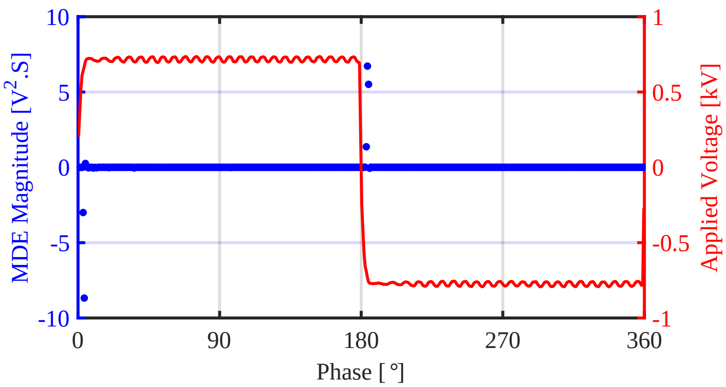

(b)

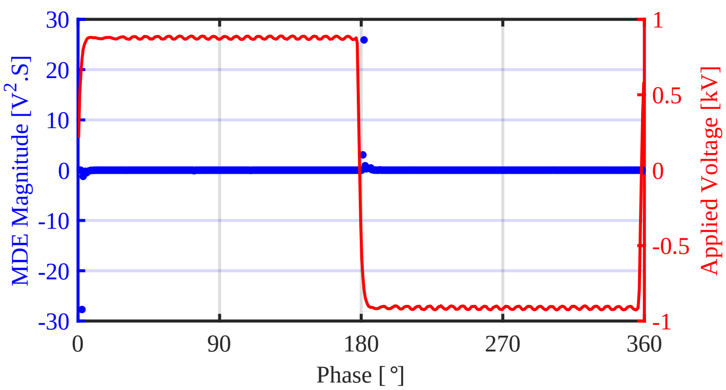

(c)

Fig. 4.7: MDE patterns caused by twisted-pair of magnet wires under square wave voltage frequency of 2 kHz and air pressure level of (a) 33 kPa, (b) 67 kPa, and (c) 101 kPa.

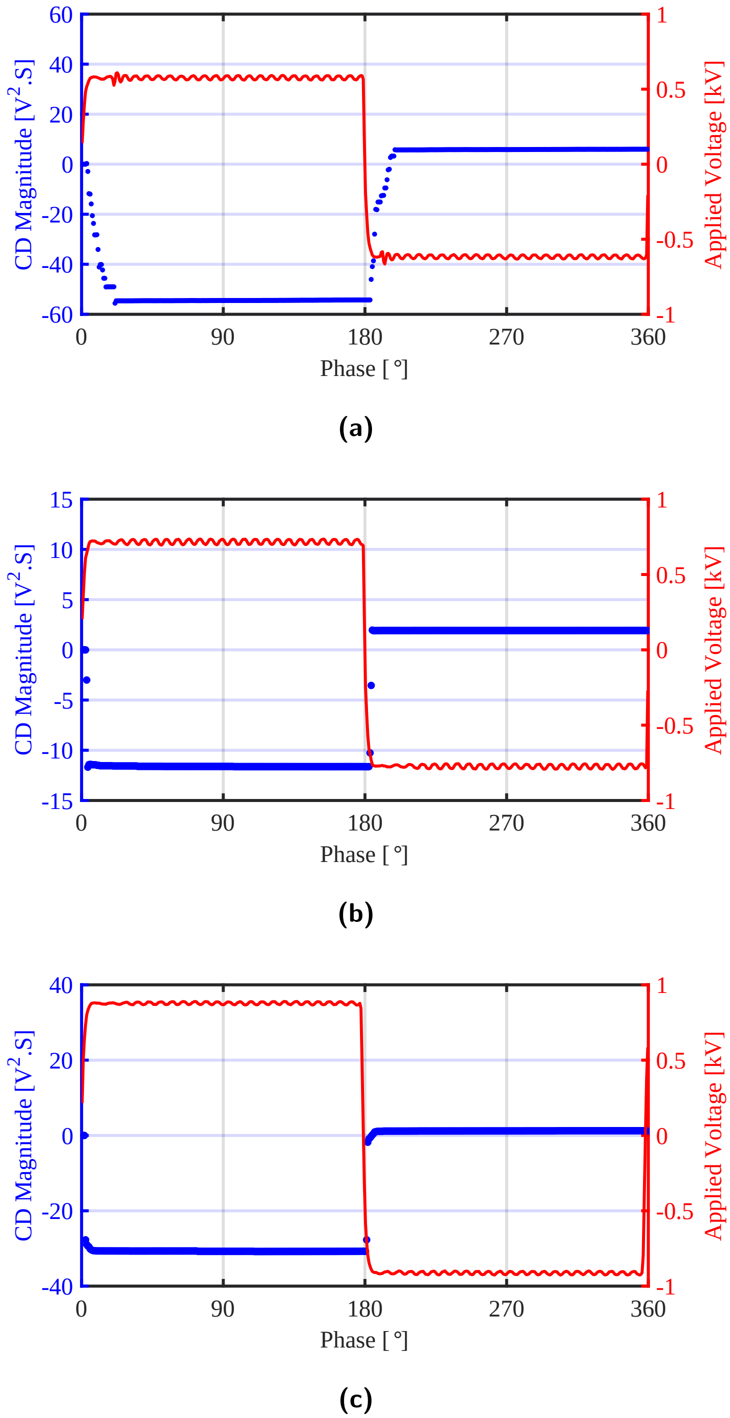

Fig. 4.8: PRCD patterns caused by twisted-pair of insulated wires under square wave voltage frequency of 2 kHz and air pressure level of (a) 33 kPa, (b) 67 kPa, and (c) 101 kPa.

respectively.

As shown in Fig. 3.11, the PDIV values of the twisted-pair magnet wires are less than the needle-plane electrode at different pressures and frequencies. Because of this, PD measurements were carried out in three steps as follows:

- The amplitude of the applied voltage is increased to 70% of the PDIV of the twisted-pair magnet wires. At this step, there is no PD to measure.
- The amplitude of the applied voltage is increased from 70% to 120% of the PDIV of the twisted-pair magnet wires. At this step, one of the PD sources which is the twisted-pair magnet wires will be activated. The measurement results have PDs generated only by the twisted-pair of magnet wires.
- The amplitude of the applied voltage is increased from 120% of PDIV of the twisted-pair magnet wires to 120% of PDIV of the needle-plane electrode. At this step, the PDs are generated by both the twisted-pair of magnet wires and needle-plane electrode. The measurement shows PDs come from both PD sources.

After each step, the measured signals are sent to a personal computer for further processing and obtaining the PRCD patterns.

4.2.1 PRCD Pattern under AC Voltage

An AC voltage with a frequency of 500 Hz is applied at the combination of the test cells. As mentioned before, the applied voltage is increased to 70% of PDIV of the twisted-pair magnet wires and then PD measurement is carried out. Fig. 4.9 shows the PRCD pattern which is related to the first step of PD measurement under an air pressure level of 101 kPa. It can be seen that the CD magnitude is constantly zero during the phase angle. The reason is that the noisy measured signal is without any PDs. Similar figures were observed for the first step of PD measurement under 33 and 67 kPa of the air pressure.

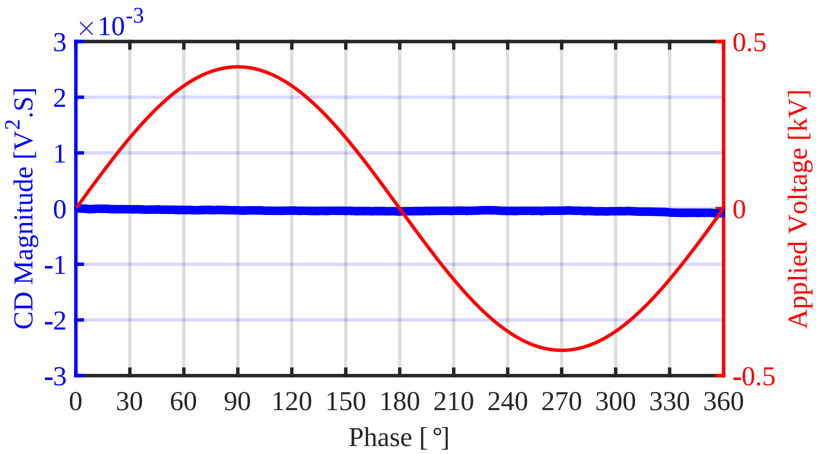

Fig. 4.9: PRCD pattern under pressure level of 101 kPa when there is no PD (first step of the measurement).

In the next step, the applied voltage is increased to 120% of PDIV of the twisted-pair magnet wires. The twisted-pair of magnet wires as a PD source is activated while the needle-plane electrode is not. The measurement contains PD pulses that come from the activated source of PD. The PRCD patterns of the second step of PD measurement are shown in Fig. 4.10. The relevant DE and MDE patterns are shown in Appendix A.

As shown in Fig. 4.10, the CD magnitude abruptly falls and then rises to a value close to zero. The PRCD pattern reveals that the PD pulses generated by a twisted-pair of magnet wires occur at both positive and negative cycles of the applied voltage and also the corresponding MDE pattern is symmetrical. Because of the symmetrical MDE pattern, the cumulative distribution of MDE in both positive and negative half cycles are equal. Therefore, the starting and ending points of CD magnitude plot are close to each other when the twisted-pair of magnet wires is activated as a PD source.

By increasing the applied voltage to 120% of PDIV of the needle-plane electrode, the corona discharges created by needle-plane electrode appear and the measurement consists of two types of PD pulses that are activated, simultaneously. Fig 4.11 shows the PRCD

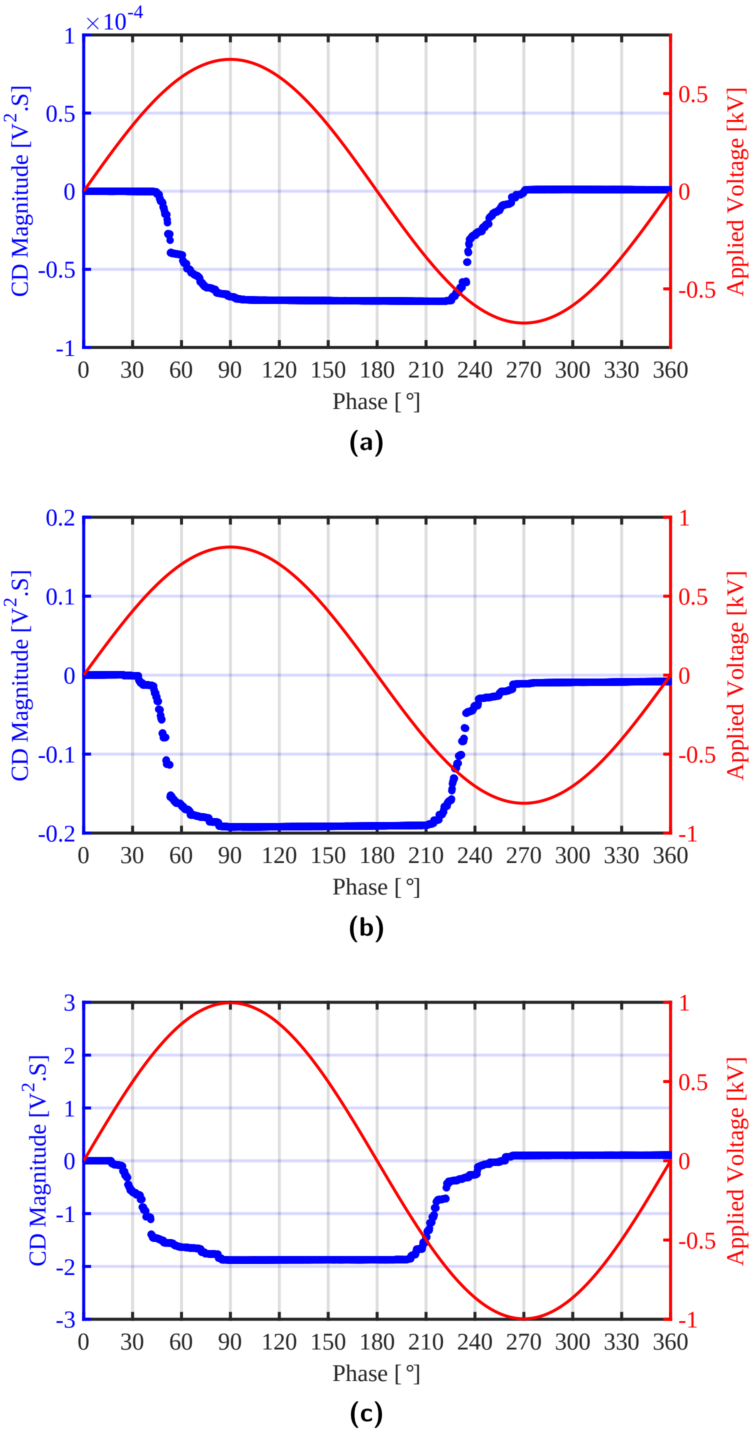

Fig. 4.10: PRCD patterns of twisted-pair magnet as an activated PD source under air pressure level of (a) 33 kPa, (b) 67 kPa, and (c) 101 kPa.

patterns of the third step of PD measurements in which both of PD sources were activated, simultaneously. It can be seen that the changes in CD magnitude at negative half cycle is more than that in the positive half cycle. It reveals that the corona discharges occur at negative half cycle of the applied voltage. The reason is that the Phase-Resolved Partial Discharge (PRPD) pattern for twisted-pair insulated wires is symmetrical. However, the PRPD pattern for needle-plane electrode is asymmetrical.

4.2.2 PRCD Pattern under Bipolar Square Wave Voltage

A bipolar square wave voltage with a frequency of 5 kHz is applied to the combination of the test cells. The test procedure is the same as in the case of the AC voltage. The applied voltage is increased to 70% of PDIV of the twisted-pair magnet wires and then the PD measurement is carried out. Fig. 4.12 shows PRCD pattern which is related to the first step of PD measurement under air pressure level of 33 kPa. It can be seen that the CD magnitude changes very slightly during the polarity reversal of the square wave voltage. This type of change is caused by switching noises which is insignificant. Therefore, the CD magnitude changes very slightly that is negligible when there is no PD activity. The same figures are observed for the first step of PD measurement under 67 and 101 kPa of air pressure.

In the next step, when the applied voltage is increased to 120% of PDIV of the twisted-pair magnet wires. The twisted-pair of magnet wires is activated as a PD source while the needle-plane electrode is not. The measurement contains PD pulses that come from the activated source. The PRCD patterns of the second step of PD measurement are shown in Fig. 4.13. The relevant DE and MDE patterns are shown in Appendix A.

As shown in Fig. 4.13, the CD magnitude abruptly falls and then rises to a value close to zero. The PD pulses that come from the twisted-pair insulated wires occur during the voltage falling and rising edge of the applied voltage for the air pressure levels of 67 and

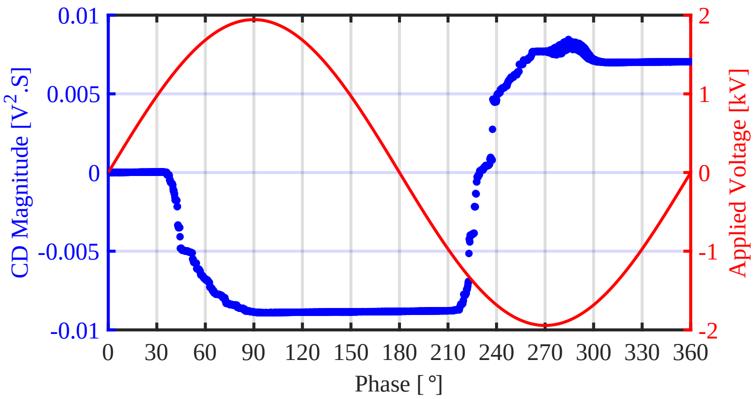

(a)

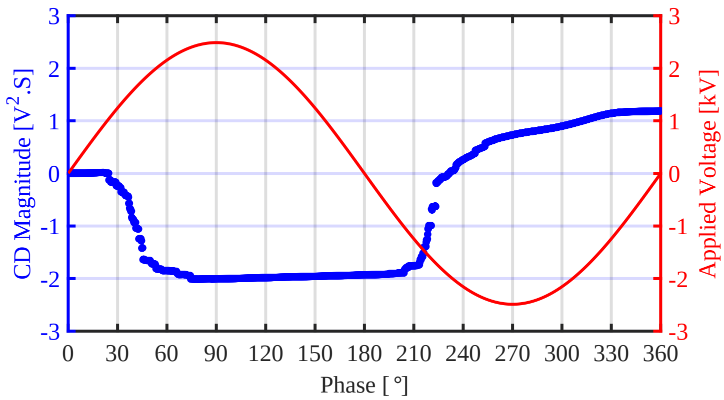

(b)

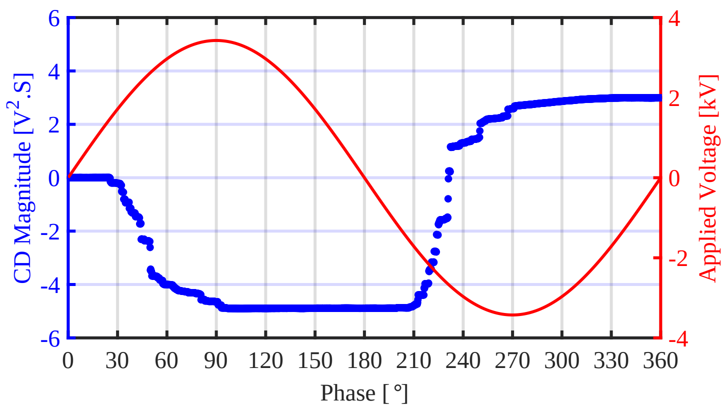

(c)

Fig. 4.11: PRCD patterns of two activated PD sources under air pressure level of (a) 33 kPa, (b) 67 kPa, and (c) 101 kPa.

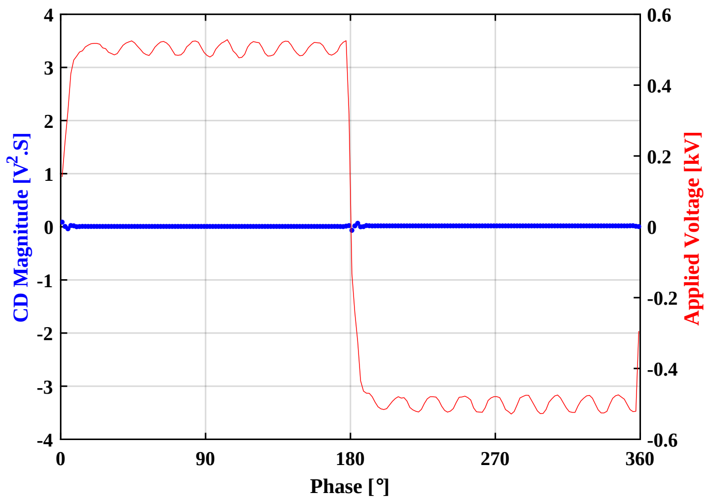

Fig. 4.12: PRCD pattern under pressure level of 33 kPa when there is no PD (first step of the measurement).

101 kPa. However, CD magnitude changes after polarity reversal of the applied voltage. Same as the case of AC voltage, PD pulses generated by a twisted-pair of magnet wires occur at both positive and negative cycles of the applied voltage. Because of the symmetrical characteristic of the MDE pattern, the cumulative distribution of MDE in both positive and negative half cycles are equal. Therefore, the starting and ending points of CD magnitude plot are close to each other when the twisted-pair of magnet wires is activated as a PD source.

Fig 4.14 shows PRCD patterns of the third step of PD measurements. It can be seen that the PD pattern changes from symmetrical to asymmetrical by increasing the applied voltage to higher than the PDIV value of the needle-plane electrode.

When the applied voltage is less than the PDIV of both PD sources, there is no PD occurrence. The zero value and the pattern of CD shows that there is no PD activity as depicted in Fig. 4.12. As the magnitude of the applied voltage becomes greater than the PDIV of twisted-pair of magnet wires, this PD source generate PD pulses while the needle-

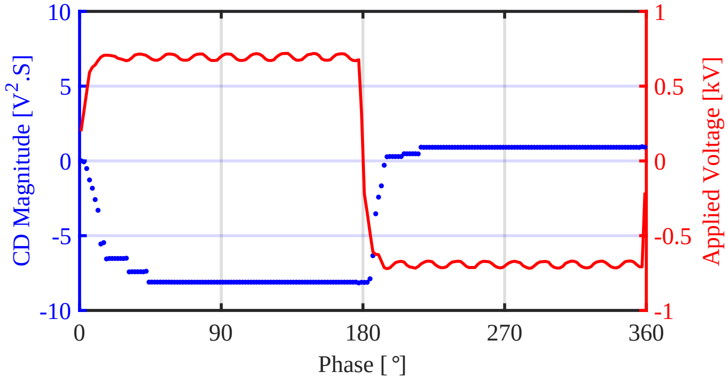

(a)

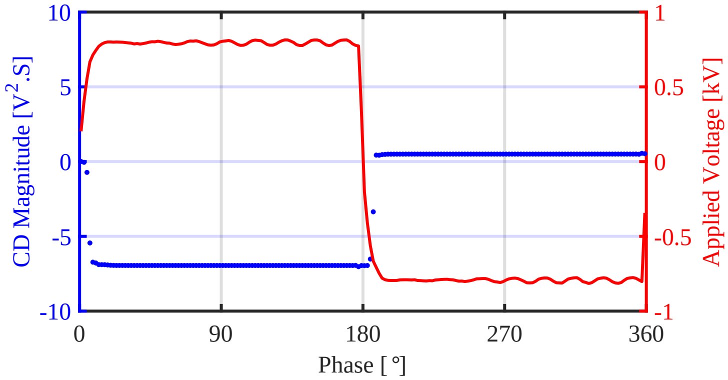

(b)

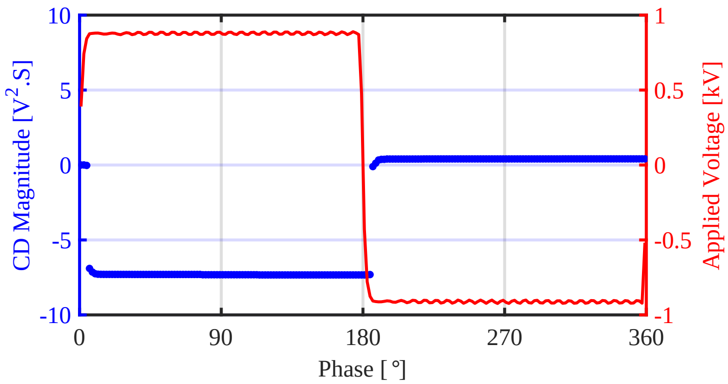

(c)

Fig. 4.13: PRCD patterns of twisted-pair magnet as an activated PD source air pressure level of (a) 33 kPa, (b) 67 kPa, and (c) 101 kPa.

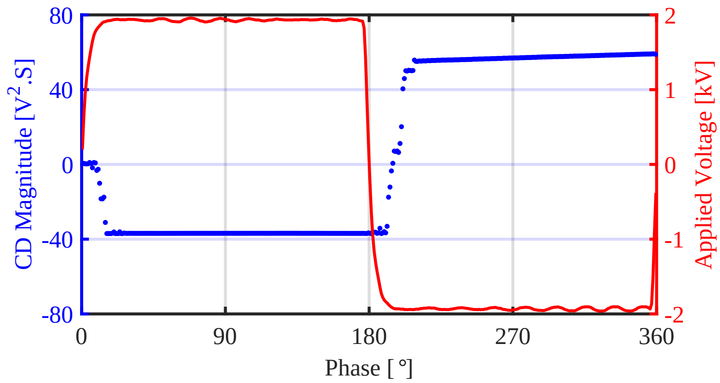

(a)

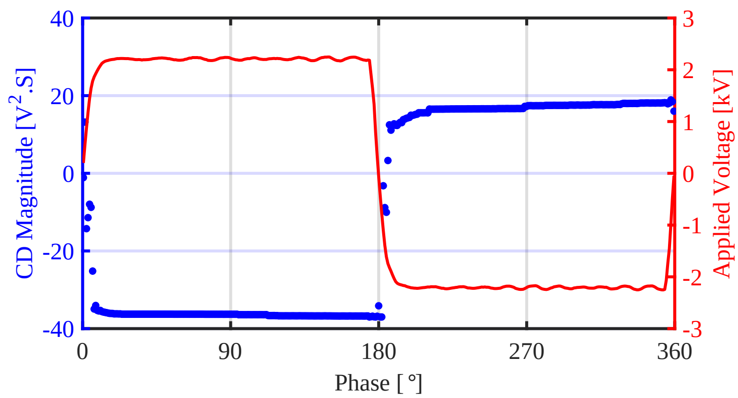

(b)

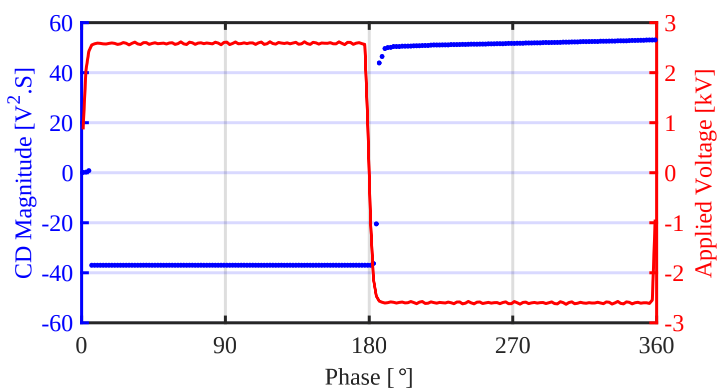

(c)

Fig. 4.14: PRCD patterns of two activated PD sources air pressure level of (a) 33 kPa, (b) 67 kPa, and (c) 101 kPa.

plane electrode is not yet active. According to Fig. 4.13, the CD magnitude abruptly falls and then rises to a value close to zero. It is obvious that the PD pattern is symmetrical for PD pulses generated by twisted-pair insulated wires. It can be seen in Fig. 4.14 that the PD pattern changes from symmetrical to asymmetrical by increasing the applied voltage to higher than 1.5 kV. The reason is that the corona discharges appear in the negative half cycle of the applied voltage that convert the symmetrical PD pattern to asymmetrical. The PD phase location can be found by the absolute value of the gradient of CD. The absolute value of gradient on phases without any PD pulses will be zero. However, the absolute value of gradient on PD phases will increase from zero to a high value.

4.3 Summary

In this chapter, phase-resolved cumulative distribution (PRCD) patterns at different levels of air pressure and frequency were presented. The PRCD pattern of single PD source as well as multiple PD sources can be obtained using the presented technique. This technique is based on the combination of the wavelet and energy techniques. It offers high performance PD detection in excessive noisy environment. The CD magnitude of the recorded noisy signal was obtained using this technique. The absolute value of the gradient of the CD magnitude revealed the applied voltage phase duration when the PDs were active. It has been proved that the PRCD pattern can be used as a fingerprint for PD characterization and identification under low air pressure and excessive noisy environment. Also, it can be implemented for condition monitoring of the insulation of aircraft electric actuators.

The results indicated that the phase-resolved pattern of the MDE for PD pulses generated by twisted-pair magnet wires is symmetrical, whereas the phase-resolved pattern of the MDE for the PD pulses caused by the needle-plane electrode is asymmetrical. As a result, when the corona discharges occur, the pattern changes from symmetrical to asymmetrical. For an asymmetrical pattern, the CD magnitude increases from a negative value to a positive value much greater than zero value in the negative half cycle of the applied voltage. In addition, it was shown that both the frequency and air pressure affect the characteristics of the PRCD pattern. It was reported that the CD magnitude decreases as the air pressure drops.

Chapter 5

Separation and Classification of Concurrent Multiple PD Sources

In Chapter 3, a PD detection method for both single PD source and multiple PD sources was presented. In Chapter 4, it was shown that the detection method is able to detect PD activity despite of the low magnitude of PD pulses and excessive noisy environment. However, the disadvantage of this method is that the positive corona discharges make identification of PD sources difficult due to overlapped patterns. The PRCD patterns generated by multi-source PDs are often partially overlapped. This has an impact on PD classification that makes PD sources so difficult to be properly identified.

By increasing the applied voltage to more than 140% of corona inception voltage (PDIV of needle-plane electrode), positive corona discharges appear. Positive corona discharges as well as negative corona discharges occur in the insulation system. Fig. 5.1 shows the MDE and PRCD patterns generated by the needle-to-plane corona discharges under atmospheric air pressure (101 kPa) and an applied voltage frequency of 50 Hz. The main observation is that the PRCD pattern shown in Fig. 5.1 is almost the same as PRCD pattern shown in Fig. 4.11 in which two PD sources (needle-plane electrode and twisted-pair magnet wires) were simultaneously activated. Because of the similar patterns, the operator who evaluates the insulation system conditions cannot recognize PD sources. Therefore, PRCD pattern for the identification of PD sources in the presence of positive corona discharges will be ineffective. In this regard, the identification of PD sources is steadily investigated in order to conduct appropriate assessment of the insulation system conditions. In this chapter, an algorithm for separation and classification of multiple concurrent PD sources is introduced.

5.1 Separation of Multi-Source PDs

There is a potential interest for MEA manufacturers to have an automated system for separation and classification of multi-source PD pulses under operation conditions. In this study, a comprehensive investigation and analysis is performed on PD pulse waveforms. Two different artificial defects, point-plane electrode and twisted-pair insulated wires, have been employed to generate PDs. The PD pulse signals are separated based on different time-domain features of signal such as risetime (RT), fall time (FT), slew rate (SR), and pulse width (PW). The time-domain features called pulse parameters describe the important fingerprints of the PD sources. Following subsections present an approach for the separation of multi-source PDs using time-domain features.

5.1.1 Measurement Procedure

The measurement procedure was performed on two types of PD sources (twisted-pair of magnet wires and needle-plane electrode) separately as well as simultaneously, according to the recommended procedure of IEC 60270 standard [13]. The experimental setup for recording the PD pulse waveform is shown in Fig. 3.3. The PD pulses were captured using a digital oscilloscope with segmented memory where a trigger level above the noise floor was used to trigger the recording. The magnitude of the applied voltage is increased to the 70% of expected PDIV for the test cell with twisted-pair of magnet wires. Since there is no

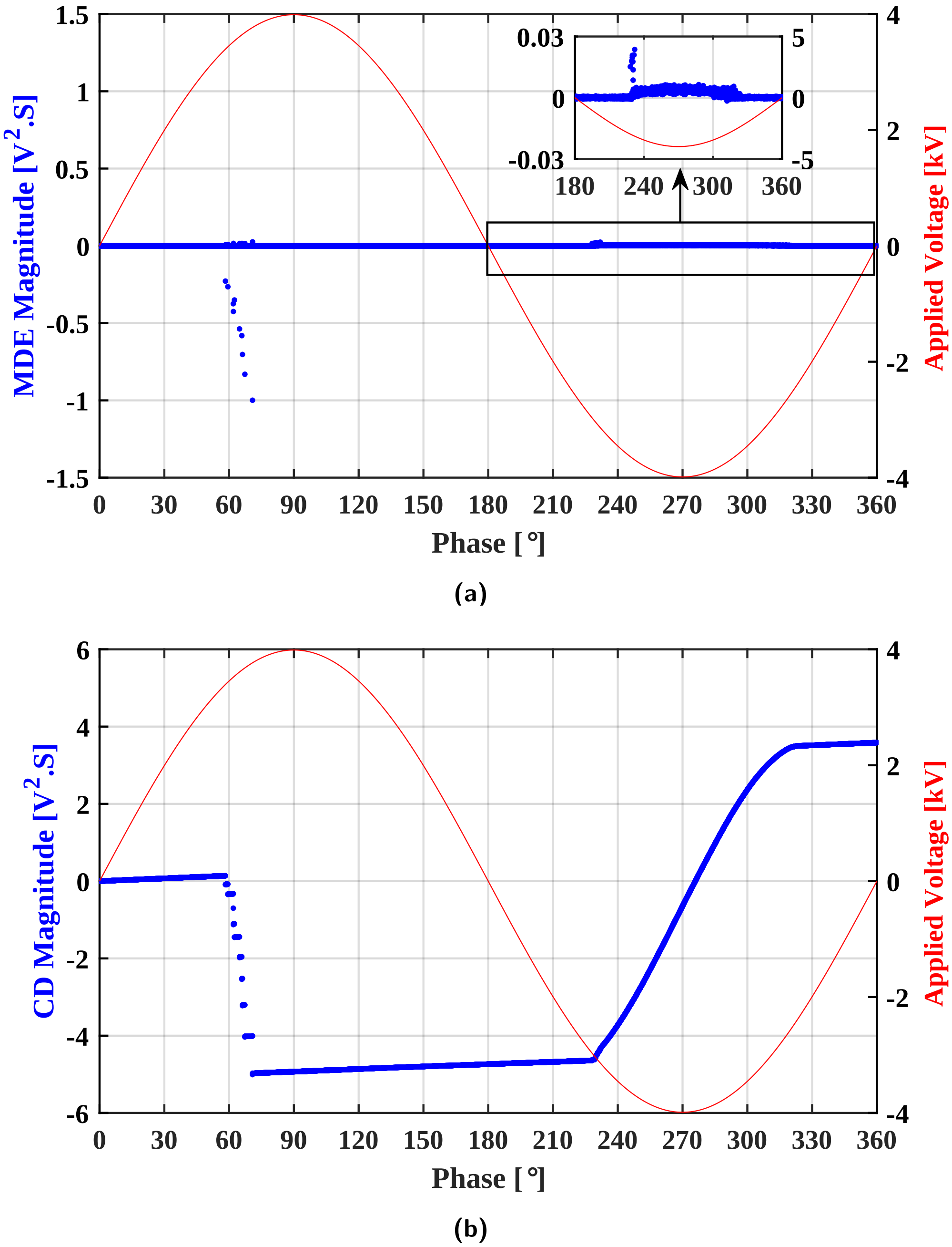

Fig. 5.1: The corona discharge patterns under applied voltage frequency of 50 Hz and atmospheric pressure (101 kPa), (a) MDE, (b) PRCD.

PD activity in the system, the oscilloscope only shows noise signal under such level of the applied voltage. Subsequently, the low trigger level of oscilloscope is adjusted higher than the continuous background noise signals. In this approach, the measurement system merely captures pulses having amplitude greater than noise signal. Once, the applied voltage is increased to 20% higher than the PD inception voltage of twisted-pair magnet wires, PD pulse signals appear. For recording PD pulse signals, PD measurements are performed at 120% of the PDIV of the test cell with needle-plane electrode. At this voltage level, both PD sources are simultaneously activated.

In order to conduct an investigation through PD pulse waveform characteristics, more than 100 PD pulse waveform under each predetermined frequency and air pressure are captured and time-domain features are extracted in order to have a better estimation of PD pulse waveform parameters.

5.1.2 Generation of PD Pulse Features

The generated time-domain features are desirable when we have an stable PD pulse signal in the presence of noisy environment. Since the measured PD pulse waveform was polluted by the background noise signals, the wavelet transform (WT) technique as described in [88] is applied to PD signals to eliminate the background noise signals. The wavelet technique provides stable PD pulse signals for further investigation. A sample of a noisy PD pulse waveform recorded by the oscilloscope and de-noised PD signal using the wavelet technique are shown in Fig. 5.2. PD measurement was conducted on the needle-plane electrode (corona discharge defect) under an AC applied voltage with the frequency of 500 Hz and an air pressure level of 101 kPa.

The de-noised PD signals were used for PD waveform analysis to separate two simultaneous PD sources. It was assumed that a given PD source generates signals that have similar waveforms. For this purpose, the time-resolved PD signals are analyzed to extract

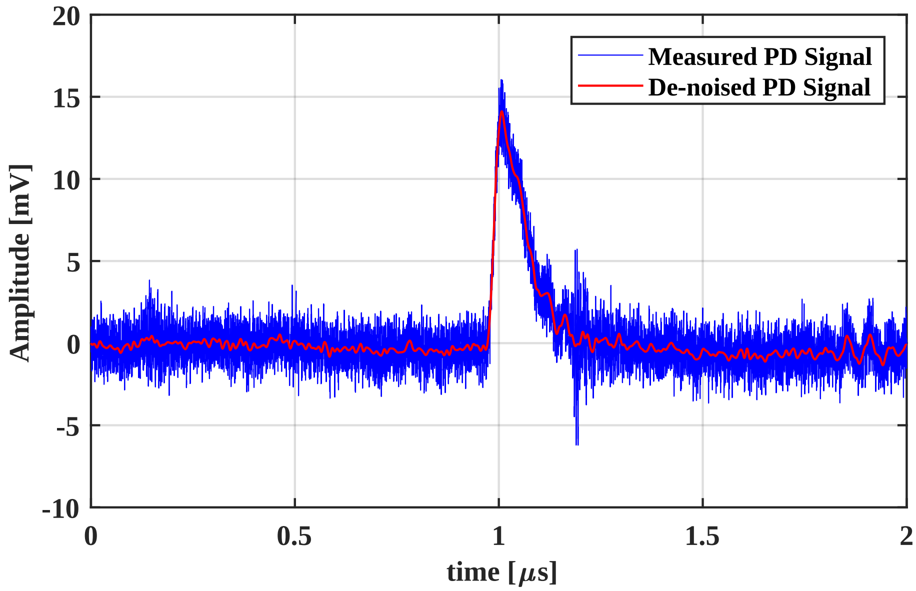

Fig. 5.2: Measured and de-noised PD signal recorded from PD measurement on needle-plane electrode.

time-domain features (i.e. RT, FT, SR, and PW) for pulse source separation under the different range of air pressures and applied voltage frequencies. Fig. 5.3 shows a de-noised PD signal and the standard definition of pulse parameters as used in this dissertation.

As presented in Fig. 5.3, the rise time (RT) is defined as the time required for PD signal to rise from 10% to 90% of its peak value. The fall time (FT) is the time required for PD pulse to fall from 90% to 10% of its peak value. The slew rate (SR) is the slope of the line connecting the 10% and 90% of PD signal peak value. The pulse width (PW) is the time difference between the same level instants (50% of PD signal peak value) of the initial and final transitions of PD signal.

5.1.3 Influence of Air Pressure on PD Pulse Features

The PD pulse parameters depend on the air pressure that varies during ascending and descending of the aircraft. Therefore, the time-domain features introduced in section 5.1.2

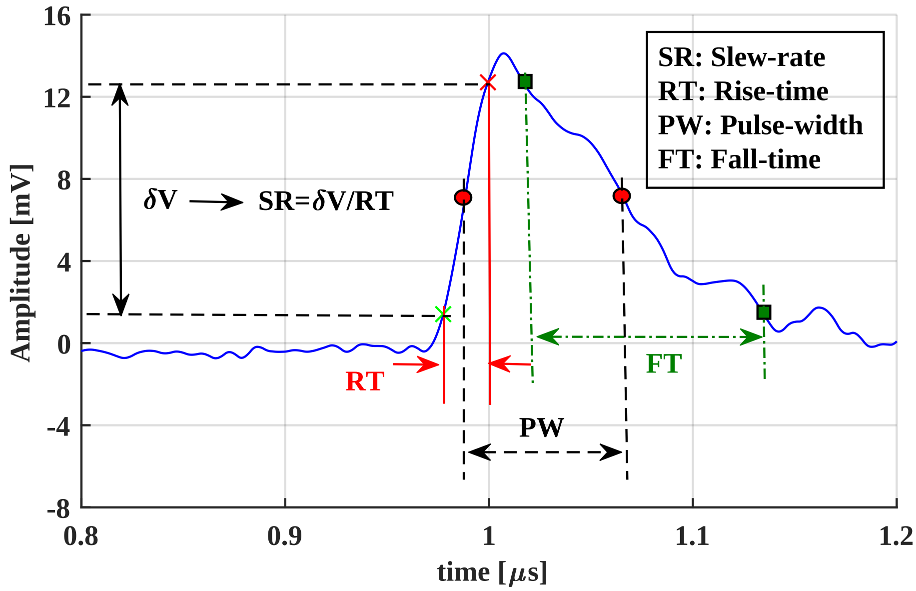

Fig. 5.3: PD pulse time-domain parameters.

are affected by air pressure.

The rise time (RT) of the measured PD pulses occurred at positive and negative half voltage cycles are shown in Tables 5.1 and 5.2 under different levels of air pressure. An AC voltage is separately applied to the test cells, that are the needle-plane electrode and twisted-pair of magnet wires. For the corona model, the amplitude of the applied voltage is raised up to 140% of the corona PDIV. At this level of voltage, the positive corona discharges may be generated.

As shown in Table 5.1, both the frequency and air pressure affect the rise time (RT) of the PD pulses generated by the PD sources. The frequency has less impact on the PD rise time than the air pressure. It is for the reason that the total duration of a PD pulse is in the range of several microseconds. The PD pulse waveform parameters will be affected by the frequency of the applied voltage if a much higher frequency (in the range of MHz) is applied to generate PDs [56]. According to Table 5.1, the value of the PD rise time increases

Table 5.1: Rise time of corona discharge pulses caused by needle-plane electrode on positive and negative half cycles of AC applied voltage.

Rise time [ns]						
	P=101 kPa		P=67 kPa		P=33 kPa	
f [Hz]	Positive half-cycle	Negative half-cycle	Positive half-cycle	Negative half-cycle	Positive half-cycle	Negative half-cycle
10	62.6	19.9	85.0	20.4	70.4	65.1
50	52.4	20.1	54.2	20.5	67.2	53.5
250	49.8	19.8	63.0	48.9	68.0	51.4
500	35.3	23.1	61.3	52.3	64.4	52.5
750	24.0	24.7	-	54.1	-	53.1
1000	-	25.2	-	37.4	-	51.0
1500	-	24.7	-	34.0	-	54.4
2000	-	22.8	-	36.3	-	53.3

Table 5.2: Rise time of partial discharge pulses caused by twisted-pair of magnet wires on positive and negative half cycles of AC applied voltage.

Rise time [ns]						
	P=101 kPa		P=67 kPa		P=33 kPa	
f [Hz]	Positive half-cycle	Negative half-cycle	Positive half-cycle	Negative half-cycle	Positive half-cycle	Negative half-cycle
10	20.8	17.6	22.1	19.5	30.4	33.2
50	20.8	18.0	23.0	19.6	30.4	31.8
250	20.6	16.9	23.2	19.1	35.3	33.3
500	20.8	16.9	23.8	19.2	33.0	30.3
750	20.9	17.3	24.0	19.0	32.7	27.5
1000	21.1	17.3	23.9	19.2	32.6	26.4
1500	21.5	17.3	24.5	18.7	31.5	25.1
2000	21.5	17.1	24.3	19.2	30.3	25.2

when the air pressure level of the test cell decreases for both of the PD pulses occurring in negative and positive half cycles. Under a pressure level of 101 kPa and a frequency of 750 Hz, the PD pulses also appear in the positive half cycle, however there is no PD pulse in the positive half cycle under the air pressure levels of 33 and 67 kPa. At higher frequency, there is no PD pulse in the positive half cycle under the air pressure levels of 33, 67 and 101 kPa. It is observed that the PD rise time for the twisted-pair of magnet wires are affected by the air pressure more than the frequency of the applied voltage. As shown in Table 5.2, the rise time of PD pulse decreases by increasing air pressure.

The fall time (FT) of the measured PD pulses occurred at positive and negative half cycles are shown in Table 5.3 and Table 5.4 for corona discharges and partial discharges caused by twisted-pair magnet wires, respectively. It is observed that frequency affects the fall time of corona discharge significantly while has little impact on the fall time of PDs caused by twisted-pair wires. It can be seen that the FT of corona discharge decreases with increasing the frequency for both of the negative and positive corona discharges as shown in Table 5.3. Under the pressure level of 33 kPa, the fall time of negative PD pulses decreases from 773 to 230 ns when the applied frequency is increased from 10 Hz to 2 kHz. It is indicated that FT is significantly raised by the environmental pressure. This pulse waveform parameter is altered from 204 to 621 ns for the needle-plane arrangement at negative half-cycle of the applied power frequency (50 Hz). During the negative half-cycle of the applied voltage, the fall time of PDs caused by the twisted-pair magnet wires decreases with increasing the frequency of the applied voltage while a slight change is observed for the positive PDs.

The pulse width (PW) of measured PD pulse waveform for both of the corona discharge and twisted-pair magnet wires are shown in Tables 5.5 and 5.6 respectively. It can be observed that the frequency has more effect on the pulse width of corona discharges at lower pressure and the value of PW decreases with increasing the frequency, whereas the

Table 5.3: Fall time of corona discharge pulses caused by needle-plane electrode on positive and negative half cycles of AC applied voltage.

Fall Time [ns]						
	P=101 kPa		P=67 kPa		P=33 kPa	
f [Hz]	Positive half-cycle	Negative half-cycle	Positive half-cycle	Negative half-cycle	Positive half-cycle	Negative half-cycle
10	187	184	354	307	820	773
50	190	204	372	329	883	621
250	193	192	363	360	850	603
500	159	116	368	349	857	736
750	150	116	-	233	-	582
1000	-	117	-	253	-	472
1500	-	114	-	252	-	300
2000	-	112	-	181	-	230

Table 5.4: Fall time of PD pulses caused by twisted-pair magnet wires on positive and negative half cycles of AC applied voltage.

Fall Time [ns]						
	P=101 kPa		P=67 kPa		P=33 kPa	
f [Hz]	Positive half-cycle	Negative half-cycle	Positive half-cycle	Negative half-cycle	Positive half-cycle	Negative half-cycle
10	70.5	60.9	84.6	69.1	116.3	93.7
50	68.8	63.8	87.0	70.1	118.1	101.2
250	71.7	58.1	82.6	68.3	114.6	88.4
500	69.4	52.2	85.9	64.9	108.7	84.4
750	72.0	49.7	89.3	64.4	108.5	84.9
1000	72.2	52.0	86.4	65.7	107.7	83.6
1500	72.4	53.2	87.4	68.8	106.4	79.8
2000	78.0	50.1	86.3	64.6	108.4	81.8

Table 5.5: Pulse width of PD pulses caused by needle-plane electrode on positive and negative half cycles of AC applied voltage.

Pulse Width [ns]						
	P=101 kPa		P=67 kPa		P=33 kPa	
f [Hz]	Positive half-cycle	Negative half-cycle	Positive half-cycle	Negative half-cycle	Positive half-cycle	Negative half-cycle
10	133	103	206	183	529	542
50	126	104	207	186	480	325
250	125	106	200	196	502	320
500	93.1	89.3	201	181	501	309
750	90.0	89.0	-	177	-	315
1000	-	93.1	-	150	-	313
1500	-	93.2	-	168	-	174
2000	-	93.4	-	143	-	141

frequency effect on the pulse width for twisted-pair magnet wires is low. The variation of PW at low pressure is high enough to distinguish the frequency effect on PD pulse width for corona discharges. Under an air pressure level of 33 kPa, the PW of pulses at negative half cycle of applied voltage decreases from 542 to 141 ns with increasing the frequency from 10 Hz to 2 kHz. It can be seen that the environmental pressure has notable effect on the width of the PD pulse. This PD pulse parameter at negative and positive half-cycle of the applied voltage increases with decreasing the air pressure for both of the electrode configurations. Under an applied frequency of 10 Hz, the PW increases from 133 to 542 ns as the environmental pressure is reduced from 101 to 33 kPa.

According to the definition of the slew rate (SR), the PD pulse amplitude and RT are the main factors to calculate the SR. The amplitude of PD pulse voltage depends on the amplitude of the applied voltage, pressure, and frequency of the applied voltage. In this study, all PD measurements are performed under a voltage level of 140% of PDIV for each frequency and pressure level. In this way, the same ratio of the applied voltage to the PD inception voltage were used for all the PD tests. The slew-rate of the measured PD pulses occurred at positive and negative half voltage cycles are given in Table 5.7 and Table 5.8.

Table 5.6: Pulse width of PD pulses caused by twisted-pair magnet wires on positive and negative half cycles of AC applied voltage.

Pulse Width [ns]						
	P=101 kPa		P=67 kPa		P=33 kPa	
f [Hz]	Positive half-cycle	Negative half-cycle	Positive half-cycle	Negative half-cycle	Positive half-cycle	Negative half-cycle
10	31.8	29.3	36.6	35.6	64	67
50	31.4	31.1	39.2	35.6	69.3	72.2
250	32.3	29.4	38.5	33.8	63.1	59.2
500	32.3	28.6	40.6	34.0	64.4	59.4
750	32.1	28.3	41.4	32.3	64.8	56.4
1000	32.3	28.4	40.1	32.9	65.3	55.8
1500	32.6	28.5	43.3	32.3	66.1	55.1
2000	34.6	28.4	33.3	39.5	66.4	52.1

It is observed that the frequency affects the slew rate of corona discharges, whereas the values of SR show slight changes with frequency for PD pulses generated by the twisted-pair magnet wires. According to Table 5.7, under pressure levels of 67 and 101 kPa, the SR value of PDs decreases by increasing the frequency from 50 Hz to 2 kHz. On the other hand, the SR value of PDs increases by increasing the frequency from 10 to 50 Hz. The value of SR decreases with frequency at negative half-cycle and under the pressure level of 33 kPa. For both types of PD sources, the value of SR decreases as the air pressure decreases and this behavior is observed for all the frequencies under different air pressure levels.

The rise time of the measured PD pulses occurred at positive and negative half cycles of the bipolar square wave voltage are shown in Table 5.9 and 5.10. The PD discharges are caused by the needle-plane electrode and twisted-pair of magnet wires under different air pressure levels. The value of fall time (FT), pulse width (PW), and slew rate (SR) are shown in Appendix B. In order to have corona discharges, the amplitude of applied voltage raised up to 140% of the corona PDIV. At this level of voltage, the positive corona discharges did not occur.

As shown in Tables 5.9 and 5.10, the rise time (RT) of discharge pulses is affected

Table 5.7: Slew rate of PD pulses caused by needle-plane electrode on positive and negative half cycles of AC applied voltage.

Slew Rate [V/μs]						
	P= 101 kPa		P= 67 kPa		P= 33 kPa	
f [Hz]	Positive half-cycle	Negative half-cycle	Positive half-cycle	Negative half-cycle	Positive half-cycle	Negative half-cycle
10	1.76	2.85	2.36	3.33	2.46	1.78
50	8.51	4.58	7.32	7.52	6.42	0.80
250	3.49	1.91	4.10	3.13	5.49	0.71
500	0.45	0.49	0.64	0.43	5.58	0.57
750	0.44	0.46	-	0.38	-	0.40
1000	-	0.42	-	0.35	-	0.32
1500	-	0.41	-	0.25	-	0.20
2000	-	0.42	-	0.19	-	0.22

Table 5.8: Slew rate of PD pulses caused by twisted-pair magnet wires on positive and negative half cycles of AC applied voltage.

Slew Rate [V/μs]						
	P= 101 kPa		P= 67 kPa		P= 33 kPa	
f [Hz]	Positive half-cycle	Negative half-cycle	Positive half-cycle	Negative half-cycle	Positive half-cycle	Negative half-cycle
10	19.1	21.2	17.6	20.6	14.4	16.2
50	24.2	23.4	22.4	24.2	18.1	18.1
250	19.2	17.2	17.7	18.9	9.1	10.3
500	17.4	15.0	14.7	17.3	10.8	9.58
750	16.3	16.4	13.1	15.9	10.6	12.9
1000	16.5	16.5	13.6	15.8	10.2	12.4
1500	17.3	16.2	12.2	15.7	10.3	13.2
2000	15.4	15.8	12.7	15.3	11.2	12.5

Table 5.9: Rise time of corona discharge pulses caused by needle-plane electrode on positive and negative half cycles of bipolar square-wave applied voltage.

Rise time [ns]						
	P=101 kPa		P=67 kPa		P=33 kPa	
f [Hz]	Positive half-cycle	Negative half-cycle	Positive half-cycle	Negative half-cycle	Positive half-cycle	Negative half-cycle
400	-	21.7	-	30.8	-	32.2
2000	-	21.3	-	29.0	-	31.9
5000	-	21.4	-	27.6	-	30.9

Table 5.10: Rise time of PD pulses caused by twisted-pair magnet wires on positive and negative half cycles of bipolar square-wave applied voltage.

Rise time [ns]						
	P=101 kPa		P=67 kPa		P=33 kPa	
f [Hz]	Positive half-cycle	Negative half-cycle	Positive half-cycle	Negative half-cycle	Positive half-cycle	Negative half-cycle
400	12.8	12.7	17.5	18.1	22.3	23.2
2000	13.1	13.3	16.2	15.5	23.9	24.2
5000	13.6	14.1	16.0	16.4	23.7	25.7

Table 5.11: Fall time of corona discharge pulses caused by needle-plane electrode on positive and negative half cycles of bipolar square-wave applied voltage.

Fall Time [ns]						
	P=101 kPa		P=67 kPa		P=33 kPa	
f [Hz]	Pos. half-cycle	Neg. half-cycle	Pos. half-cycle	Neg. half-cycle	Pos. half-cycle	Neg. half-cycle
400	-	92.6	-	146	-	192
2000	-	80.5	-	133	-	103
5000	-	79.0	-	109	-	96.2

Table 5.12: Fall time of PD pulses caused by twisted-pair magnet wires on positive and negative half cycles of bipolar square-wave applied voltage.

Fall Time [ns]						
	P=101 kPa		P=67 kPa		P=33 kPa	
f [Hz]	Pos. half-cycle	Neg. half-cycle	Pos. half-cycle	Neg. half-cycle	Pos. half-cycle	Neg. half-cycle
400	64.8	62.8	93.3	115	62.8	99.3
2000	69.3	73.6	85.9	103	73.3	82.6
5000	70.7	72.4	65.7	93.4	117	124

by the air pressure. The rise time of the discharge pulses increases when the air pressure reduces. This means that the frequency of pulses decreases. The same happens for the fall time of discharges pulses according to Tables 5.11 and 5.12. On the other hand, the voltage frequency does not have a significant influence on the rise time.

As indicated in Tables 5.13 and 5.14, the pulse width (PW) of corona discharges at first increases by reducing the air pressure level and then decreases. The PW of corona discharges that occur under a pressure level of 33 kPa is higher than those under a pressure level of 101 kPa.

As shown in Tables 5.15 and 5.16, the slew rate (SR) of discharge pulses is affected by the air pressure. The value of SR increases with air pressure because the SR value depends on the pulse amplitude and rise time. At lower levels of air pressure, the PD pulse amplitude

Table 5.13: Pulse width of corona discharge pulses caused by needle-plane electrode on positive and negative half cycles of bipolar square-wave applied voltage.

Pulse width [ns]						
	P=101 kPa		P=67 kPa		P=33 kPa	
f [Hz]	Pos. half-cycle	Neg. half-cycle	Pos. half-cycle	Neg. half-cycle	Pos. half-cycle	Neg. half-cycle
400	-	72.4	-	142	-	116
2000	-	67.8	-	195	-	93.0
5000	-	46.1	-	164	-	109

Table 5.14: Pulse width of PD pulses caused by twisted-pair magnet wires on positive and negative half cycles of bipolar square-wave applied voltage.

Pulse width [ns]						
	P=101 kPa		P=67 kPa		P=33 kPa	
f [Hz]	Pos. half-cycle	Neg. half-cycle	Pos. half-cycle	Neg. half-cycle	Pos. half-cycle	Neg. half-cycle
400	42.7	43.8	54.3	56.8	41.6	43.4
2000	39.9	42.6	51.6	47.6	41.0	41.7
5000	39.1	41.0	42.3	43.4	66.7	53.0

Table 5.15: Slew rate of corona discharge pulses caused by needle-plane electrode on positive and negative half cycles of bipolar square-wave applied voltage

Slew Rate [V/μs]						
	P=101 kPa		P=67 kPa		P=33 kPa	
f [Hz]	Pos. half-cycle	Neg. half-cycle	Pos. half-cycle	Neg. half-cycle	Pos. half-cycle	Neg. half-cycle
400	-	1.50	-	0.65	-	0.41
2000	-	0.65	-	0.54	-	0.29
5000	-	0.58	-	0.48	-	0.26

Table 5.16: Slew rate of PD pulses caused by twisted-pair magnet wires on positive and negative half cycles of bipolar square-wave applied voltage

Slew Rate [V/μs]						
	P=101 kPa		P=67 kPa		P=33 kPa	
f [Hz]	Pos. half-cycle	Neg. half-cycle	Pos. half-cycle	Neg. half-cycle	Pos. half-cycle	Neg. half-cycle
400	187	200	68.0	52.3	30.8	29.1
2000	172	180	84.8	89.0	38.4	38.7
5000	160	168	82.9	91.2	35.0	24.9

is smaller while the rise time is greater that results in smaller SR value.

To illustrate the effect of air pressure on PD pulse waveform parameters, it is assumed that the needle electrode is energized with a positive polarity voltage. When the applied voltage magnitude reaches the PDIV of the corona discharge, electron avalanches slowly start to grow toward the tip of the electrode. The densities of electrons, negative and positive ions are very low at the beginning point of the corona PD pulse. During the rise time (RT), the densities of these three particles raise significantly because of the development of electron avalanches. Consequently, the amplitude of corona current pulse rises rapidly and reaches to the maximum value. The number of electrons has an important role in the ionization region during rise time of discharge pulses. The number of gas particles reduces with decreasing the air pressure. The generation rate of free electrons decreases due to the lower number of gas particles, which results in increase of the rise time of PD pulse. After the maximum value of PD current pulse, the electron avalanches will be absorbed by the tip of the needle and the positive ions are taken away from the tip of the needle due to the electric field coincidentally. At the fall-time interval, the amplitude of corona current starts to decreases because of a reduction in the number of electrons. Because of higher drift velocity of the electrons, they disappear rapidly. Subsequently, positive ions in the vicinity of the tip of the needle create an electric field between the positive ions and the needle tip. This electric field weakens the local electric field nearby the tip of the needle, which results in ending of the electron avalanche formation since the local electric field is lower than the onset electric field. Therefore, the fall time is determined by the drift velocity of positive ions as they move toward the plane electrode. It has been reported that the positive ions drift faster at higher air pressure levels [38]. As a result, the fall time of corona PD pulse increases with decreasing the air pressure and hence more time is needed for positive ions to cross the air gap completely. When the rise time and fall time of the PD pulses increase, the width of PD pulse raises. Increasing the rise time and reduction in the amplitude of

PD under low air pressure result in the decrease of the slew-rate [38].

5.1.4 Feature Analysis

Previously, it was reported how the time-domain features (RT, FT, SR, and PW) are generated. Three of the generated time-domain features are selected and represented in a three-dimensional (3D) space and the calculated features of all PD signals are projected into the 3D space. Multi-source dataset is separated based on the feature analysis. The benefit of this separation is that the overlapping level of the PD sources is reduced which results in the improvement of classification for multiple-PD sources. In this low dimensional map space, the multi-source classes are relatively discriminated. Each PD source shows a cloud of data points (clusters) that are mapped in different positions.

As mentioned, the defect models are simulated by needle-plane electrode and the twisted-pair magnet wires. Because of this, there were two types of clusters associated to artificial PD sources. The location and dispersion of the clusters in 3D space are used for separation of superimposed PD sources.

5.2 Multi-Source PD Classification

Classification of PD sources based on the statistical moments of time-domain feature distributions is performed after the separation. To statistically analyze the PD data, the distribution of time-domain features are used for PD identification of the mixed PD signals. Normal and Weibull distributions, which are the most commonly used for insulation evaluation are employed [89]. Normal and Weibull distributions are the important statistical operators used for random values of PD pulse waveform features. The probability distributions of features associated with Normal and Weibull functions are determined in this section. The statistical moments of probability distribution are subsequently computed for further evaluation and discrimination of PD sources. The statistical moments of Normal distribution (skewness and kurtosis) and the parameters of Weibull distribution (shape and scale) are employed for classification. The classification of concurrent PD sources is achieved using a nonlinear version of Support Vector Machine (SVM) which is called Kernel SVM (KSVM). In this approach, PD pulses are recognized and separated from noise pulses based on pulse signal parameters.

5.2.1 Probabilistic Analysis

The probabilistic analysis provides diagnostic tools for identification of PD sources. The clusters associated with PD sources are analyzed using a probabilistic method. Each of the clusters has data points that have information from the time-domain features. The distribution of each time-domain feature related to each cluster was fitted by the probability function to generate well-discriminative fingerprints. The Probability Density Function (PDF) of features may be described in terms of two parameters. The parameters of Normal function are mean (μ) and standard deviation (σ). The parameters of Weibull function are scale (α) and shape (β), which are estimated by means of maximum likelihood method. Accordingly, the probability density function (PDF) of a Normal and Weibull distributions are given by

$$N(x|\mu,\sigma) = \frac{1}{\sqrt{2\sigma^2}}.e(-\frac{(x-\mu)^2}{2\sigma^2}) \tag{5.1}$$

$$W(x|\alpha,\beta) = \frac{\beta}{\alpha}(\frac{x}{\alpha})^{\beta-1}.e(-(\frac{x}{\alpha})^{\beta}) \tag{5.2}$$

where x is the random variable.

The most frequently statistical moments of PDF are skewness and kurtosis. Skewness is a measure of the lack of PDF histogram symmetry around the mean value (μ) and kurtosis is a measure of the PDF histogram sharpness. The skewness and kurtosis values are normalized by σ^3 and σ^4, respectively. Skewness (S) and kurtosis (K) of the normal distribution are defined by

$$S = \frac{\sum_1^N (x_i - \mu)^3}{N.\sigma^3} \tag{5.3}$$

$$K = \frac{\sum_1^N (x_i - \mu)^4}{N.\sigma^4} \tag{5.4}$$

where x_i is the value of each data point, N is the total number of data points, μ is the mean of distribution and σ is the standard deviation of the data distribution.

If the value of skewness is positive, it means that the bulk of the data points is at the right side of the mean value. However, the skewness becomes negative value when most of the distribution is skewed to the left side of mean value. The positive kurtosis indicates that the distribution has a sharper and higher peak compared to the normal distribution. On the other hand, a distribution of data points with negative kurtosis implies a flatter and lower peak relative to a normal curve.

In order to generate fingerprints of each PD defect, statistical moments (S, K, α, β) of respective feature distributions are considered. There are four time-domain features and each of the features has four statistical moments. Totally, there are sixteen statistical moments that can be referred as the fingerprints of the PD sources. The PD source fingerprints will be used to classify an unknown PD source.

5.2.2 Support Vector Machine

Generally, the probability estimation of multi-sources data points is performed with respect to the individual classes of single-sources. The outcome of this analysis is the generation of PD sources fingerprints. However, the value of these estimated fingerprints will not indicate which one of the single-sources had contribution in constructing the mixed PD sample. This occurs sometimes due to the scattering of multi-source data points close to the single source which has no role in the formation of those samples. Reliance on the estimated fingerprints obtained from the probabilistic analysis may mislabel the class of PD pulse sources instead of constitutive PD source. However, performing a correct and powerful feature generation in conjunction with utilizing a high performance classifier can enhance the estimation power of the classification algorithm via generating discriminating features from raw PD signals. This will help to exactly recognize the constitutive single-sources which contributed to the mixed-sources PD sample. Tackling these points by the developed algorithm demonstrates its importance to have a high successful rate of classification for the multiple concurrent PD sources.

There are various classification algorithms that are used for PD signal classifications. The algorithms that are frequently used are fuzzy logic algorithm [90], probabilistic neural network [91], Bayesian [92], and support vector machine [93, 94]. Among them, support vector machine (SVM) is the robust and powerful algorithm for multiple PD sources classification. SVM is one of the supervised method for discrimination of different classes. The goal of SVM algorithm is to design hyperplanes that classify all the training data points. The hyperplane classifiers leave the maximum margin between different classes and the data points that are located within the margin are misclassified. Depending on the complexity of feature values, nonlinear classifiers can be employed to separate a number of classes. When the classes are not linearly separable, any attempt to identify hyperplanes may lead to inaccurate and indeterminate classification [95].

In this thesis, a nonlinear version of SVM is utilized for discriminating different classes known as Kernel SVM (KSVM) because of the complexity of computed statistical moments. This algorithm uses a set of Kernel functions to map the input features space into infinite dimensional features space. Since the kernel functions are non-linear transformation, no assumption and human assessment beforehand is required to determine whether data is linearly separable or not. Therefore, using the SVM algorithm provides a good generalization for implementing in practical conditions. The SVM algorithm outputs are generated based on a unique solution in the optimization problem while other algorithms such as neural networks may have multiple solution in solving the problem. Because of this reason, other algorithms are not robust [95, 96].

The general idea of KSVM is to map the data (x_i) in the input space into Hilbert feature space (H) using a nonlinear map [95]. The transformation of the input data (x_i) into Hilbert feature space (H), which is a space with infinite number of dimensions, is done using a feature map ϕ:

$$x \rightarrow \phi(x) \in H \tag{5.5}$$

In the nonlinear SVM algorithm, a Kernel function is required to be applied in the SVM algorithm. This mathematical function must satisfy the Mercer's condition [95]:

$$K(x, x_i) =< \phi(x), \phi(x_i) > \tag{5.6}$$

where K is a Kernel function.

We need to select a suitable kernel function instead of working with the feature mapping ϕ. In this dissertation, the Radial-Basis Function (RBF) is adopted as a Kernel function that is given by

$$K(x, x_i) = exp(-\frac{\|x - x_i\|^2}{2\sigma^2}) \tag{5.7}$$

where σ is the RBF kernel width parameter which is a positive real number and free parameter. This kernel function defines a mapping into a higher unknown dimensions. To have a good generalization capability and avoid inaccurate classification of training features vectors, the KSVM algorithm maximizes the margin while minimizing the cost function which does not depend on the dimensionality of the feature space. The cost function is given by

$$J(\omega, \omega_0, \zeta) = \frac{1}{2}\|\omega\|^2 + C\sum_{i=1}^{N}\zeta_i \tag{5.8}$$

subject to

$$y_i[\omega^T\phi(x_i) + \omega_0] \geq 1 - \zeta_i \quad \text{and} \quad \zeta_i \geq 0 \quad \text{for} \quad i = 1, 2, ..., N$$

where ω and ω_0 define the optimal separation hyperplane. C is a regularization and smoothing parameter that balance the trade-off between the margin width and classification error. In practice, the output of the SVM algorithm for the exact separation of the training may cause poor generalization due to overlapping of the class-conditional distributions. Hence, some of the training data points are permitted to be located on the wrong side of the decision boundary considering a penalty. The penalty for misclassified training data points, which is known as the slack variable ζ, is a linear function of the distance from the boundary margin and positive parameter. As shown above, the quadratic programming (QP) is formulated as a quadratic objective function and linear inequality constraints. This problem can be transformed to its duality, in which inequality constraints are satisfied. It is stated equivalently by its Wolfe dual form and given by

$$\max_{\lambda}(\sum_{i=1}^{N}\lambda_i - \frac{1}{2}\sum_{i,j}\lambda_i\lambda_j y_i y_j K(x_i, x_j)) \tag{5.9}$$

subject to

$$0 \leq \lambda_i \leq C \quad \text{for} \quad i = 1, 2, ..., N \quad \text{with} \quad \sum_{i=1}^{N}\lambda_i y_i = 0$$

where λ_i are the Lagrange multipliers related to misclassified the data points. To end, in the high dimensional mapped feature space, the SVM makes use of a linear classifier, which is associated to to a non-linear classifier in the original space, to assign the class of each new data via calculating

$$g(x) = sgn[\sum_{i=1}^{N} \lambda_i y_i K(x_i, x) + \omega_0] \tag{5.10}$$

where sgn is the sign function.

The KSVM classification algorithm for the discrimination of multiple concurrent PD sources is developed based on the time-domain fingerprints. These fingerprints are calculated from the statistical moments of the PD pulse parameters.

5.3 Algorithm for Separation and Classification of Concurrent Multiple PD Sources

In this section, the proposed algorithm is presented for the separation and classification of the concurrent multiple PD sources at different air pressure levels and applied frequencies. The multiple PD source dataset is fed to the algorithm for separation and then classification. Once the separation is accomplished based on feature analysis, the probabilistic analysis is conducted on each of the separated data points (clusters) to find the statistical moments as PD source fingerprints. Once the PD source fingerprints (S, K, α, β) obtained from conducting probabilistic analysis on the separated data points (clusters), the fingerprint data sets can be employed as the input data for the classification task. There are sixteen statistical moments (PD source fingerprints) for each cluster that are fed to the KSVM algorithm for the classification. The classification input data have to be utilized for both training and testing purposes. The performance of the algorithm is evaluated based on the classification accuracy rate using the available sets of data. The flowchart of the proposed algorithm for separation and classification is shown in Fig. 5.4.

In this thesis, the leave-one-out method has been implemented for the validation of the algorithm because of its higher efficiency and lower computational complexity [95]. In this method, N measured samples, containing samples from each of the classes, are used.

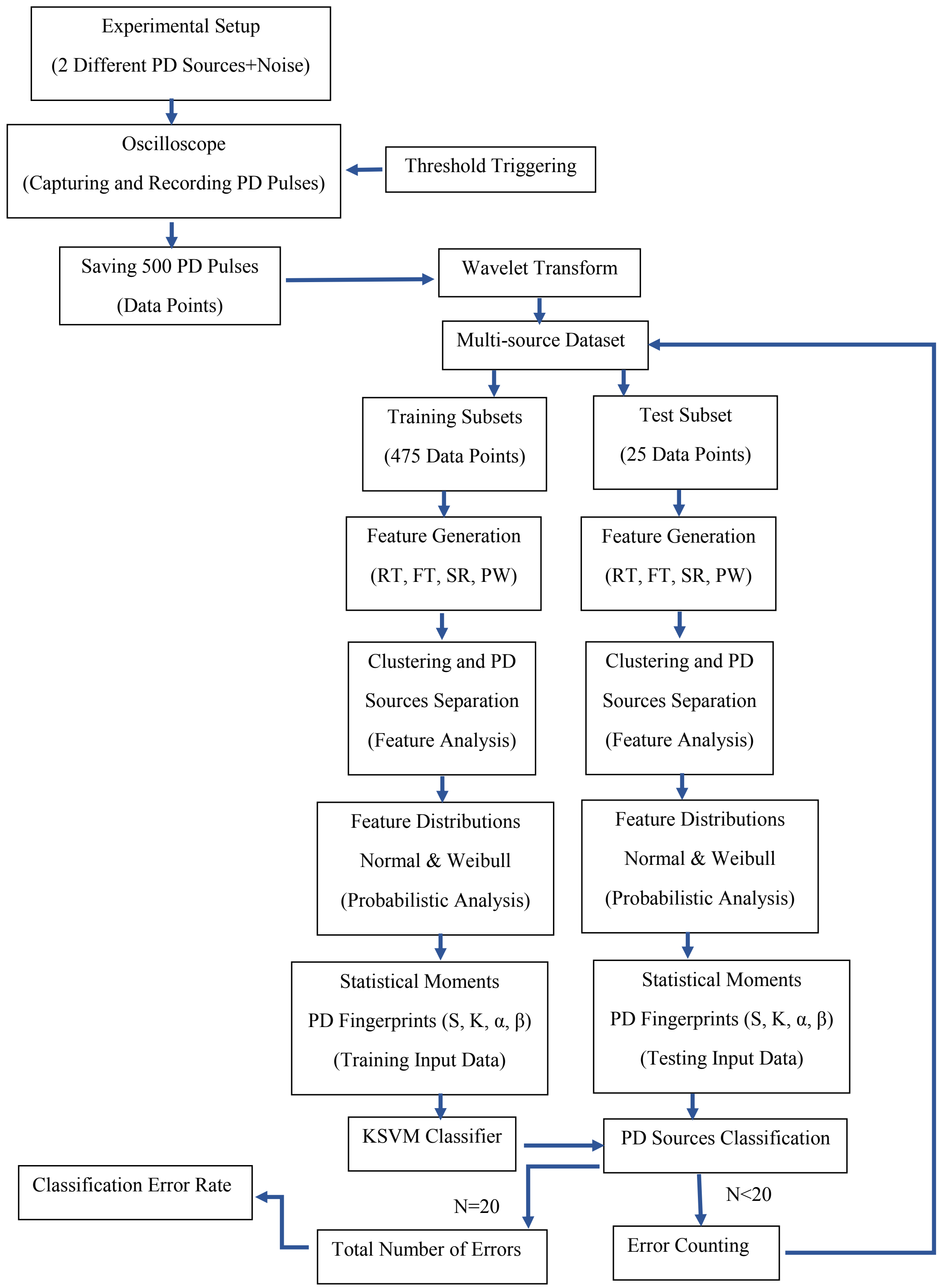

Fig. 5.4: Flowchart of the proposed algorithm.

From the measured test samples, m samples are excluded for testing and $N - m$ samples are allocated for constructing the training part of the algorithm. Next, the test samples are passed through the trained classifier and misclassification error is calculated. This procedure is repeated N times and each time a different sample is excluded for the testing. Thus, all samples are used for the training and exactly once for the testing and the independence between training and test sets is maintained. As mentioned in Section 3.2, two test cells with different electrode arrangements have been selected for PD measurements that result in two PD sources. The PD signals and background noises create three observations. These observations are corona discharges (positive and negative), partial discharges created by twisted-pair magnet wires, and noise signals. Under bipolar square wave applied voltage, corona discharges, discharges created by twisted-pair magnet wires, and switching noise signals make three observations. Because of these three observations, the 3-fold cross validation has been selected over leave-one-out method to perform a comprehensive evaluation of classification. In order to carry out a comprehensive performance evaluation of the KSVM classifier, the consecutive 500 PD pulses were captured from the experimental setup shown in Fig. 3.3. A multi-source dataset matrix with 500 data points is created. This multi-source data set was divided equivalently into 20 subsets ($N = 20$). Based on leave-one-out method, 19 subsets (475 data points) were used for training and 1 subset (25 data points) assigned for testing and this procedure is repeated 20 times. In each repetition, the training subsets as well as the test subset are separated into three different clusters, needle-to-plane corona discharges, PDs caused by twisted-pair magnet wires, and noises. The training clusters are classified based on their statistical moments using KSVM. The statistical moments of the test clusters are compared with the trained data for classification. When the cluster is correctly classified, it is counted as a correct prediction. Otherwise, it is an incorrect prediction (error). Finally, the classification accuracy is reported to evaluate the performance of the proposed algorithm. Classification accuracy (CA) is the ratio of correct predictions over total predictions. CA will be estimated via the so-called Confusion Matrix (CM) [95]:

$$CA = \frac{1}{C \times N} \sum_{i=1}^{C} CM(i,i) \tag{5.11}$$

where N is the repetition number ($N = 20$) and C is the number of classes ($C = 3$). The CA matrix shows the number of correct predictions for each of the classes (class i) with diagonal elements ($CA(i,i)$) while the other elements ($CA(i,j), i \neq j$) represent mislabeled classes. Each row of confusion matrix indicates an expected class, whereas each column represents a predicted class [95]. The error rate (ER) known as misclassification rate is calculated from classification accuracy. The relation between the classification accuracy (CA) and error rate (ER) for the confusion matrix is given by [95]:

$$ER = 1 - CA \tag{5.12}$$

5.4 Results and Discussions

5.4.1 Separation of PD Sources

Two electrode configurations are energized in parallel to simultaneously generate PD pulses with different nature of PD sources. The needle-plane electrode and twisted-pair magnet wires are separately mounted in the test cells. The test cell with the twisted-pair magnet wires has a lower PDIV compared to the test cell with the needle-plane electrode. The applied voltage is increased to 140% of the maximum PDIV of the parallel test cells combination. Under this level of applied voltage, the measured signal contains PD pulses that come from the test cells and the switching noises. The time duration of measured PD signal is adjusted for each frequency and air pressure level to record more than 500 consecutive PD pulses. As discussed in the previous chapter, using PRPD pattern for discriminating multiple activated PD sources may give incorrect interpretation of PD signal. In this section, the results of developed algorithm for the separation of multiple PD sources are presented.

It was shown that the rise and fall time of corona discharges generated by the needle-plane electrode are higher than the PD pulses caused by twisted-pair wires, so the twisted-pair PD pulses are faster than corona pulses in air. The pulse width of corona discharges is higher compared to the twisted-pair wires while the slew rate is lower. Due to the effect of air pressure and applied frequency, the distribution of these features overlap with each other in the 3D space considering only three PD pulse features. Therefore, it would be beneficial to take into account all the calculated parameters as features to avoid overlapping. For the separation of PD defects, three features that have lower standard deviation were selected to constitute a three-dimensional space. The reason is that the feature values are distributed over a narrower range and function more effectively for discriminating purpose. The experimental results collected from separate PD tests on the needle-plane electrode and twisted-pair magnet wires (shown in Section 5.1.3), are used for the separation of PD sources activated simultaneously due to the existence of similarity between PD pulses with the same nature.

As mentioned before, there are four features that are rise time, fall time, pulse width, and slew rate. Three features out of four can be selected as separation features for the 3D map. The selected features are used to create a combination. Therefore, four feature combinations can be generated that are:

1. Rise time, fall time, pulse width (RT, FT, PW)
2. Rise time, slew rate, pulse width (RT, SR, PW)
3. Fall time, slew rate, pulse width (FT, SR, PW)
4. Rise time, fall time, slew rate (RT, FT, SR)

Fig. 5.5 shows the separation map of two activated PD defects based on PD pulse feature analysis. The AC applied voltage frequency and the air pressure are 500 Hz and

33 kPa, respectively. Each data point (PD pulse) is mapped into 3D space at a different position. The data points that have similar PD pulse parameters (same nature) make a cluster with the same characteristics. To discriminate between PD sources, the effective combinations of features are selected and shown in Fig. 5.5. The first combination and the second combination are selected as the effective combinations. The 3D map of other feature combinations for separation are shown in Appendix B.

It can be seen that there are four discriminated clusters. The two clusters (#1 and #2) placed in the upper part of Fig. 5.5a are associated with PD pulses generated by needle-plane electrode (corona discharges) according to the feature values. Under an AC applied voltage, the characteristics of positive and negative corona discharges are strikingly different. According to the tables illustrated in Appendix B, the fall time and pulse width values of needle-to-plane corona discharges are much higher than the twisted-pair magnet wires. Because of this, the cluster #3 on the lower part of the map is related to the PD pulses generated by the twisted-pair of magnet wires. We can then consider that cluster #4 is related to the noise signals. It can be seen that the discrimination between noise signals and PD pulses is unclear when the first feature combination is used. On the other hand, Fig. 5.5b shows that the noise signal cluster is separated from the other clusters. Also, the feature values of positive corona discharges are higher in comparison to the negative corona discharges. Because of this, cluster #1 located on upper part is related to the positive corona discharges. However, it is observed that the clusters of positive and negative PD pulses generated by the twisted-pair magnet wires have overlapped each other because of similar characteristics.

Fig. 5.6 shows the separation map of two activated PD defects in which the PD measurement was conducted under 500 Hz AC applied voltage and an air pressure level of 101 kPa. According to Table 5.1 and Table 5.2, the rise time of discharge pulses are close to each other. The fall time and pulse width of corona discharge pulses are greater than PD pulses

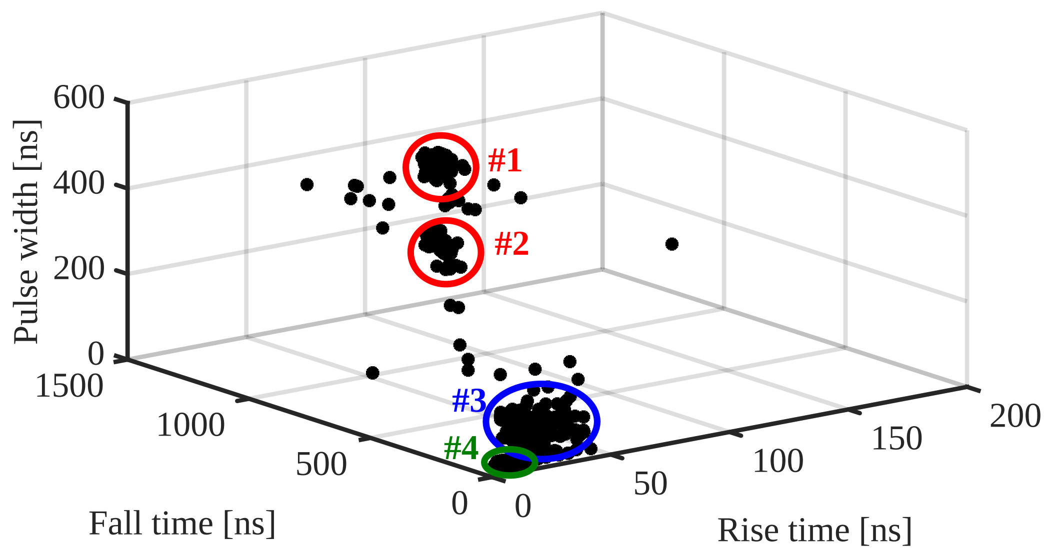

(a)

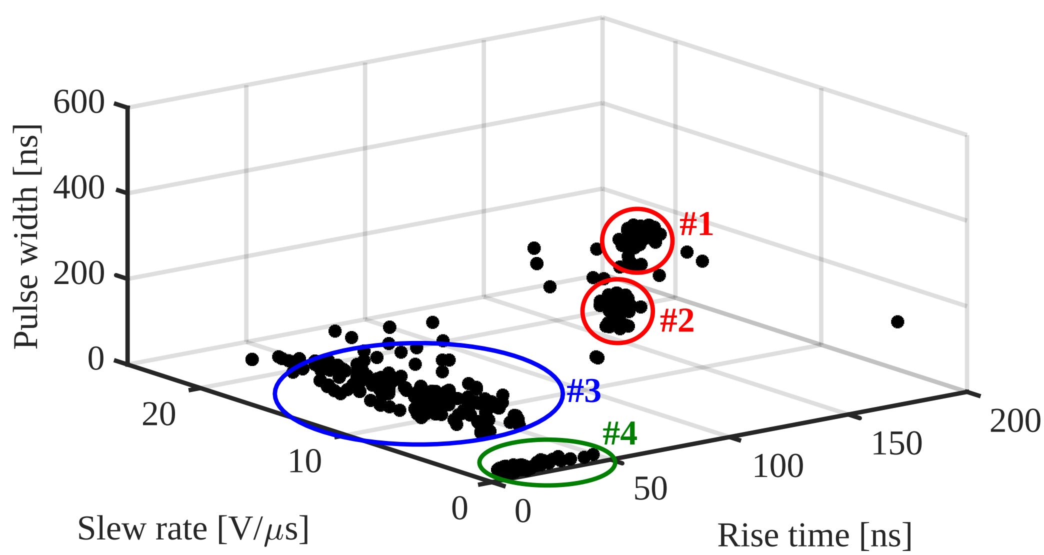

(b)

Fig. 5.5: The separation map of the first (a) and the second (b) feature combinations under AC applied voltage frequency of 500 Hz and sub-atmospheric pressure of 33 kPa.

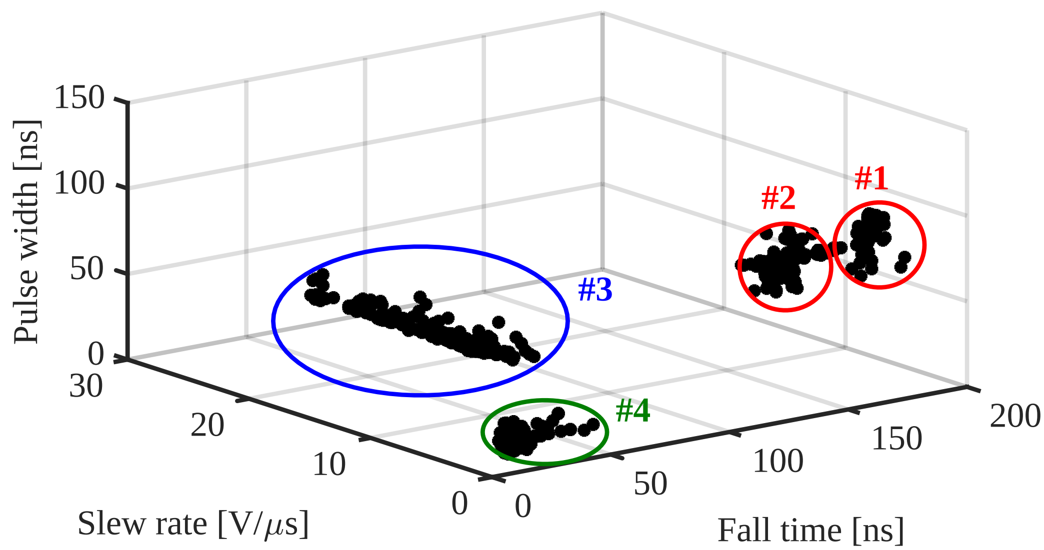

Fig. 5.6: The separation map of the third feature combination under AC applied voltage frequency of 500 Hz and atmospheric pressure of 101 kPa.

caused by twisted-pair wires according to the tables illustrated in Appendix B (Table 5.3 to Table 5.8). However, the slew rate of PD pulses caused by wisted-pair wires is significantly higher than the needle-plane electrode. Because of this, the third feature combination (FT, SR, PW) was selected to map data points in the 3D space to discriminate PD sources. The 3D map of other feature combinations for separation are shown in Appendix B. It is clear that all clusters are separated from each other perfectly. It can be seen that the data points inside noise cluster are squeezed together and is the smallest cluster. It demonstrates that the feature values of pulses generated by switching noises are altered in a very small range in comparison to the other cluster and the noise points are lumped into a highly densed cluster.

The separation map of the two activated PD defects under bipolar square wave voltage is shown in Fig. 5.7. The PD measurement was carried out under an air pressure level of 33 kPa and a frequency of 5kHz. The most effective feature combination was used for

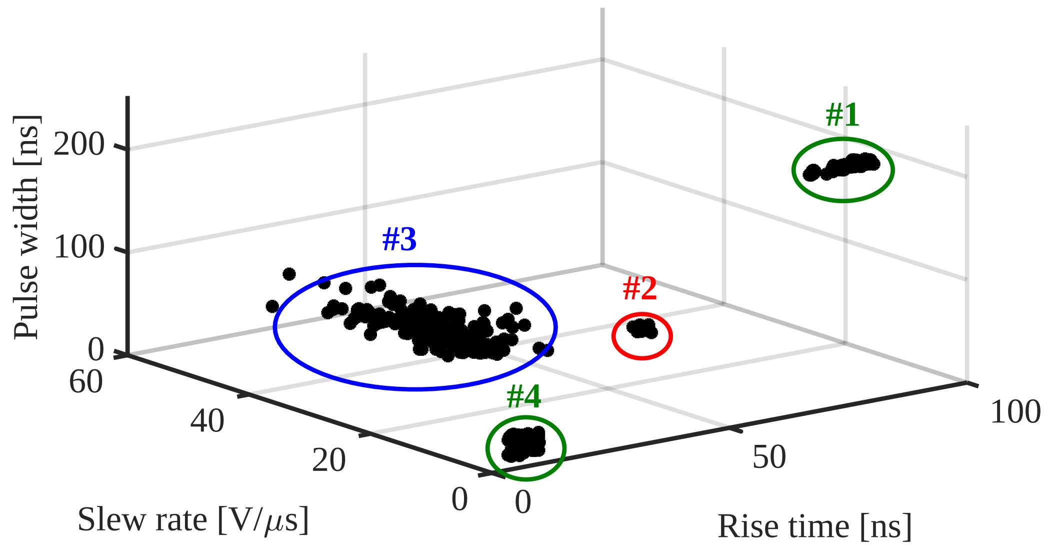

Fig. 5.7: The separation map of the third feature combination under bipolar square wave voltage, voltage frequency of 5 kHz and sub-atmospheric pressure of 33 kPa.

separation. The separation map of other combinations are provided in Appendix B. The features used are the rise time, slew rate, and pulse width. The polarity reversal of the applied square wave voltage generates pulses that may interfere with PD pulses.

According to the Tables 5.9 and 5.10, it is obvious that the clusters (#1 and #4) placed in the upper and lower part of Fig. 5.7 are not related to PD or corona pulses. The data points of cluster #1 were generated during polarity reversal of the applied voltage. On the other hand, the data points of cluster #4 were generated to the noise signals. Cluster #2 is associated to corona discharges, however cluster #3 is related to the partial discharges caused by twisted-pair magnet wires.

It is clearly shown in Figs. 5.5-5.7 that the separation of simultaneous PD sources can be effectively done via discovering patterns in the PD data based on the time-domain features. This exploring intrinsic characteristics leads to organize the PD date into discriminated classes, which is called unsupervised learning approach. In order to find class label for large amount of PD data points, clustering criterion is an essential part of the separation task.

5.4.2 Classification of PD Sources

In this thesis, the probabilistic analysis was used for PD classification of the mixed PD data. To generate fingerprints for the classification of PD sources, Normal and Weibull Probability Density Functions (PDF) were fitted on the distribution of PD pulse features. The distribution of PD pulse features are determined based on clustering structure. Accordingly, the probability density function of Normal and Weibull distributions PD data shown in Fig. 5.5a is presented in the following.

Fig. 5.8 shows the probability density function (PDF) of the rise time for both of the Weibull and normal functions. It indicates that the rise time of PD pulses generated by the corona discharges are higher than the PD pulses occur between the turns of twisted-pair magnet wires. The separation of pulses caused by corona discharge and switching noises can only be performed via considering rise time as the discrimination feature. However, a significant overlap exist between the PDF of all pulse sources in both of the fitted functions. Therefore, it is not accurate to conduct PD identification in the presence of concurrent PD sources specially under sub-atmospheric pressures. It obviously can be seen that the separation of pulse sources based on the rise time results in incorrect PD source identification as depicted in Fig. 5.8.

As such, other pulse parameters must be considered in PD identification procedure to facilitate the discrimination between PD sources. Figures 5.9 and 5.10 indicate the PDF of fall-time and pulse-width distributions for different pulse sources. It can be seen that the PDF of fall times are completely separated from each other as well as pulse width. Because of this, the identification of PD sources can be carried out based on the fall-time and pulse-width features.

Therefore, multiple PD source identification based on one feature leads to incorrect

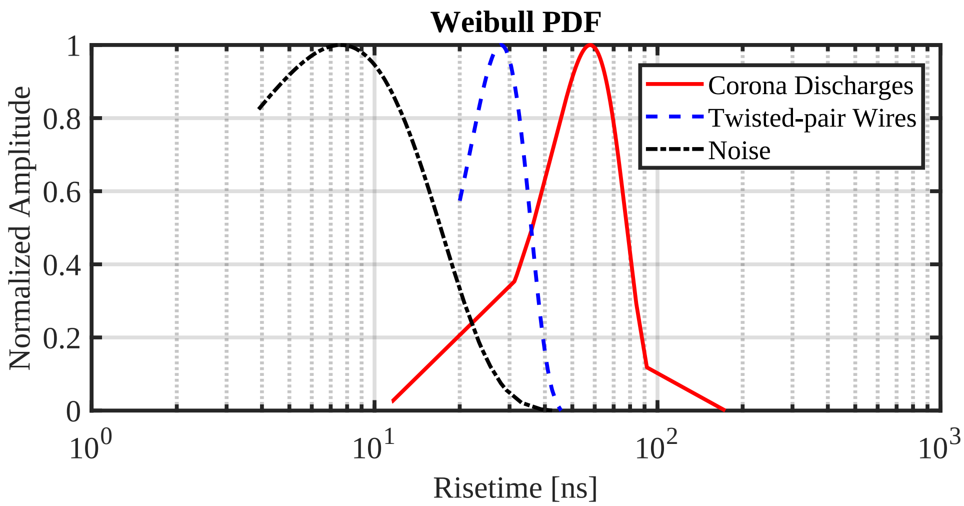

(a)

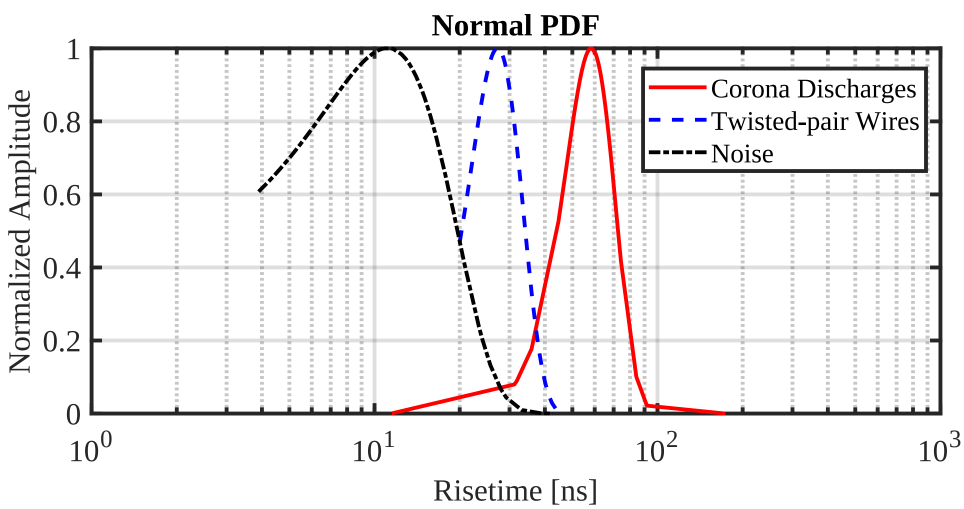

(b)

Fig. 5.8: Weibull (a) and Normal (b) distribution of rise time for applied frequency of 500 Hz and air pressure level of 33 kPa.

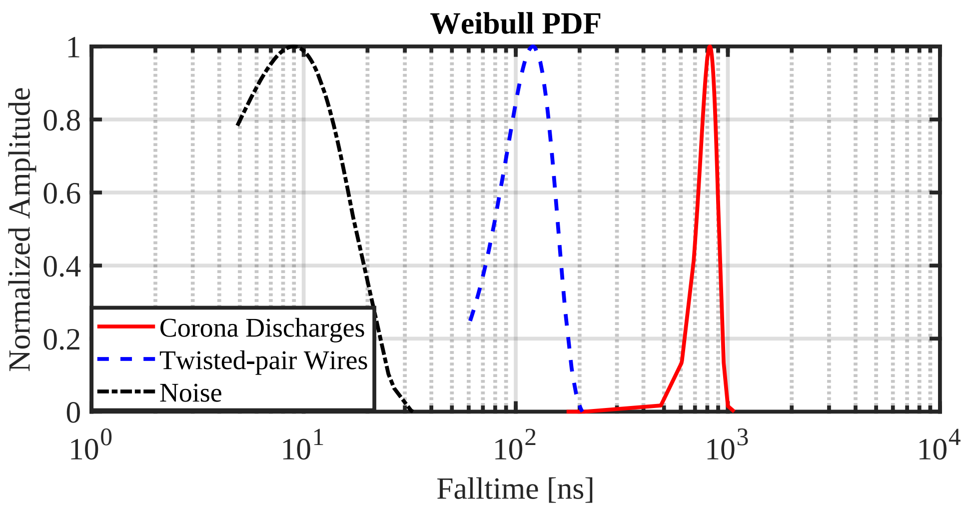

(a)

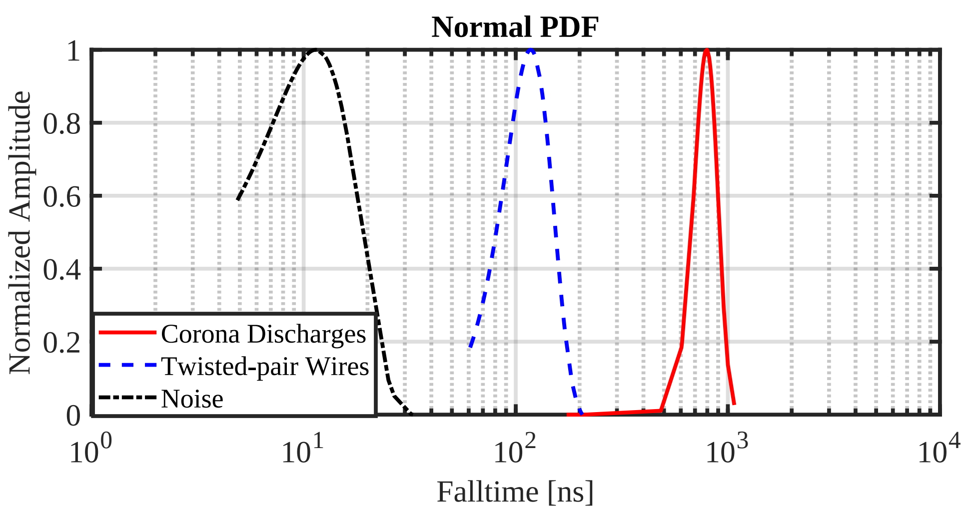

(b)

Fig. 5.9: Weibull (a) and Normal (b) distribution of fall time for applied frequency of 500 Hz and air pressure level of 33 kPa.

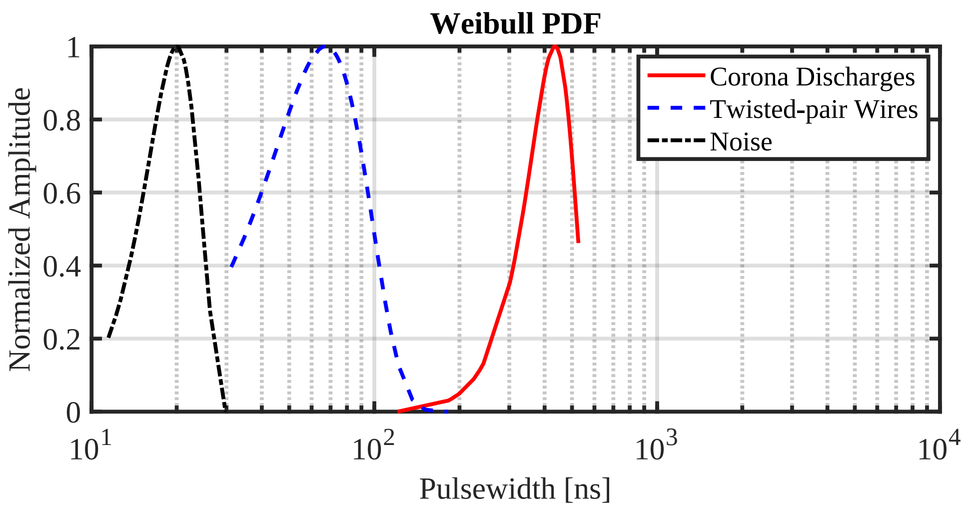

(a)

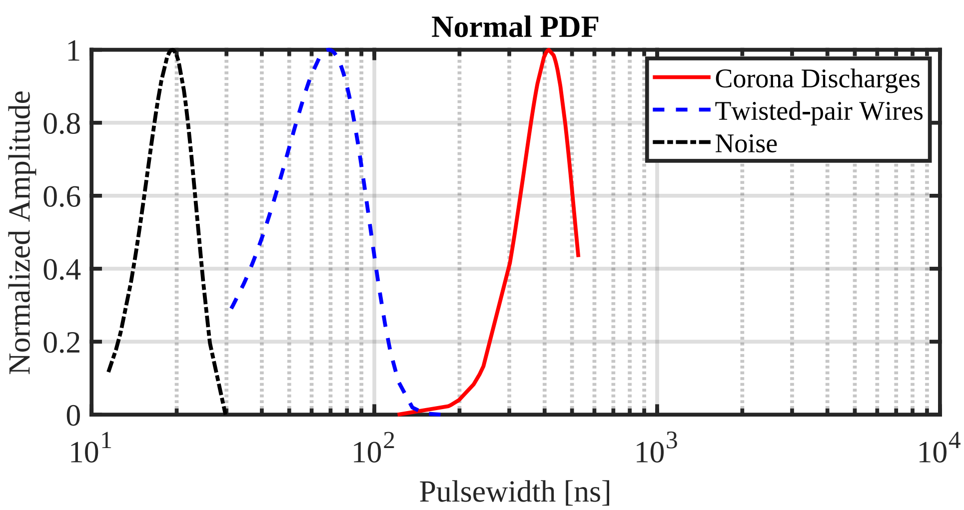

(b)

Fig. 5.10: Weibull (a) and Normal (b) distribution of pulse width for applied frequency of 500 Hz and air pressure level of 33 kPa.

results due to the overlap between the distribution of the features. Hence, an effective approach is to perform the discrimination of simultaneous PD sources based on the different pulse features. For instance, the rise time feature can be employed to separate corona signals from noise signals, however it is not effective to discriminate PD signals created by the twisted-pair wires from corona signals. For identification of twisted-pair magnet wire from other sources, the fall time and pulse width can be used.

The same explanation for PD identification of the mixed PD data, which is shown in Fig. 5.6 is presented in Appendix B. To have a powerful approach for the separation of pulse sources, different pulse parameters such as rise time, slew rate, fall time and pulse width are taken into account as discrimination features. Figs. B.6-B.9 show the PDF of the Normal and Weibull distributions of features for the measurement of PD under an AC voltage with a frequency of 500 Hz and a pressure level of 101 kPa. As shown in Fig. B.6, the rise time feature is inefficient for the PD source separation. However, the fall time feature is the most effective one for separation.

To produce a dataset from the distributions of PD pulse features, probabilistic analysis is performed. For this purpose, the skewness (S) and kurtosis (K) parameters of Normal distribution of the pulse time-domain feature are calculated under each predetermined frequency and air pressure. In addition, scale (α) and shape (β) parameters of Weibull distribution are obtained via data fitting. As mentioned in 5.2.1, each of the pulse features generates four statistical moments. There are four time-domain features that results in sixteen statistical moments. The statistical moments can be referred as the fingerprints of each PD source. The PD source fingerprints will be used to classify an unknown PD source. Due to low dimensionality of the features space associated with single-source PDs, principal component analysis (PCA) is not employed to construct a low dimensional space. In fact, this dimensionality-reduction technique is useful when there is a high dimensional feature space [95]. The calculated statistical moments for two case study are presented in

Table 5.17: The Statistical Moments of Feature Distribution associated with different sources of pulses

PD pulse sources		Needle-to-Plane		Twisted-pair wires		Noise	
PD pulse features		A	B	A	B	A	B
Rise time	S	-2.107	0.984	2.018	2.080	2.415	2.450
	K	6.942	4.684	7.774	8.743	9.545	9.751
	α	7.559e-8	4.496e-8	3.509e-8	3.428e-8	1.173e-8	1.163e-8
	β	20.101	10.309	2.203	2.351	1.686	1.685
Fall time	S	-4.141	-0.352	-0.024	-0.136	2.343	2.329
	K	31.288	2.626	1.353	1.824	8.241	8.239
	α	35.432e-8	43.122e-8	9.312e-8	9.442e-8	1.250e-8	1.249e-8
	β	16.308	12.539	5.434	6.622	1.965	1.972
Slew rate	S	1.532	0.125	1.050	0.281	2.734	2.757
	K	7.447	2.889	5.500	2.547	10.770	10.972
	α	0.49e+6	0.59e+6	11.6e+6	11.0e+6	0.07e+6	0.07e+6
	β	4.742	8.649	2.304	2.711	0.001	1.027
Pulse width	S	0.282	0.579	-0.162	-0.217	0.575	0.576
	K	2.657	3.852	1.834	2.439	4.107	4.022
	α	18.343e-8	25.102e-8	6.776e-8	7.114e-8	2.045e-8	2.036e-8
	β	9.698	17.080	4.350	5.149	4.321	4.282

Table 5.17. The results for case (A) are obtained from performing PD measurements under the applied frequency of 500 Hz at the air pressure level of 67 kPa, and the results for case (B) are calculated from conducting PD test under frequency of 1 kHz and sub-atmospheric pressure of 33 kPa. The results of probabilistic analysis can be used to design a classification system of multi-source PD.

To conduct a comprehensive assessment of the proposed algorithm, PD measurement were performed under the AC applied voltage frequency of 500 , 1000 and 2000 Hz at the air pressure levels of 101, 67 and 33 kPa.

Table 5.18 indicates the classification accuracy rates and the corresponding confusion matrix for different range of air pressure and frequency. The two-class experimental setup and the noise signals create 3-by-3 confusion matrix. These accuracy rates are obtained based on the class labels that are allocated to the unknown multi-source test data. The

Table 5.18: The classification accuracy rate and confusion matrix for each of the PD measurements using the developed algorithm

Air pressure (kPa)	33				67				101			
f (Hz)	Accuracy Rate %	C1	C2	C3	Accuracy Rate %	C1	C2	C3	Accuracy Rate %	C1	C2	C3
500	98.3	19	1	0	100.0	20	0	0	98.3	20	0	0
		0	20	0		0	20	0		0	19	1
		0	0	20		0	0	20		0	0	20
1000	98.3	19	1	0	100.0	20	0	0	100.0	20	0	0
		0	20	0		0	20	0		0	20	0
		0	0	20		0	0	20		0	0	20
2000	88.33	17	2	1	73.3	5	10	5	98.3	20	0	0
		0	20	0		0	20	0		1	19	0
		0	0	20		0	0	20		0	0	20
Overall %	94.98											

Class C1: Corona in air, Class C2: Twisted-pair magnet wires, Class C3: Noises

developed algorithm shows high classification rates under wide range of frequency and sub-atmospheric pressures. It can be seen that the classification accuracy rate is decreased with increasing the frequency under the constant air pressure level of 33 kPa. This can be related to the effect of frequency on the distribution of pulse parameters as discussed in pulse waveform analysis section. In addition, It is clearly observed that error rate is higher at high frequency range of 2000 Hz and sub-atmospheric pressures. This result indicates the complexity of performing separation and classification of simultaneous activated PD sources at low air pressure, however, the accuracy rates of the proposed algorithm is high enough under sub-atmospheric pressures.

5.5 Summary

In this study, a time-saving and efficient method for on-line monitoring of MEA insulation operations as well as separation and classification of PD pulses under sub-atmospheric air pressures was introduced based on effective statistical features.

In this chapter, the variation of PD pulse parameters was investigated from low to high frequencies and under air pressure levels of 33 kPa, 67 kPa and 101 kPa. It was observed that the rise time, fall time and pulse width of PD pulses increase with reducing the air pressure while the slew rate decreases. The rationale for this observation was attributed to the low electron generation rate at low air pressure which affects the discharge mechanism.

An algorithm has been proposed for the separation and classification of multi-source PDs which may be active simultaneously in the insulation system of aircraft. The PRPD pattern of multi-source PDs may be partially overlapped which makes it extremely hard to identify the sources of PD pulses. To overcome this difficulty, a comprehensive method was developed based on the probabilistic analysis of statistical features. In this thesis, time-domain parameters related to the PD pulse waveform were extracted and analyzed. The parameters that describe the time-domain characteristics of PD pulse waveform are rise time, slew rate, fall time and pulse width. The proposed algorithm assumes that the PD sources with the same nature generate PD pulse waveforms with similar characteristics.

To separate the multi-source PDs, the mixed PD dataset was projected on to the 3D map space. Each PD pulse, which was associated with a data point, was located in the map space depending on its time-domain parameters. The result of this procedure was the separated clusters of data points related to multi-source PDs. After performing separation based on the PD pulse waveform of PD pulses, the probabilistic analysis was carried out on each of the separated clusters to generate the required fingerprints for training and testing of the classifier. Skewness (S) and kurtosis (K) parameters of the Normal distribution and scale (α) and shape (β) parameters of Weibull distribution were selected as the fingerprints of each PD sources. KSVM classifier was used for the classification considering the extracted feature distributions as feature vectors.

Chapter 6

Conclusions and Future Work

6.1 Conclusions

In this thesis, development, testing, and evaluation of two methods for the identification of single and multiple concurrent PD sources in a range of air pressure and applied frequency were presented. In the first method, the PD sources were recognized based on the combination of wavelet and differential energy techniques while in the second method, the identification of PD sources were performed based on time-domain features.

To evaluate the effectiveness of the proposed methods, two small-scale artificial laboratory test cells were developed to simulate two different sources PD which may occur in the insulation system of an aircraft. The first test cell contains a needle-plane electrode to model corona discharges in air. The second test cell contains a twisted-pair of magnet wires to simulate PDs which may happen in the windings of electric actuators. The air pressure of the test cells was adjustable by using a vacuum pump. PD measurements were individually and simultaneously performed on the test cells at the air pressure levels of 33, 67 and 101 kPa. The applied frequency for PD tests on the individual test cell was in the range of 10, 50, 250, 500, ..., 5000 Hz.

The first method, which was based on the combination of wavelet and differential energy techniques, was able to detect PD pulses under extremely noisy contaminated environment and low air pressure. This PD recognition method consists of two parts: a high order of Symlet wavelet family for removing the background noise from the measured signal and a differential energy based technique for removing switching noises and generating the PRCD pattern. The variation in the obtained PRCD pattern can be used for monitoring the insulation condition in the presence of single and simultaneous multi-source PDs. It was shown that the PRCD pattern can be used as a fingerprint for PD identification under low air pressure and excessive noisy environment.

The results indicated that the phase-resolved pattern of the MDE for PD pulses caused by twisted-pair magnet wires is symmetrical. However, the phase-resolved pattern of the MDE for PD pulses caused by needle-plane electrode is asymmetrical. When the corona discharges occur, the pattern changes from symmetrical to asymmetrical. For the asymmetrical pattern, the CD magnitude increases from a negative value to a positive value much greater than zero on the negative half cycle of the applied voltage. In addition, it was shown that both the frequency and air pressure affect the characteristics of the PRCD pattern. It was also shown that the CD magnitude decreases as the air pressure drops.

The drawback of the PRCD pattern is that the pattern in the presence of positive corona discharges will be ineffective for PD identification because of the similarity of PRCD patterns. To mitigate this disadvantage, a comprehensive method was developed based on the probabilistic analysis of statistical features. An algorithm was developed for the separation and classification of multi-source PDs. This algorithm operates based on the assumption that there is a correlation between the nature of PD sources and their PD pulse waveform. In this developed algorithm, the probabilistic analysis was conducted on the PD pulse parameters related to each PD source in order to generate fingerprints for the classification of multiple, simultaneously-activated PD sources. For this purpose, Normal and Weibull distributions of the PD pulse parameters were estimated. Next, the kernelized version of SVM was adopted as an effective classifier using the statistical moments of the pulse parameters distributions. The benefit of employing KSVM in the proposed algorithm is that the PD sources were classified with high accuracy. As a result, this method will be practical to be used for PD source identification in the insulation system of more-electric aircraft.

In addition, the effect of frequency and air pressure on the PD inception voltage (PDIV) of the artificial PD sources as well as detailed characteristics of the PD pulse waveforms were investigated experimentally. It was concluded that both the frequency and air pressure affect the discharge mechanism. Under AC applied voltage, the value of PDIV decreases with decreasing the air pressure, whereas increasing the applied voltage frequency causes a reduction of the PDIV. Under bipolar square wave voltage, the air pressure has significant effect on PDIV, however the frequency of the applied voltage has no influence.

It was observed that a drop in the air pressure level results in an increase of the risetime, fall time, and pulse width of the PD pulse waveform while the slew rate decreases. Increasing the frequency of the power supply has less effect on the PD pulse parameters. It was observed that PD pulses are generated at both positive and negative half voltage cycles when the frequency of the AC applied voltage is less than 750 Hz. This causes faster degradation of the insulation system due to the higher amplitude of the PD pulses at the positive half cycle. For frequencies higher than 750 Hz, the PD pulses were observed only in the negative half cycle under an AC applied voltage of 40% higher than the PDIV.

In summary, the results of the proposed methods for partial discharge recognition show that the single and multiple PD sources can be successfully identified at different levels of air pressure. This identification system is able to continuously monitor the insulation system of a more-electric aircraft (MEA), and help to identify PD sources in early stages which leads to safe operation of an aircraft.

6.2 Future Work

In this thesis, a PD detection algorithm was proposed which aims to detect PDs at excessively noisy low air pressure environment. The proposed method can be implemented for on-line and off-line PD measurements. In addition, an algorithm was developed based on the time-domain features of the PD pulse waveforms to separate and classify the concurrent PD sources. The results demonstrate that both of the proposed algorithms are practical for monitoring the insulation condition in the aircraft power system. The future research which could enrich the research presented in this thesis is presented as follows:

- In this thesis, PD measurements were performed in order to investigate the effect of air pressure and the frequency of the applied voltage on the PD pulse waveform characteristics at room temperature. Due to the temperature drop at high altitude, the effect of temperature could be investigated on the discharge mechanism.
- The effect of humidity was not considered in this study. The humidity has effects on the partial discharge inception voltage. The relative humidity at high altitude is lower than the sea level. The effect of humidity on partial discharges can be considered.
- The PD sources considered in this thesis were a needle-plane electrode and a twisted-pair of magnet wires. Different PD sources such as PDs between motor winding and stator slot, impregnated winding motors, and various electrode arrangements could be employed to generate PD pulses of different nature.
- Sine and square voltage waveforms were used for PD tests and performing separation and classification. In order to control the amount of power delivered to the actuators in the electric power system of the aircraft, Pulse-width Modulation (PWM) technique is used [70]. Hence, the impact of this repetitive voltage waveform on the PDIV and PRCD pattern could be evaluated.

- In order to generate features for the separation and classification of PD sources, time-domain parameters of PD pulse waveform were utilized. Further, feature generation could be done via calculating frequency-domain parameters such as dominant frequency of the PD pulse.

- Different classifiers such as fuzzy logic, neural networks or logistic regression could be used for the classification of concurrent PD sources and their reliability and accuracy rates could be compared with the proposed algorithm.

- The samples are aged during multiple tests that can affect the experimental results. In order to detect any changes in the test samples, the change-point analysis which is a powerful statistical approach can be used.

References

[1] [Online]. Available: http://www.boeing.com/commercial/787/#/family

[2] R. Rui and I. Cotton, "Impact of low pressure aerospace environment on machine winding insulation," in *2010 IEEE International Symposium on Electrical Insulation*, June 2010, pp. 1–5.

[3] K. Emadi and M. Ehsani, "Aircraft power systems: technology, state of the art, and future trends," *IEEE Aerospace and Electronic Systems Magazine*, vol. 15, no. 1, pp. 28–32, Jan 2000.

[4] T. Billard, C. Abadie, and T. Lebey, "Partial discharge testing in aeronautic environment on magnet wire and feeder cables," in *2016 IEEE Electrical Insulation Conference (EIC)*, June 2016, pp. 101–104.

[5] D. G. Kasten, X. Liu, S. A. Sebo, D. F. Grosjean, and D. L. Schweickart, "Partial discharge measurements in air and argon at low pressures with and without a dielectric barrier," *IEEE Transactions on Dielectrics and Electrical Insulation*, vol. 12, no. 2, pp. 362–373, April 2005.

[6] E. Sili, F. Koliatene, and J. P. Cambronne, "Pressure and temperature effects on the paschen curve," in *Annual Report Conference on Electrical Insulation and Dielectric Phenomena (CEIDP)*. Cancun, Mexico: IEEE, October 2011, pp. 464–467.

[7] D. F. Grosjean, D. L. Schweickart, D. G. Kasten, S. A. Sebo, and X. Liu, "Development of procedures for partial discharge measurements at low pressures in air, argon and helium," *IEEE Transactions on Dielectrics and Electrical Insulation*, vol. 15, no. 6, pp. 1535–1543, December 2008.

[8] K. R. Wheeler, D. A. Timucin, I. X. Twombly, K. F. Goebel, and P. F. Wysocki, "Aging aircraft wiring fault detection survey," NASA Ames Research Center, Moffett Field CA 94035, techreport 1, Jun. 2007.

[9] J. G. Sarkozi and N. A. Evers, "Current transformers for partial discharge detection on aircraft cables and wires," USA Patent US7 145 345B2, 2006.

[10] A. Krivda, "Automated recognition of partial discharges," *IEEE Transactions on Dielectrics and Electrical Insulation*, vol. 2, no. 5, pp. 796–821, Oct. 1995.

[11] H. Janani, B. Kordi, and M. J. Jozani, "Classification of simultaneous multiple partial discharge sources based on probabilistic interpretation using a two-step logistic regression algorithm," *IEEE Transactions on Dielectrics and Electrical Insulation*, vol. 24, no. 1, pp. 54–65, Feb. 2017.

[12] E. Kuffel, W. Zaengl, and J. Kuffel, *High Voltage Engineering: Fundamentals*, 2nd ed. Newnes, August 2000.

[13] *High-voltage test techniques - Partial discharge measurements*, IEC 60270 International Standard, Rev. 3, December 2000.

[14] D. Xiao, *Gas Discharge and Gas Insulation*, ser. Energy and Environment Research in China. Springer, 2015.

[15] Y. P. Raizer, V. I. Kisin, and J. E. Allen, *Gas Discharge Physics.* Springer, 2011.

[16] R. Arora and W. Mosch, "High voltage and electrical insulation engineering," in *High voltage and electrical insulation engineering*, 2011.

[17] E. Husain and R. S. Nema, "Surface discharge studies with uniform field electrodes at low pressures," *IEEE Transactions on Electrical Insulation*, vol. EI-16, no. 2, pp. 128–133, April 1981.

[18] H. Okubo, S. Yuasa, K. Ota, N. Hayakawa, and M. Hikita, "Discharge characteristics under non-uniform electric field in he, ar and air at low pressures," *IEEE Transactions on Dielectrics and Electrical Insulation*, vol. 4, no. 4, pp. 450–455, Aug 1997.

[19] H. Okubo, Y. Yamano, A. Ohashi, and K. Kato, "Vacuum discharge phenomena under non-uniform field conditions," in *The 18th International Symposium on Discharges and Electrical Insulation in Vacuum*, vol. 1, Aug 1998, pp. 93–100.

[20] E. Li and J. M. K. MacAlpine, "Negative corona in air using a point/cup electrode system," *IEEE Transactions on Dielectrics and Electrical Insulation*, vol. 7, no. 6, pp. 752–757, Dec 2000.

[21] J. M. K. MacAlpine and L. Erning, "Positive corona in air using a point/cup electrode system," *IEEE Transactions on Dielectrics and Electrical Insulation*, vol. 10, no. 2, pp. 307–311, 04 2003.

[22] D. L. Schweickart, D. F. Grosjean, D. G. Kasten, X. Liu, and S. A. Sebo, "Partial discharge measurements at low pressures with and without a dielectric barrier," in *The 17th Annual Meeting of the IEEE Lasers and Electro-Optics Society*, Oct 2004, pp. 462–465.

[23] M. Tabrizchi and F. Rouholahnejad, "Corona discharge ion mobility spectrometry at reduced pressures," *Review of Scientific Instruments*, vol. 75, no. 11, pp. 4656–4661, nov 2004.

[24] ——, "Comparing the effect of pressure and temperature on ion mobilities," *Journal of Physics D: Applied Physics*, vol. 38, no. 6, p. 857, 2005.

[25] X. Liu, "Partial discharge detection and analysis in low pressure environments," Ph.D. dissertation, The Ohio State University, Department of Electrical and Computer Engineering, The Ohio State University, 2006.

[26] X. Liu, D. G. Kasten, and S. A. Sebo, "Partial discharge measurements for a twisted pair of insulated conductors at low pressures in air, argon and helium," in *Conference Record of the 2006 IEEE International Symposium on Electrical Insulation*, June 2006, pp. 286–289.

[27] C. Forssen and H. Edin, "Partial discharges in a cavity at variable applied frequency part 1: measurements," *IEEE Transactions on Dielectrics and Electrical Insulation*, vol. 15, no. 6, pp. 1601–1609, December 2008.

[28] ——, "Partial discharges in a cavity at variable applied frequency part 2: measurements and modeling," *IEEE Transactions on Dielectrics and Electrical Insulation*, vol. 15, no. 6, pp. 1610–1616, December 2008.

[29] D. L. Schweickart, D. F. Grosjean, D. G. Kasten, S. A. Sebo, and X. Liu, "Low-pressure partial-discharge measurements: Monitoring the insulation integrity of aircraft power wiring systems," in *International Power Modulators and High-Voltage Conference*. Las Vegas, NE, USA: IEEE, May 2008, pp. 568–571.

[30] X. Bian, L. Wang, J. M. K. Macalpine, Z. Guan, J. Hui, and Y. Chen, "Positive corona inception voltages and corona currents for air at various pressures and humidities," *IEEE Transactions on Dielectrics and Electrical Insulation*, vol. 17, no. 1, pp. 63–70, February 2010.

[31] X. Bian, X. Meng, L. Wang, J. M. K. Macalpine, Z. Guan, and J. Hui, "Negative corona inception voltages in rod-plane gaps at various air pressures and humidities," *IEEE Transactions on Dielectrics and Electrical Insulation*, vol. 18, no. 2, pp. 613–619, April 2011.

[32] P. Sattari, G. S. P. Castle, and K. Adamiak, "A numerical model of trichel pulses in air; the effect of pressure," *Journal of Physics: Conference Series*, vol. 301, no. 1, p. 012058, 2011.

[33] P. Sattari, C. F. Gallo, G. S. P. Castle, and K. Adamiak, "Trichel pulse characteristics - negative corona discharge in air," *Journal of Physics D: Applied Physics*, vol. 44, no. 15, p. 155502, 2011.

[34] G. W. Trichel, "The mechanism of the negative point to plane corona near onset," *Phys. Rev.*, vol. 54, pp. 1078–1084, Dec 1938.

[35] S. J. He, J. Ha, Y. H. Han, Z. Q. Liu, and S. Q. Guo, "Trichel pulses in a negative corona discharge in air at low pressure," *Journal of Physics: Conference Series*, vol. 418, no. 1, p. 012091, 2013.

[36] A. Cavallini, L. Versari, and L. Fornasari, "Feasibility of partial discharge detection in inverter-fed actuators used in aircrafts," in *Annual Report Conference on Electrical Insulation and Dielectric Phenomena (CEIDP)*. Shenzhen, China: IEEE, October 2013, pp. 1250–1253.

[37] C. Abadie, T. Billard, and T. Lebey, "Influence of pressure on partial discharge spectra," in *2016 Electrical Insulation Conference (EIC)*. Montreal, QC: IEEE, Jun. 2016, pp. 507–510.

[38] L. Xuebao, C. Xiang, L. Tiebing, L. Dayong, C. Bo, and F. Yuke, "Influence of air pressure on the detailed characteristics of corona current pulse due to positive corona discharge," *Physics of Plasmas*, vol. 23, no. 12, p. 123516, 2016.

[39] T. Liu, Y. Xiao, Y. Lu, X. Huang, Q. Li, and Z. Wang, "Effect of voltage frequency on surface discharge characteristics and aging process," in *2017 IEEE Electrical Insulation Conference (EIC)*, June 2017, pp. 463–466.

[40] G. Dong, T. Liu, M. Zhang, Q. Li, and Z. Wang, "Effect of voltage waveform on partial discharge characteristics and insulation life," in *2018 12th International Conference on the Properties and Applications of Dielectric Materials (ICPADM)*, May 2018, pp. 144–147.

[41] Y. Zhou, Z. Zhou, L. Zhang, Y. Zhang, Y. Mo, and J. Sun, "Characterization and comprehension of corona partial discharge in air under power frequency to very low frequency voltage," *Plasma Science and Technology*, vol. 20, no. 5, p. 054016, 2018.

[42] B. X. Ming, Z. J. Yu, Y. Wei, W. S. Wei, Q. Lei, L. XueBao, and L. HaiBing, "The role of low air pressure in the variation of negative corona-generated space charge in a rod to plane electrode," *High Voltage*, vol. 3, no. 2, pp. 126–132, 2018.

[43] C. Emersic, C. Zhang, I. Cotton, R. Lowndes, S. Rowland, and R. Freer, "Degradation of printed circuit board coatings due to partial discharge," in *2015 Electrical Insulation Conference (EIC)*. Seattle, Washington, USA: IEEE, Jun. 2015.

[44] C. Emersic, R. Lowndes, I. Cotton, S. Rowland, and R. Freer, "The effects of pressure and temperature on partial discharge degradation of silicone conformai coatings," *IEEE Transactions on Dielectrics and Electrical Insulation*, vol. 24, no. 5, pp. 2986–2994, oct 2017.

[45] G. C. Stone, M. K. W. Stranges, and D. G. Dunn, “Common questions on partial discharge testing: A review of recent developments in IEEE and IEC standards for offline and online testing of motor and generator stator windings,” *IEEE Industry Applications Magazine*, vol. 22, no. 1, pp. 14–19, jan 2016.

[46] R. Bartnikas, “Partial discharges. their mechanism, detection and measurement,” *IEEE Transactions on Dielectrics and Electrical Insulation*, vol. 9, no. 5, pp. 763–808, Oct 2002.

[47] L. Li, J. Tang, and Y. Liu, “Partial discharge recognition in gas insulated switchgear based on multi-information fusion,” *IEEE Transactions on Dielectrics and Electrical Insulation*, vol. 22, no. 2, pp. 1080–1087, April 2015.

[48] G. Stone, E. Boulter, I. Culbert, and H. Dhirani, *Electrical Insulation for Rotating Machines: Design, Evaluation, Aging, Testing, and Repair*, 1st ed. Wiley-IEEE Press, January 2014.

[49] G. C. Stone, C. Chan, and H. G. Sedding, “Relative ability of UHF antenna and VHF capacitor methods to detect partial discharge in turbine generator stator windings,” *IEEE Transactions on Dielectrics and Electrical Insulation*, vol. 22, no. 6, pp. 3069–3078, December 2015.

[50] S. Committee, *IEEE Guide for the Measurement of Partial Discharges in AC Electric Machinery*, IEEE Std 1434 IEEE Standard, Rev. 2, 2014.

[51] R. Candela and A. Contin, “A portable instrument for the location and identification of defects generating pd,” in *Electrical Insulation Conference (EIC)*. Annapolis, Maryland: IEEE, June 2011, pp. 468–472.

[52] K. Wang, R. Liao, L. Yang, J. Li, S. Grzybowski, and J. Hao, “Optimal features selected by nsga-ii for partial discharge pulses separation based on time-frequency representation and matrix decomposition,” *IEEE Transactions on Dielectrics and Electrical Insulation*, vol. 20, no. 3, pp. 825–838, Jun. 2013.

[53] C. Hudon and M. Belec, “Partial discharge signal interpretation for generator diagnostics,” *IEEE Transactions on Dielectrics and Electrical Insulation*, vol. 12, no. 2, pp. 297–319, Apr. 2005.

[54] M. Cacciari, A. Contin, and G. C. Montanari, “Use of a mixed-weibull distribution for the identification of pd phenomena [rotating machines],” *IEEE Transactions on Dielectrics and Electrical Insulation*, vol. 2, no. 4, pp. 614–627, Aug. 1995.

[55] A. Cavallini, G. C. Montanari, A. Contin, and F. Pulletti, “A new approach to the diagnosis of solid insulation systems based on pd signal inference,” *IEEE Electrical Insulation Magazine*, vol. 19, no. 2, pp. 23–30, March-April 2003.

[56] A. Cavallini, G. C. Montanari, F. Puletti, and A. Contin, "A new methodology for the identification of pd in electrical apparatus: properties and applications," *IEEE IEEE Transactions on Dielectrics and Electrical Insulation*, vol. 12, no. 2, pp. 203–215, Apr. 2005.

[57] A. Contin and S. Pastore, "Classification of partial discharge signals by means of auto-correlation function evaluation," in *IEEE International Symposium on Electrical Insulation*, Toronto, Ontario, Canada, 2006, pp. 302–303.

[58] ——, "Classification and separation of partial discharge signals by means of their auto-correlation function evaluation," *IEEE Transactions on Dielectrics and Electrical Insulation*, vol. 16, no. 6, pp. 1609–1622, Dec. 2009.

[59] T. Pinpart and M. D. Judd, "Differentiating between partial discharge sources using envelope comparison of ultra-high-frequency signals," *IET Science, Measurement & Technology*, vol. 4, no. 5, pp. 256–267, Sep. 2010.

[60] L. Hao, P. L. Lewin, J. A. Hunter, D. J. Swaffield, A. Contin, C. Walton, and M. Michel, "Discrimination of multiple pd sources using wavelet decomposition and principal component analysis," *IEEE Transactions on Dielectrics and Electrical Insulation*, vol. 18, no. 5, pp. 1702–1711, Oct. 2011.

[61] P. Wang, H. Xu, J. Wang, W. Wang, and A. Cavallini, "Effect of repetitive impulsive voltage duty cycle on partial discharge features and insulation endurance of enameled wires for inverter-fed low voltage machines," *IEEE Transactions on Dielectrics and Electrical Insulation*, vol. 24, no. 4, pp. 2123–2131, Sep. 2017.

[62] J. Tang, W. Li, and Y. Liu, "Blind source separation of mixed pd signals produced by multiple insulation defects in gis," *IEEE Transactions on Power Delivery*, vol. 25, no. 1, pp. 170–176, Jan. 2010.

[63] M. X. Z. et al., "Classification and separation of partial discharge ultra-high-frequency signals in a 252 kv gas insulated substation by using cumulative energy technique," *IET Science, Measurement & Technology*, vol. 10, no. 4, pp. 316–326, Jul. 2016.

[64] J. A. Ardila-Rey, J. M. Martinez-Tarifa, G. Robles, and M. V. Rojas-Moreno, "Partial discharge and noise separation by means of spectral-power clustering techniques," *IEEE Transactions on Dielectrics and Electrical Insulation*, vol. 20, no. 4, pp. 1436–1443, Aug. 2013.

[65] J. M. Martinez-Tarifa, J. A. Ardila-Rey, and G. Robles, "Automatic selection of frequency bands for the power ratios separation technique in partial discharge measurements: part i, fundamentals and noise rejection in simple test objects," *IEEE Transactions on Dielectrics and Electrical Insulation*, vol. 22, no. 4, pp. 2284–2291, Aug. 2015.

[66] J. A. Ardila-Rey, J. M. Martinez-Tarifa, and G. Robles, “Automatic selection of frequency bands for the power ratios separation technique in partial discharge measurements: part ii, pd source recognition and applications,” *IEEE Transactions on Dielectrics and Electrical Insulation*, vol. 22, no. 4, pp. 2293–2301, Aug. 2015.

[67] J. C. Chan, H. Ma, and T. K. Saha, “Time-frequency sparsity map on automatic partial discharge sources separation for power transformer condition assessment,” *IEEE Transactions on Dielectrics and Electrical Insulation*, vol. 22, no. 4, pp. 2271–2283, Aug. 2015.

[68] A. Baug, N. R. Choudhury, R. Ghosh, S. Dalai, and B. Chatterjee, “Identification of single and multiple partial discharge sources by optical method using mathematical morphology aided sparse representation classifier,” *IEEE Transactions on Dielectrics and Electrical Insulation*, vol. 24, no. 6, pp. 3703–3712, Dec. 2017.

[69] H. Janani, N. D. Jacob, and B. Kordi, “Automated recognition of partial discharge in oil-immersed insulation,” in *IEEE Electrical Insulation Conference (EIC), Seattle, WA, 2015, pp. 467-470.*, Seattle, WA, Jun. 2015, pp. 467–470.

[70] A. Eid, H. El-Kishky, M. Abdel-Salam, and M. T. El-Mohandes, “On power quality of variable-speed constant-frequency aircraft electric power systems,” *IEEE Transactions on Power Delivery*, vol. 25, no. 1, pp. 55–65, Jan 2010.

[71] T. Billard, T. Lebey, and F. Fresnet, “Partial discharge in electric motor fed by a pwm inverter: off-line and on-line detection,” *IEEE Transactions on Dielectrics and Electrical Insulation*, vol. 21, no. 3, pp. 1235–1242, June 2014.

[72] M. Ashtiani and S. Shahrtash, “Partial discharge pulse localization in excessive noisy data window,” *IEEE Transactions on Dielectrics and Electrical Insulation*, vol. 22, no. 1, pp. 428–435, Feb. 2015.

[73] W. Hauschild, A. Cavallini, and G. C. Montanari, “Effect of supply voltage frequency on testing of insulation system,” *IEEE Transactions on Dielectrics and Electrical Insulation*, vol. 13, no. 5, pp. 1189–1191, Oct. 2006.

[74] L. Hao, P. L. Lewin, and S. G. Swingler, “Improving detection sensitivity for partial discharge monitoring of high voltage equipment,” *Measurement Science and Technology*, vol. 19, no. 5, p. 055707, 2008.

[75] A. A. Bajwa, S. Habib, and M. Kamran, “An investigation into partial discharge pulse extraction methods,” *International Journal of Electrical Power & Energy Systems*, vol. 73, pp. 964–982, 2015.

[76] F. Alrumayan, I. Cotton, and A. Nelms, “Partial discharge testing of aerospace electrical systems,” *IEEE Transactions on Aerospace and Electronic Systems*, vol. 46, no. 2, pp. 848–863, April 2010.

[77] *Winding wires Test methods Part 5: Electrical properties*, IEC 60851-5 International Standard, Rev. 3, July 2008.

[78] A. Cavallini, L. Lusuardi, D. R. Meyer, and S. Machipeddy, "Modelling partial discharge inception in magnet wires at different altitudes," in *2016 IEEE Conference on Electrical Insulation and Dielectric Phenomena (CEIDP)*, Oct 2016, pp. 449–452.

[79] N. C. Sahoo, M. M. A. Salama, and R. Bartnikas, "Trends in partial discharge pattern classification: a survey," *IEEE Transactions on Dielectrics and Electrical Insulation*, vol. 12, no. 2, pp. 248–264, April 2005.

[80] E. M. Lalitha and L. Satish, "Wavelet analysis for classification of multi-source pd patterns," *IEEE Transactions on Dielectrics and Electrical Insulation*, vol. 7, no. 1, pp. 40–47, Feb 2000.

[81] D. Evagorou, A. Kyprianou, P. L. Lewin, A. Stavrou, V. Efthymiou, A. C. Metaxas, and G. E. Georghiou, "Feature extraction of partial discharge signals using the wavelet packet transform and classification with a probabilistic neural network," *IET Science, Measurement Technology*, vol. 4, no. 3, pp. 177–192, May 2010.

[82] H. Janani, "Partial discharge source classification using pattern recognition algorithms," Ph.D. dissertation, University of Manitoba, Department of Electrical and Computer Engineering, University of Manitoba, Winnipeg, Manitoba, Canada, 2016.

[83] B. Efron, "The bootstrap and modern statistics," *Journal of the American Statistical Association*, vol. 95, no. 452, pp. 1293–1296, 2000.

[84] A. C. Davison and D. V. Hinkley, *Bootstrap Methods and their Application*, Har/Dskt, Ed. Cambridge University Press, 1997.

[85] A. N. Esfahani, S. Shahabi, G. C. Stone, and B. Kordi, "Investigation of corona partial discharge under variable frequency and air pressure," in *2018 Electrical Insulation Conference (EIC), San Antonio, TX, USA, 17 - 21 June 2018*. IEEE, 2018.

[86] Y. Zhang, Q. Xia, Z. Jiang, and J. Ouyang, "Trichel pulse in various gases and the key factor for its formation," *Scientific Reports*, vol. 7, no. 2, pp. 1–8, Aug. 2017.

[87] A. W. Ali, "The electron avalanche ionization of air and a simple air chemistry model," Naval research laboratory, Washington, D.C., NRL Memorandum Report, Apr. 1982.

[88] F. Alvarez, J. Ortego, F. Garnacho, and M. A. Sanchez-Uran, "A clustering technique for partial discharge and noise sources identification in power cables by means of waveform parameters," *IEEE Transactions on Dielectrics and Electrical Insulation*, vol. 23, no. 1, pp. 469–481, February 2016.

[89] *IEEE Guide for the Statistical Analysis of Electrical Insulation Breakdown Data*, IEEE standard Standard, 2005.

[90] A. Contin, A. Cavallini, G. C. Montanari, G. Pasini, and F. Puletti, "Digital detection and fuzzy classification of partial discharge signals," *IEEE Transactions on Dielectrics and Electrical Insulation*, vol. 9, no. 3, pp. 335–348, 2002.

[91] E. Gulski and A. Krivda, "Neural networks as a tool for recognition of partial discharges," *IEEE Transactions on Dielectrics and Electrical Insulation*, vol. 28, no. 6, pp. 984–1001, 1993.

[92] H. Ma, J. C. Chan, T. K. Saha, and C. Ekanayake, "Pattern recognition techniques and their applications for automatic classification of artificial partial discharge sources," *IEEE Transactions on Dielectrics and Electrical Insulation*, vol. 20, no. 2, pp. 468–478, April 2013.

[93] S. Poyhonen, M. Conti, A. Cavallini, G. C. Montanari, and F. Filippetti, "Insulation defect localization through partial discharge measurements and numerical classification," in *IEEE International Symposium on Industrial Electronics*, vol. 1, Ajaccio, France, 2004, pp. 417–422.

[94] R. M. Sharkawy, R. S. Mangoubi, T. k. Abdel-Galil, M. M. A. Salama, and R. Bartnikas, "Svm classification of contaminating particles in liquid dielectrics using higher order statistics of electrical and acoustic pd measurements," *IEEE Transactions on Dielectrics and Electrical Insulation*, vol. 14, no. 3, pp. 669–678, 2007.

[95] S. Theodoridis and K. Koutroumbas, *Pattern Recognition*, 4th ed. Elsevier, 2009.

[96] H. Janani and B. Kordi, "Towards automated statistical partial discharge source classification using pattern recognition techniques," *IET High Voltage*, vol. 3, no. 3, pp. 162–169, September 2018.

Appendix A

Differential Energy (DE) Pattern

DE patterns for single PD source and multiple PD sources are shown in this appendix at different air pressure levels and frequencies. The PD sources were needle-plane electrode and twisted-pair of magnet wires. MDE and PRCD patterns demonstrated in Chapter 4 were generated by these DE patterns.

A.1 Single Source DE Pattern

In this section, DE pattern related to needle-plane electrode or twisted-pair of magnet wires as a PD source has been presented.

Fig. A.1 and Fig. A.2 show DE patterns produced by needle-plane electrode under AC and square voltage waveforms, respectively.

Fig. A.3 and Fig. A.4 show DE pattern produced by twisted-pair of magnet wires under AC and square voltage waveforms, respectively.

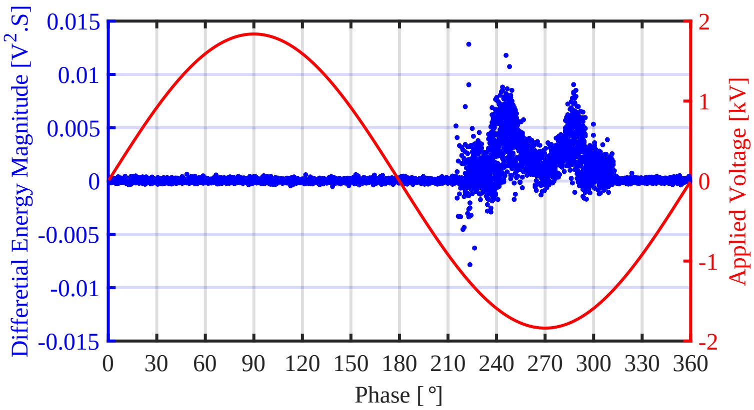

(a)

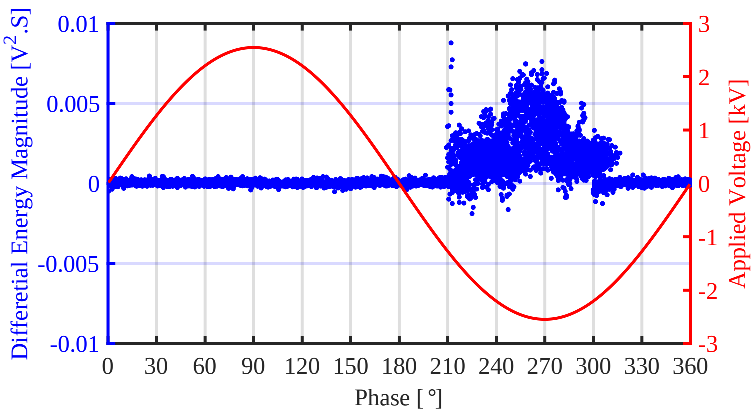

(b)

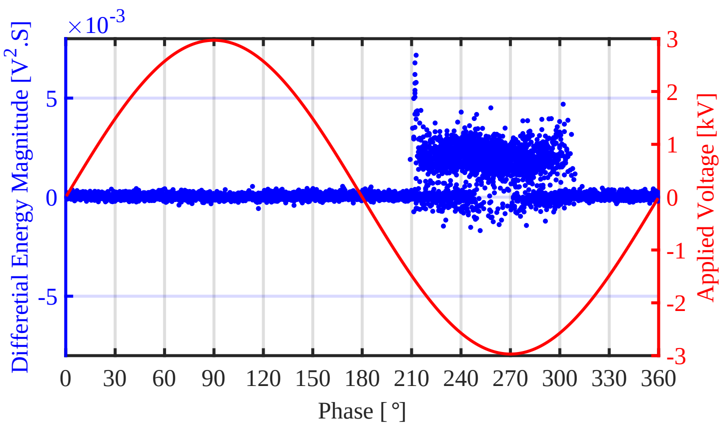

(c)

Fig. A.1: DE patterns for corona discharges under AC voltage frequency of 1 kHz for air pressure levels of (a) 33 kPa, (b) 67 kPa, and (c) 101 kPa

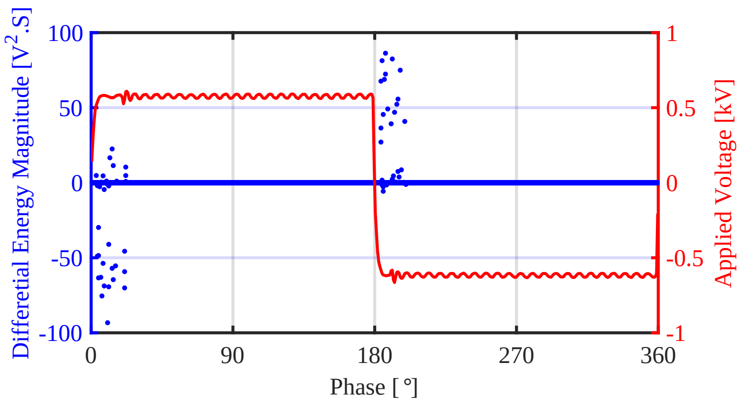

(a)

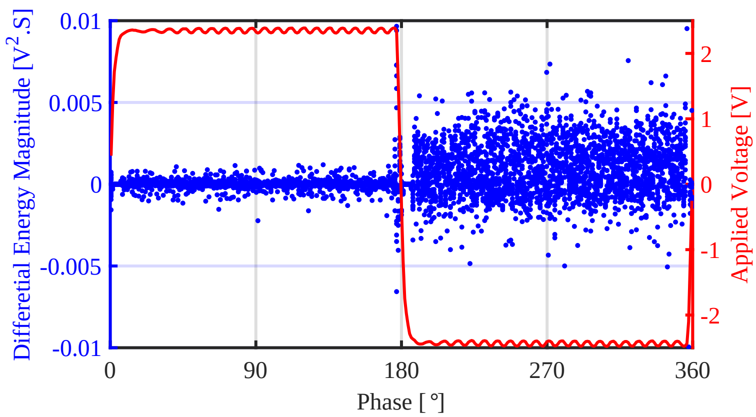

(b)

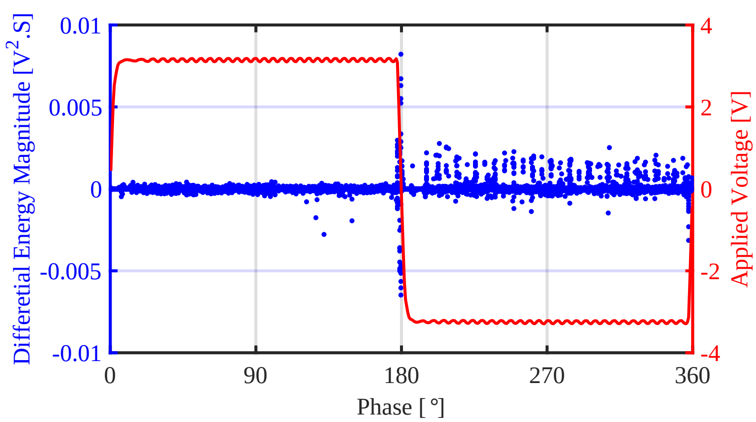

(c)

Fig. A.2: DE patterns for corona discharges under square wave voltage frequency of 2 kHz for air pressure levels of (a) 33 kPa, (b) 67 kPa, and (c) 101 kPa

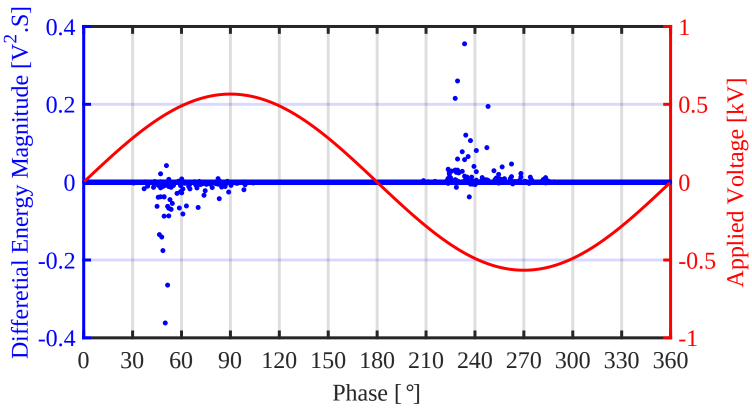

(a)

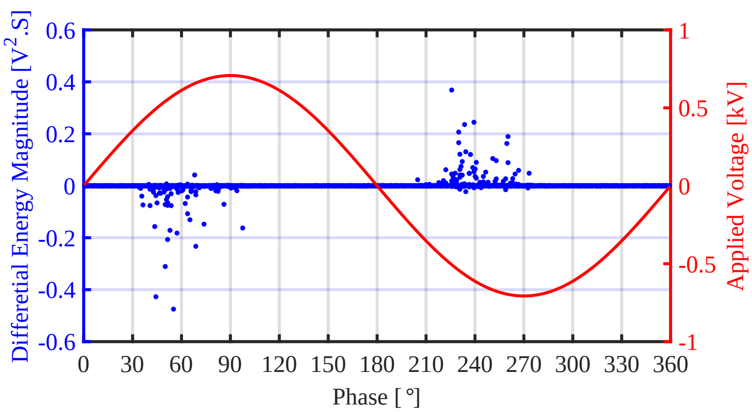

(b)

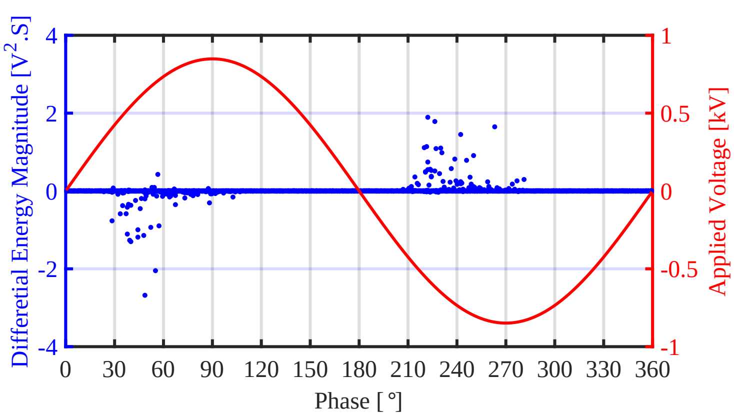

(c)

Fig. A.3: DE patterns produced by twisted-pair of magnet wires under AC voltage frequency of 1 kHz for air pressure levels of (a) 33 kPa, (b) 67 kPa, and (c) 101 kPa

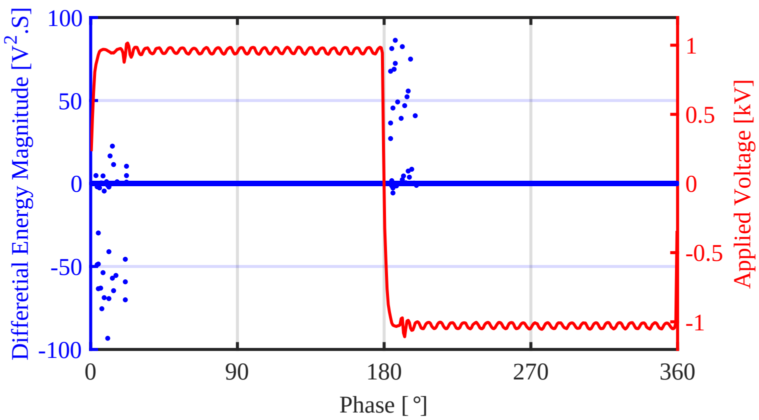

(a)

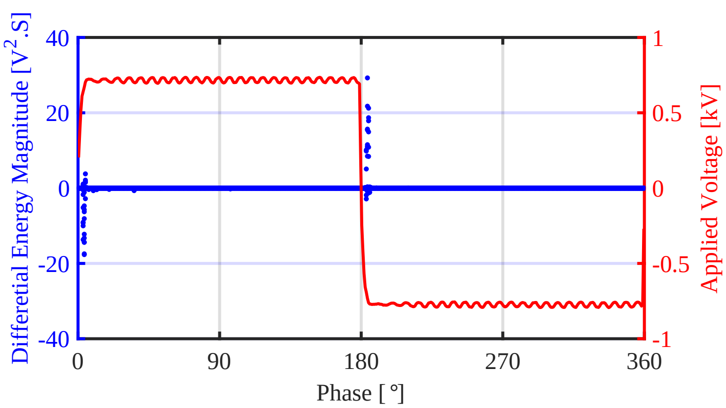

(b)

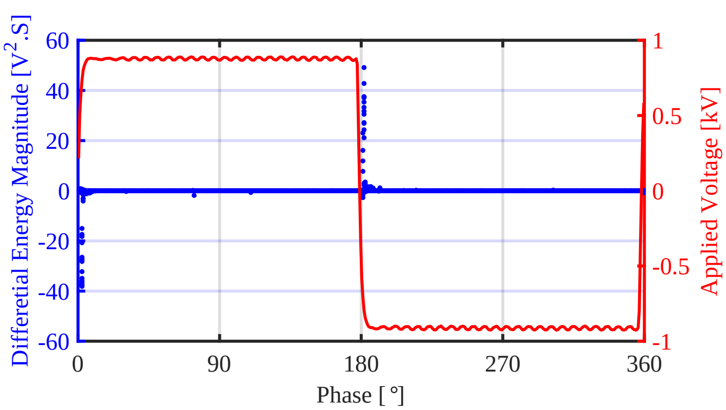

(c)

Fig. A.4: DE patterns produced by twisted-pair of magnet wires under square wave voltage frequency of 2 kHz for air pressure levels of (a) 33 kPa, (b) 67 kPa, and (c) 101 kPa

A.2 Multi Source DE Pattern

In this section, DE and MDE patterns related to needle-plane electrode and twisted-pair of magnet wires as activated PD sources have been presented.

Fig. A.5 and Fig. A.6 show DE and MDE patterns produced by two activated PD sources that are needle-plane electrode and twisted-pair of magnet wires under AC voltage waveform.

Fig. A.7 and Fig. A.8 show DE and MDE patterns produced by two activated PD sources that are needle-plane electrode and twisted-pair of magnet wires under square voltage waveform.

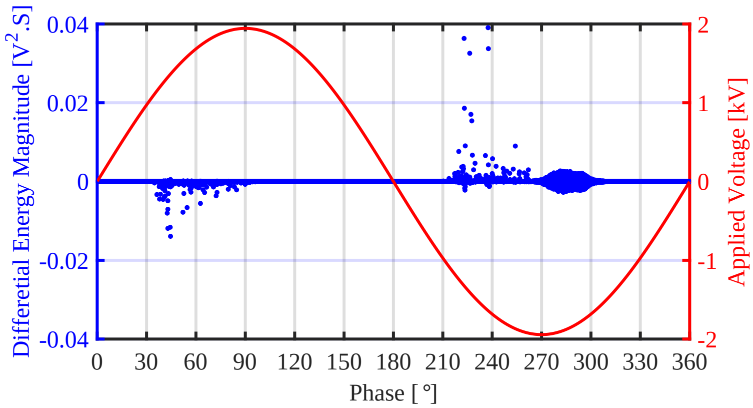

(a)

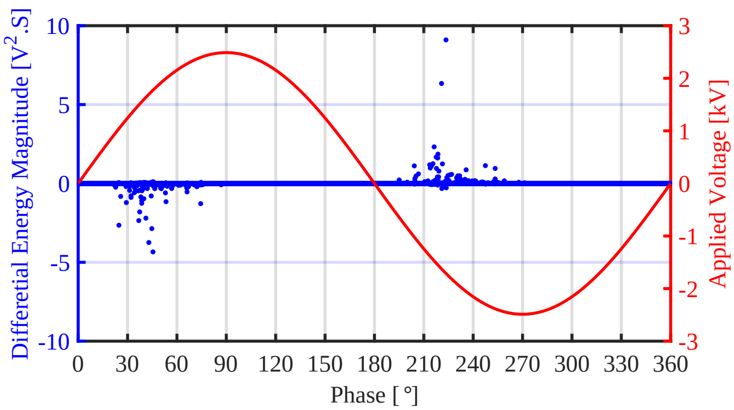

(b)

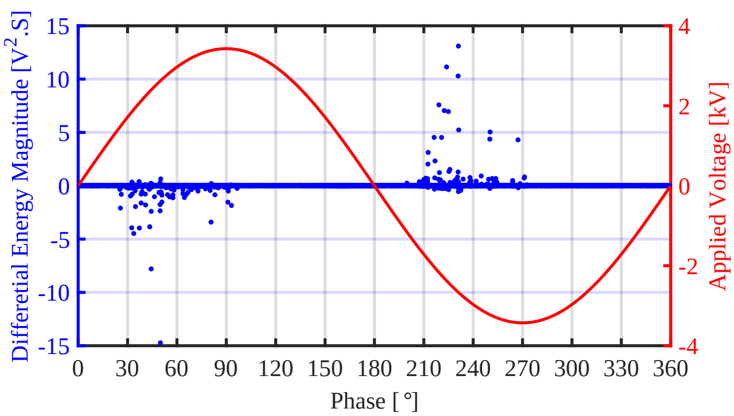

(c)

Fig. A.5: DE patterns produced by two activated PD sources under AC voltage frequency of 500 Hz for air pressure levels of (a) 33 kPa, (b) 67 kPa, and (c) 101 kPa

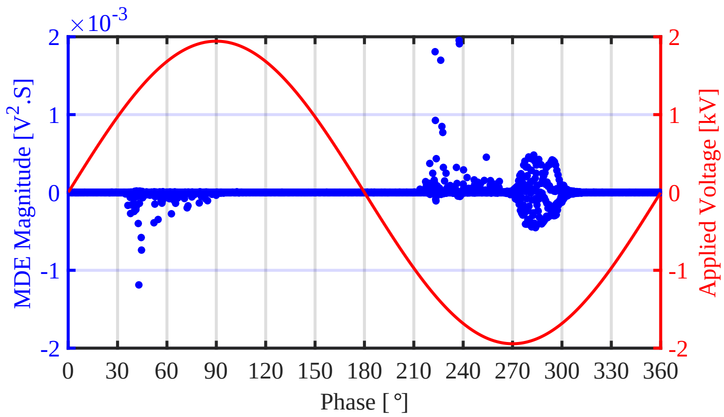

(a)

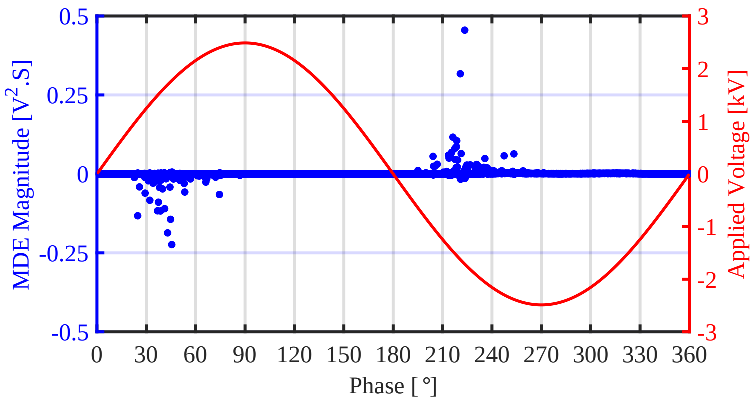

(b)

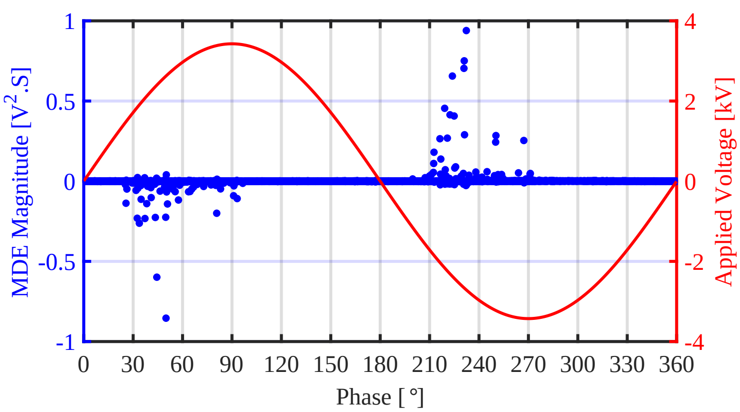

(c)

Fig. A.6: MDE patterns produced by two activated PD sources under AC voltage frequency of 500 Hz for air pressure levels of (a) 33 kPa, (b) 67 kPa, and (c) 101 kPa

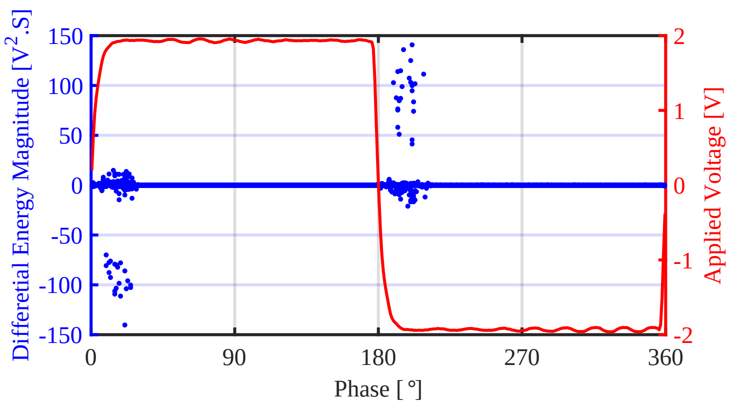

(a)

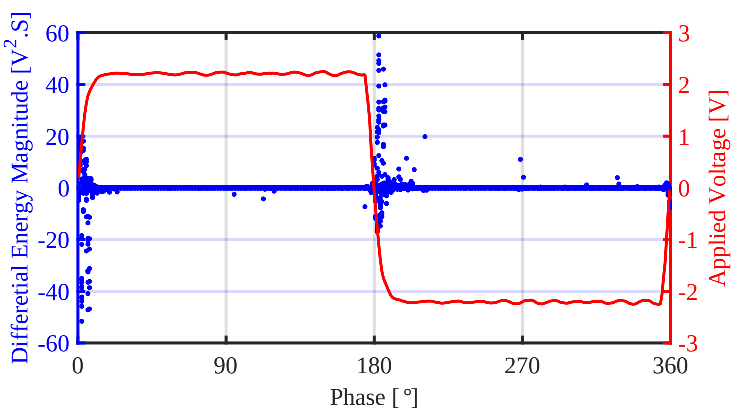

(b)

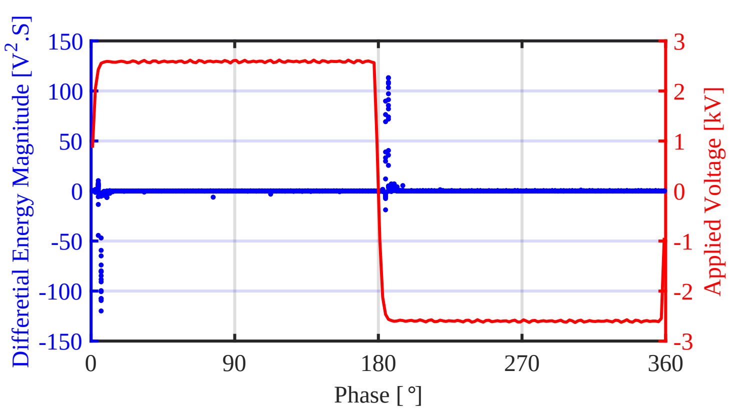

(c)

Fig. A.7: DE patterns produced by two activated PD sources under square wave voltage frequency of 5 kHz for air pressure levels of (a) 33 kPa, (b) 67 kPa, and (c) 101 kPa

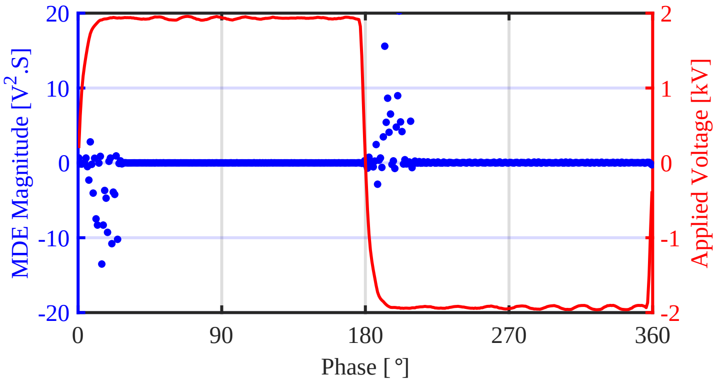

(a)

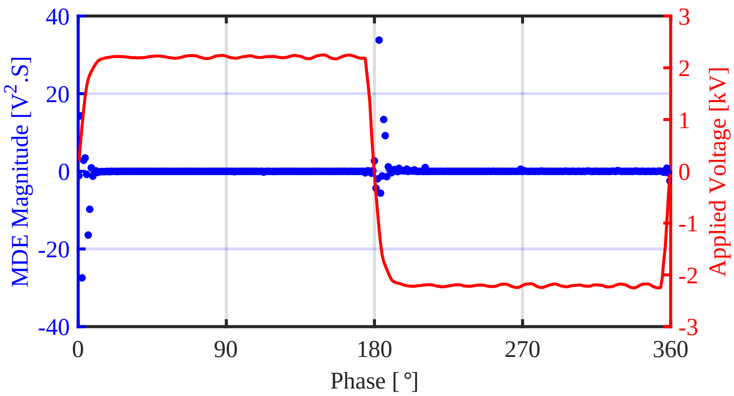

(b)

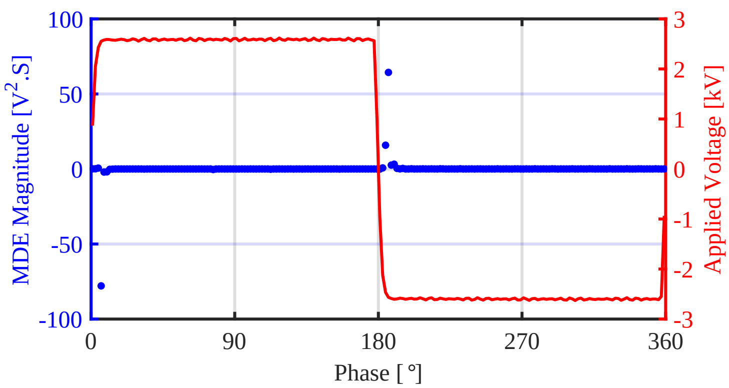

(c)

Fig. A.8: MDE patterns produced by two activated PD sources under square wave voltage frequency of 5 kHz for air pressure levels of (a) 33 kPa, (b) 67 kPa, and (c) 101 kPa

Appendix B

Separation and Classification of Concurrent PD Sources

In this section, the separation of PD sources in 3D space, and the Probability density function of Normal and Weibull distributions of PD data are indicated. The PDF of Normal and Weibull distributions were carried out based on PD data clustering shown in separation map. Accordingly, the probability density function (PDF) of a Normal and Weibull distributions were calculated to find PD waveform characteristics.

B.1 PD Sources Separation Map

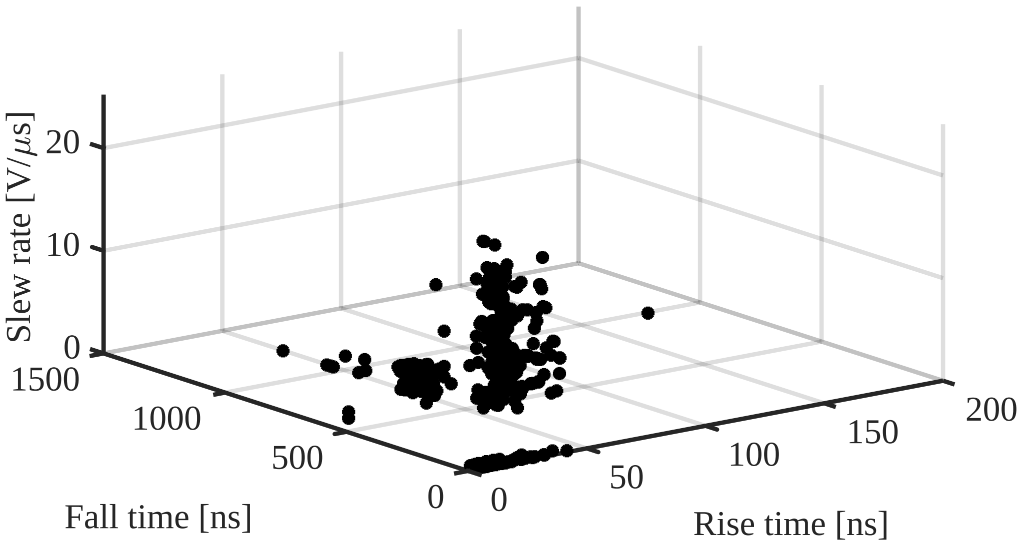

Fig. B.1: The separation map of PD sources under AC applied voltage frequency of 500 Hz and sub-atmospheric pressure of 33 kPa

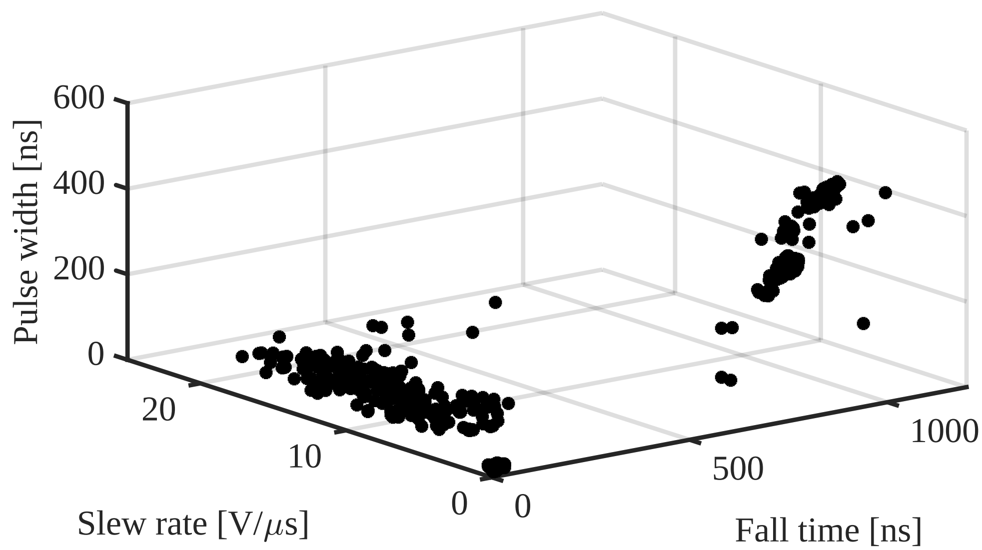

Fig. B.2: The separation map of PD sources under AC applied voltage frequency of 500 Hz and sub-atmospheric pressure of 33 kPa

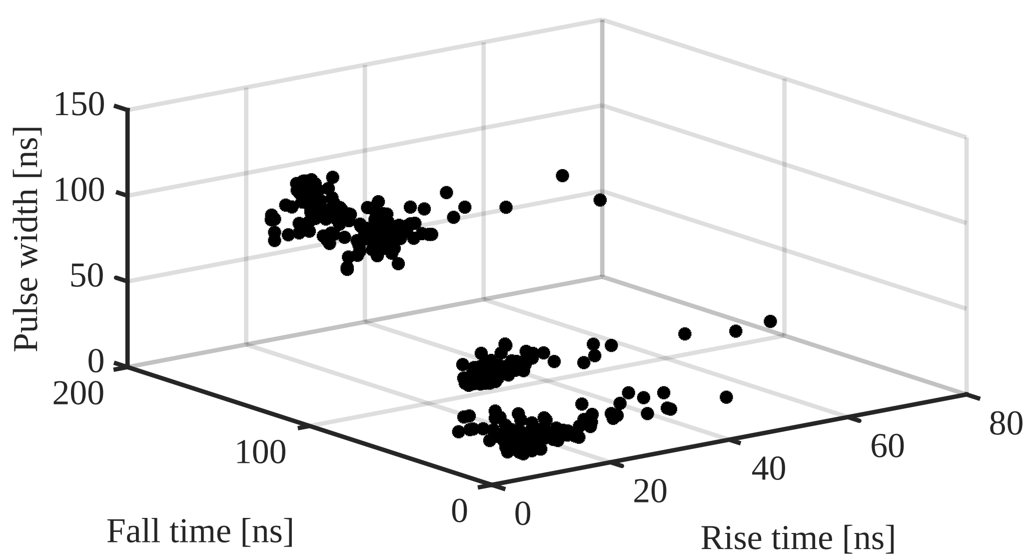

Fig. B.3: The separation map of PD sources under AC applied voltage frequency of 500 Hz and atmospheric pressure of 101 kPa

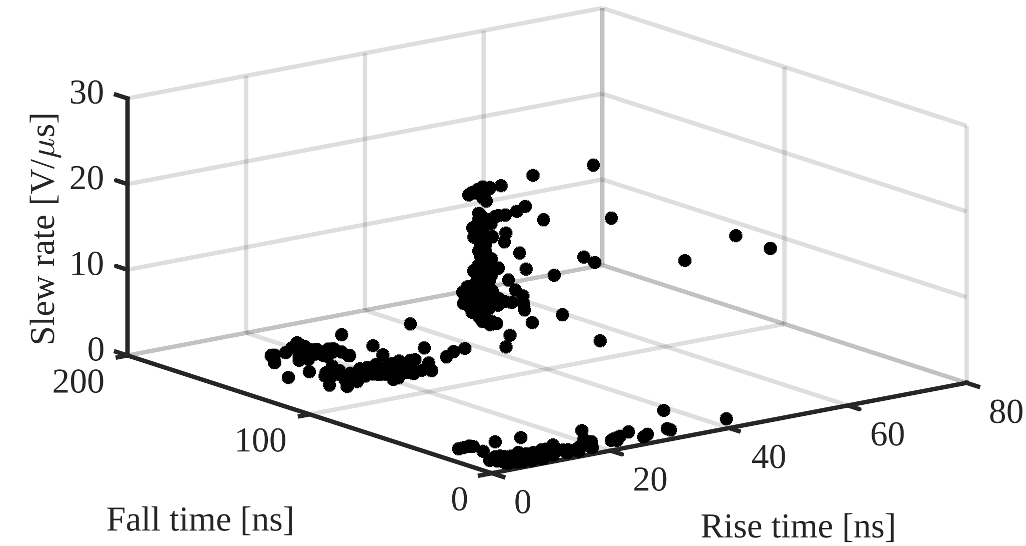

Fig. B.4: The separation map of PD sources under AC applied voltage frequency of 500 Hz and atmospheric pressure of 101 kPa

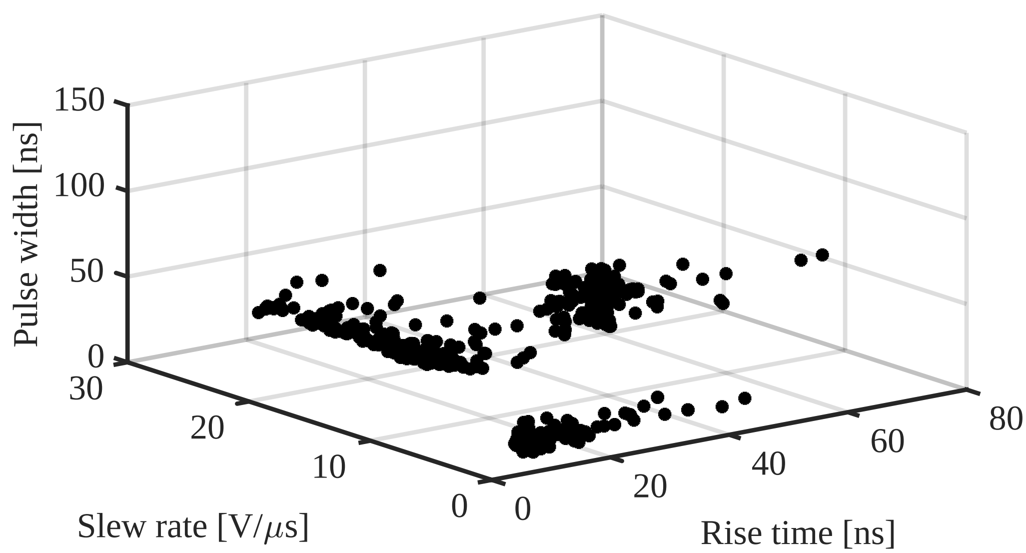

Fig. B.5: The separation map of PD sources under AC applied voltage frequency of 500 Hz and atmospheric pressure of 101 kPa

B.2 Probability Density Function

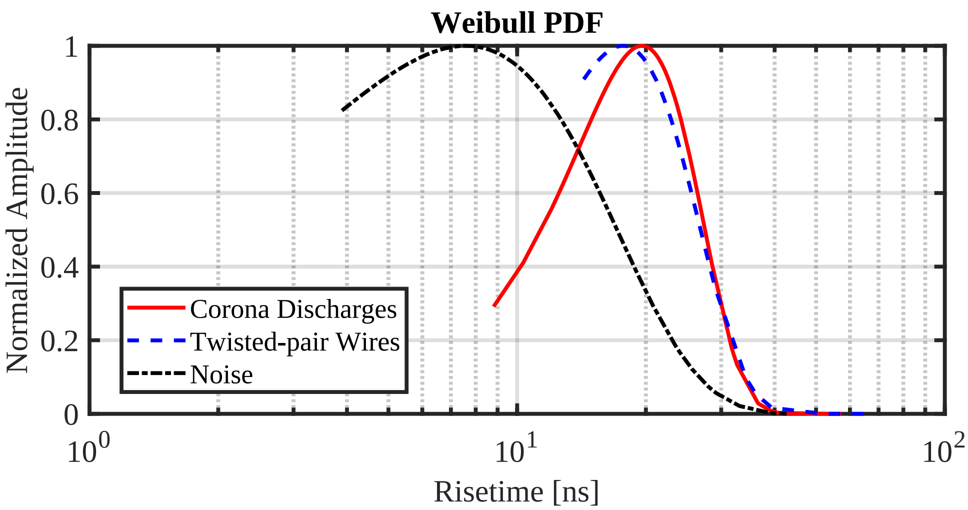

(a)

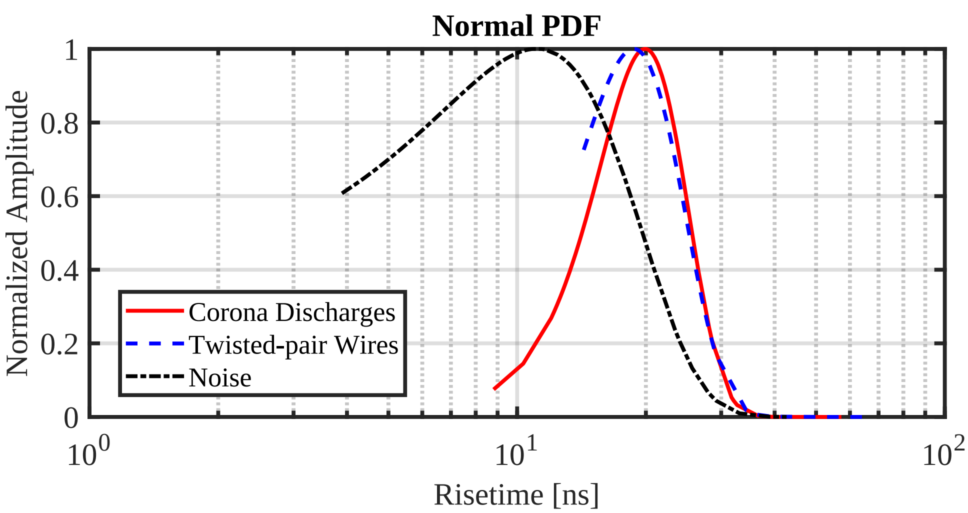

(b)

Fig. B.6: Weibull (a) and Normal (b) distribution of rise time for applied frequency of 500 Hz and air pressure level of 101 kPa.

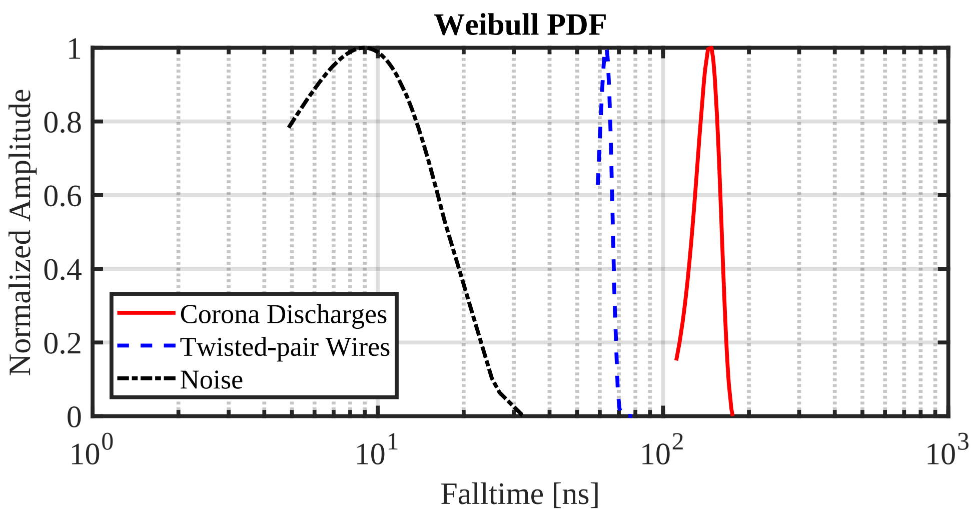

(a)

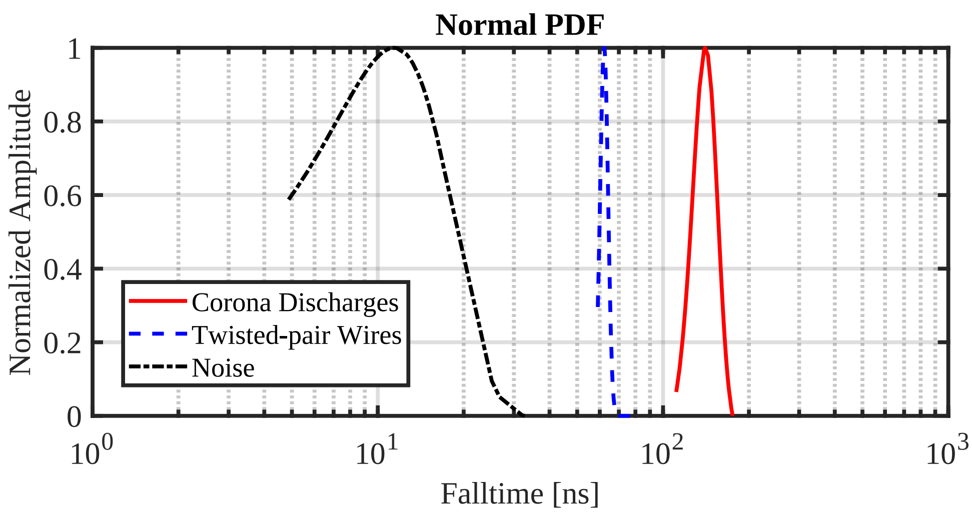

(b)

Fig. B.7: Weibull and Normal distribution of fall time for applied frequency of 500 Hz and air pressure level of 101 kPa.

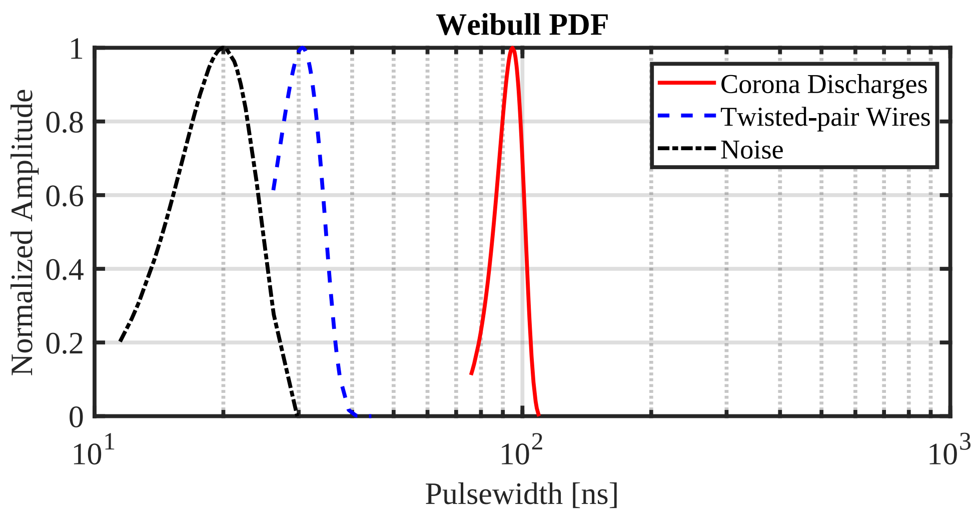

(a)

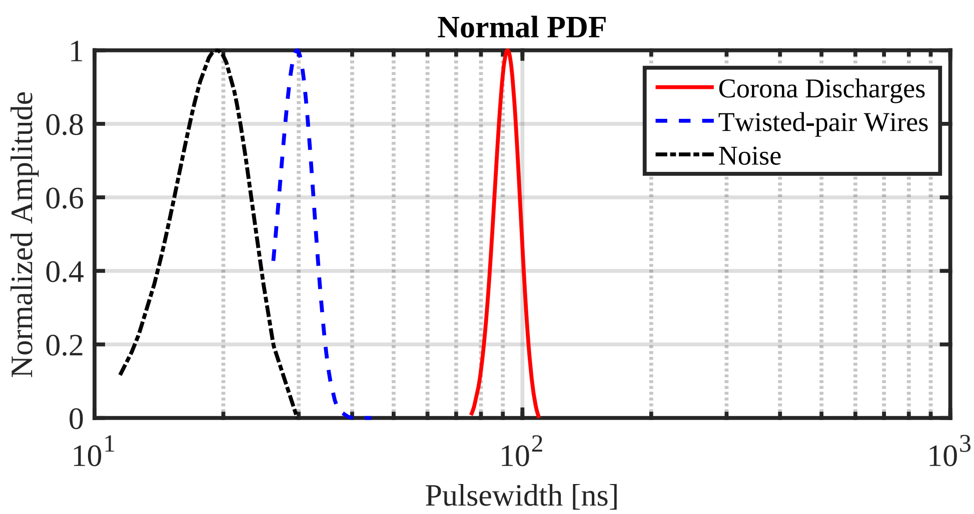

(b)

Fig. B.8: Weibull and Normal distribution of pulse width for applied frequency of 500 Hz and air pressure level of 101 kPa.

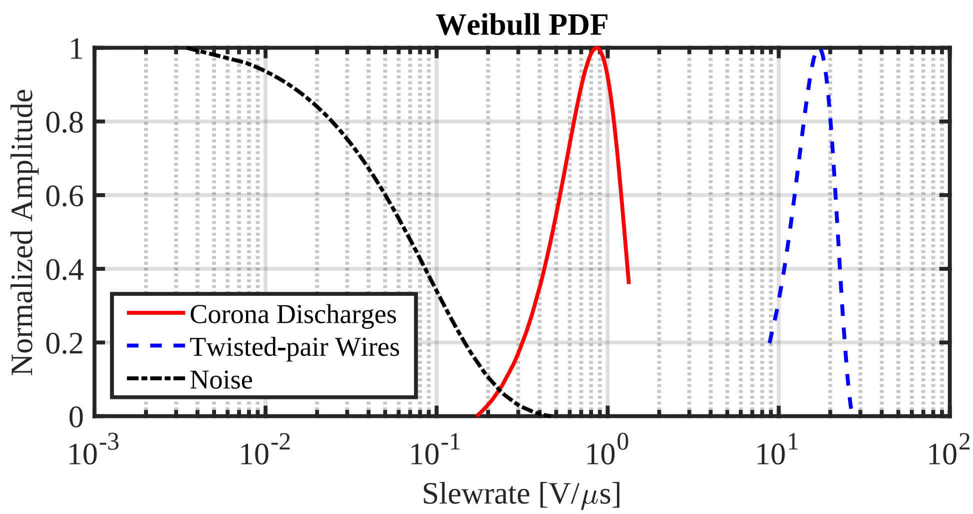

(a)

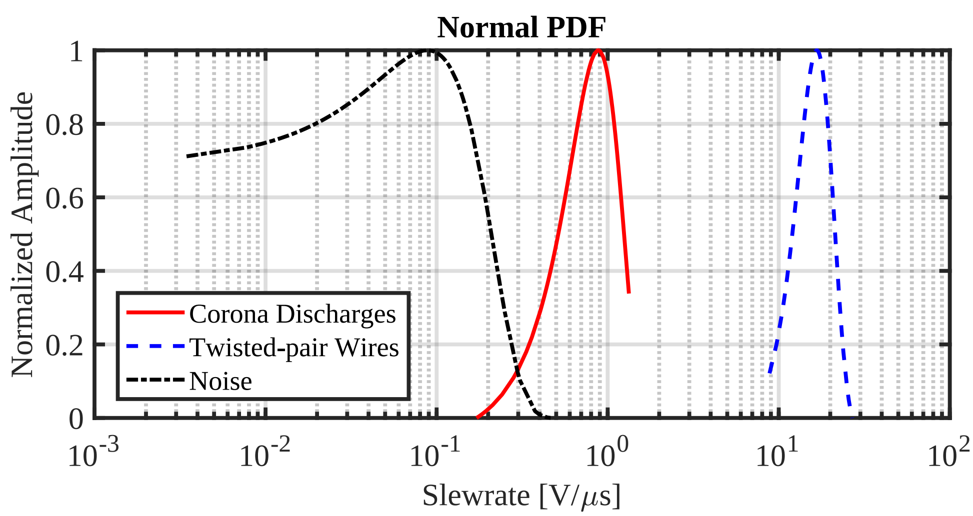

(b)

Fig. B.9: Weibull and Normal distribution of pulse width for applied frequency of 500 Hz and air pressure level of 101 kPa.